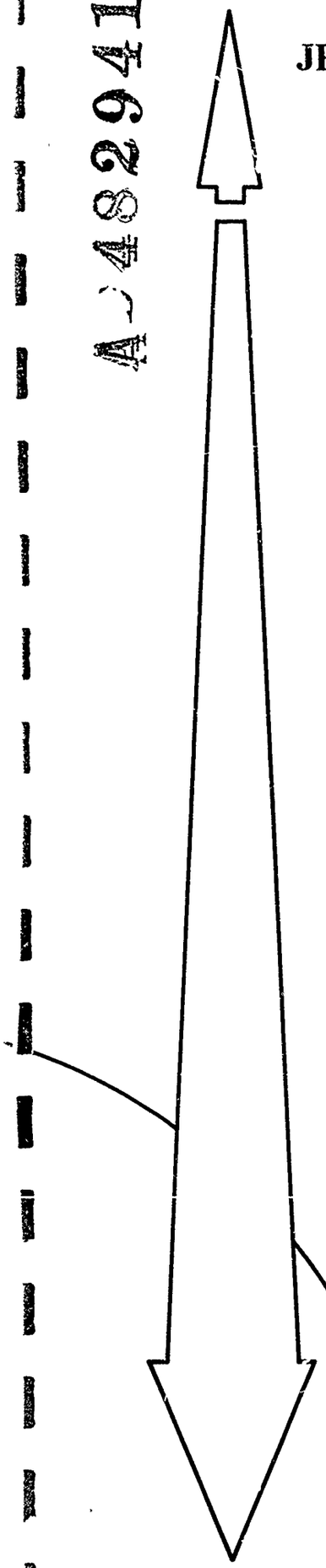

JPC 418

Report Number
TM-66-1

The Interaction of a Finite Amplitude Pressure Disturbance with a Combustion Region

by

G. M. Lehmann

Technical Memorandum

Contracts

Nonr 1100(21)

AFOSR 753-65

January 1966

JET PROPULSION CENTER
PURDUE UNIVERSITY

SCHOOL OF MECHANICAL ENGINEERING
LAFAYETTE, INDIANA

PURDUE UNIVERSITY

AND

PURDUE RESEARCH FOUNDATION

Lafayette, Indiana

Report No. TM-66-1

The Interaction of a Finite Amplitude Pressure Disturbance with a Combustion Region

by

G. M. Lehmann

Technical Memorandum

Contracts

Nonr 1100(21)

AFOSR 753-65

Jet Propulsion Center

Purdue University

February 1966

Approved by:

_____

B. A. Reese

Date: _____

ACKNOWLEDGMENTS

The author wishes to thank Professors S. N. B. Murthy and J. R. Osborn who conceived the original problem and guided the research. The author also wishes to thank the Director of the Purdue Jet Propulsion Center, Dr. M. J. Zucrow, Atkins Professor of Engineering, for his interest in and supervision of the research program. The author is indebted to Dr. R. B. Lawhead of Rocketdyne Corporation who made pressure-time traces of the reflection of a nonuniform shock from a burning propellant surface available and Mr. Carl Oberg of the same corporation who prepared the traces. The excellent work of Mrs. Sandy Lowe who typed the final draft of the thesis and Frank Bennett who prepared the drawings are also gratefully acknowledged.

The author is also indebted to his wife, Marilyn, who typed the rough draft and spent many hours proofreading the preliminary and final drafts.

The research reported herein was sponsored jointly by the Power Branch, Office of Naval Research, Washington 25, D. C., and the Air Force Office of Scientific Research under contracts Nonr 1100(21) and AFOSR 753-65 respectively. Reproduction in full or in part for any use of the United States Government is permitted.

TABLE OF CONTENTS

LIST OF TABLES

Table | Page

LIST OF ILLUSTRATIONS

ABSTRACT

One of the more important processes occurring during unstable combustion in propulsion systems is the process in which the finite amplitude pressure disturbance interacts with the combustion region. The interaction process is important because through that process the combustion region imparts energy to the disturbance. The aforementioned phenomenon is studied by analyzing the interaction of a nonuniform shock with the combustion region at the surface of a burning solid propellant.

The postulated combustion region comprises three separate zones: (a) a decomposition zone in which the gases evolved from the propellant surface decompose exothermically, (b) an induction zone in which the decomposed gases are heated and induction reactions take place, and (c) a flame zone in which a rapid exothermic chemical reaction takes place. The decomposition rate in the decomposition zone and the chemical reaction rate in the flame zone are assumed to be governed by Arrhenius type functions. Heat transfer, molecular diffusion, bulk viscosity, and property change due to chemical reaction are also included. Physical and transport properties were assigned

based upon the assumption that the propellant being burned was composed of 80 per cent ammonium perchlorate and 20 per cent polybutadiene-acrylic acid polymer. The solid propellant is treated as an elastic solid of semi-infinite extent.

Because of the complexity of the problem investigated solutions were obtained by numerically integrating the related equations. The numerical integration was performed upon an IBM 7094 digital computer. Calculations were made employing three different steady state combustion pressures, 250, 500, and 1000 psia. The initial amplitude of the nonuniform shock employed in the calculations ranged from 2.5 to 150 psi. The results of the calculations are given in the form of an amplification ratio which is defined as the amplitude of the shock front after interaction with the combustion region divided by its amplitude before.

The results indicated that the amplification ratio of the non-uniform shock decreases with increasing initial amplitude for each of the aforementioned combustion pressures. Also, for any given initial amplitude the amplification of the shock decreases with increasing steady state combustion pressure.

In addition to calculating the amplitude of the shock as it propagated through the combustion region, the individual effects of each process occurring in the combustion region which produced a change in the amplitude of the shock were determined. Such results indicated that the amplification or attenuation of the shock is determined by the sum of the following: (a) the amplifying effect of the

chemical heat additon and molecular weight change during chemical reaction, (b) the attenuating effects of the solid propellant as it abosrbs energy during the shock's reflection from its surface and absorbs heat from the gases near its surface, and (c) the amplifying or attenuating effect of the velocity gradient immediately behind the shock. The effect of molecular diffusion and bulk viscosity upon the amplification of the shock were found to be higher order quantities.

The results of the present analysis are consistent with experimental data obtained in T-burners using propellants with compositions similar to that employed in the present analysis and data obtained from pulsing burning propellants with a nonuniform shock.

Although the analysis has been applied to one specific combustion region, it can be applied to other regions whose combustion reactions and products occur primarily in the gaseous phase.

1.0 INTRODUCTION

Cyclic oscillation of the combustion pressure has frequently been observed in chemical combustion chambers which have very high energy release rates per unit volume. The peak to peak amplitude of those oscillations may be very small or may be of an order of magnitude as high as the mean combustion pressure. The oscillations have been most frequently encountered in the combustion chambers of rocket motors although they have also been observed in ramjet and gas turbine engine combustion chambers. The presence of those cyclic oscillations has been loosely called combustion instability but is more accurately termed combustion pressure oscillation. Combustion pressure oscillation with any sizable peak to peak amplitude is usually undesirable because in addition to producing vibrations its presence in the combustion chamber increases the heat transfer to the chamber walls. In both liquid and solid propellant rocket motors the oscillation may cause off-design performance or actual mechanical failure of the combustion chamber. Most of the rocket development programs in the United States, particularly for the liquid propellant motors, have had to deal with combustion pressure oscillation. In many cases the problem of eliminating the oscillations increases the development time and cost of the program.

The combustion pressure oscillation generally falls into one of two classes and is termed either a high or low frequency oscillation.

The high frequency oscillation, as indicated by the name, not only oscillates at a much higher frequency than the low frequency type, but is also a different phenomenon. When low frequency combustion pressure oscillation occurs the combustion pressure oscillates in phase as a unit at all points in the chamber. The cause of the low frequency oscillation has been traced to a coupling of the propellant feed system to the combustion chamber. The low frequency oscillation can usually be eliminated by properly redesigning the feed system to uncouple it from the combustion chamber. The combustion pressure does not oscillate as a unit in high frequency pressure oscillation, but modes of oscillation occur similar to the acoustic modes of oscillation in a right circular cylinder. High frequency oscillations are considered to be caused by a coupling of the pressure oscillation with the energy release rate in the combustion region. The combustion chamber geometry and the propellant being burned determine the mode and frequency of pressure oscillation. Normally not more than one mode and one frequency of oscillation are observed at one time, although more than one mode and one frequency sometime occur. The mode and frequency of oscillation is described in terms of the possible modes and frequencies of acoustic oscillation in a right circular cylinder, i.e., tangential, longitudinal, radial, etc., and first harmonic, second harmonic, etc. respectively. The uncoupling of the pressure oscillation and the combustion rate in the high frequency oscillation is much more difficult to deal with than the uncoupling of the feed system and the combustion chamber in the low frequency one. The high frequency oscillation is

usually eliminated by costly time consuming cut and try methods. The possibility of elimination of the oscillation from solid propellant motors has been greatly improved by the discovery that the addition of powdered aluminum to the propellant will help or completely eliminate the oscillation. To eliminate the oscillation in solid propellant motors the composition of the propellant is usually altered by adding powdered aluminum and/or changing the oxidizer particle size. For liquid propellant motors the injector design is repeatedly changed to try and uncouple the pressure oscillation from the chemical reaction rate, or baffles and/or acoustic liners are inserted into the combustion chamber to damp the oscillation.

Many theories have been proposed to help explain the high frequency combustion pressure oscillation phenomenon (1)* but to date only general qualitative results have been obtained. The theories which have been developed can be grouped into two broad categories, acoustic theories and nonacoustic theories. The acoustic theories, also termed linear theories, assume that a very small amplitude pressure oscillation is present in the combustion chamber. All nonlinear effects are ignored and, further, the problem is assumed to remain acoustic in nature independent of any growth in amplitude of the oscillation. A desirable feature of acoustic theories is that the geometry of the combustion chamber can be readily included in the analysis; however, a drawback of the method is that it is impossible to include the processes occurring

* Numbers in parentheses refer to references presented in the bibliography (Section 9.0)

in the combustion region and still have an analytically solvable problem. Solutions to acoustic theories can predict qualitatively the conditions under which an acoustic oscillation will grow beyond acoustic proportions. Most of the theories developed to date dealing with high frequency combustion pressure oscillation are of the acoustic type.

The nonacoustic theories, also termed nonlinear theories, assume the oscillation is of finite amplitude and so retain the nonlinearities in the conservation equations. Also the nonlinearities introduced by the presence of transport processes are sometimes included. Because of the difficulties involved in the solution of nonlinear equations, results are usually of a numerical nature. Nonacoustic theories allow the combustion process to be represented by a reasonably realistic model; however, the geometry of the combustion chamber is not as effectively brought into the analysis as in acoustic theory. Nonlinear solutions are usually reduced to the calculation of the propagation of a single pressure pulse in a combustion chamber.

Numerous experimental findings show that satisfactorily performing rocket motors of different types can be caused to exhibit combustion pressure oscillation by pulsing them with relatively large pressure disturbances (2)(3). As a consequence, the "pulsing" or "bombing" of rocket motors during performance testing is practiced quite generally in evaluating the susceptibility of a given rocket motor to pressure oscillation. It is apparent from the experimental evidence of the appearance of the aforementioned nonacoustic phenomenon that nonlinear

theories should be developed to study combustion pressure oscillation. While acoustic theories are helpful they are not adequate for the study of combustion pressure oscillation.

The study reported herein employs a nonacoustic theory and is concerned with the interaction of a finite amplitude pressure disturbance with the different physico-chemical processes occurring in the combustion region at the surface of a burning solid propellant. The objective of the study is to determine the manner in which the amplitude of the pressure disturbance changes as it propagates through the combustion region normal to the burning surface. It is also hoped that insight into the mechanisms which cause amplification of the disturbance will be gained in the process of making the study.

1.1 Processes in Gaseous, Liquid, and Solid Propellant Rocket Motors

The nature and distribution of the physico-chemical processes occurring in a rocket motor are such that for the purpose of analysis the combustion chamber may be divided into reasonably well-defined regions. The latter are basically the same whether the rocket motor under consideration burns liquid propellant, an end-burning solid propellant grain, premixed gaseous propellant, or an unmixed gaseous propellant. Starting at the fore end of the rocket motor, the following regions can be defined:

(1) a source region,

(2) a combustion region,

(3) a combustion products region, and

(4) a nozzle region.

The combustion region can be further divided into one or more preparation zones and a flame zone, depending on the type of propellant being burned. The source region and the preparation zones will, of course, be markedly different for each type of rocket motor and it is in those portions of the combustion chamber where the greatest differences in the analyses of the different types of rocket motors will appear.

An outline for the aforementioned regions containing a brief description of the processes which occur in each of them will be discussed for rocket motors burning each of the three types of propellant.

1.1.1 Gaseous Propellant Rocket Motor

Source Region. This region is bounded on the fore side by a plane, semi-reflecting, heat-absorbing wall from which issues (at specified locations) gaseous propellant at a prescribed rate.

Combustion Region. This region can be further divided into zones with each zone described as follows:

(1) A mixing zone (absent from motors using mixed gaseous propellant), wherein mixing of the gaseous oxidizer and fuel takes place and a small amount of heating of the gases occurs.

(2) An induction zone, wherein heating of the gaseous propellant occurs which, in turn, causes induction reactions to take place.

(3) A flame zone, wherein the following processes occur: chemical reaction (liberating heat), heat transfer, molecular diffusion between the reactant and the product, and bulk viscosity dissipation.

Combustion Products Region. In this region the gases have a fairly homogeneous composition. A low rate of heat transfer to the walls of the combustion chamber occurs.

Nozzle Region. The gases flow through the nozzle according to some (non-equilibrium) process. Some heat is transferred to the walls of the nozzle.

1.1.2 Liquid Propellant Rocket Motor

Source Region. The region is bounded on the fore side by a reflecting, plane, heat-absorbing wall from which droplets of liquid fuel and oxidizer are emitted at a prescribed rate and according to some given size and geometric distribution.

Combustion Region. This region is further divided into four zones with each zone described as follows:

(1) A droplet breakup zone, wherein the droplets break up (mainly through collision). The zone must be modified if one of the propellants is injected above its critical pressure.

(2) A vaporization and decomposition zone, wherein the fine droplets vaporize and decompose due to heating.

(3) An induction zone, wherein the gases are heated causing induction reactions to occur (the induction zone may contain some droplets in the flowing medium).

(4) A flame zone, wherein the following processes occur: chemical reaction (liberating heat), heat transfer, molecular diffusion between the reactant and combustion product, and bulk viscosity dissipation.

Combustion Products Region. In this region the gases have a fairly homogeneous composition. A low rate of heat transfer to the walls of the combustion chamber occurs.

Nozzle Region. The gases flow through the nozzle according to some (non-equilibrium) process. Some heat is transferred to the walls of the nozzle.

1.1.3 End-Burning Grain Solid Propellant Rocket Motor

Source Region. This region is bounded on the fore end by the reasonably planar surface of the heat-absorbing viscoelastic solid propellant. The surface recedes parallel to itself and may emit solid particles in addition to gases and vapors from its surface.

Combustion Region. This region is further divided into three zones with each of the zones described as follows:

(1) A decomposition zone, wherein the materials evolved from the propellant surface decompose and mix; they may or may not release heat in the process.

(2) An induction zone, wherein heating of the gases causes induction reactions to occur.

(3) A flame zone, wherein the following processes occur: chemical reaction (liberating heat), heat transfer, molecular diffusion between reactant and combustion product, and bulk viscosity dissipation.

Combustion Products Region. In this region the gases have a fairly homogeneous composition. A low rate of heat transfer to the walls of the combustion chamber occurs.

Nozzle Region. The gases flow through the nozzle according to some (non-equilibrium) process. Some heat is transferred to the walls of the nozzle.

The flowing medium in each of the regions of a solid propellant motor will be composed of two phases (gases and solid particles) if the solid propellant contains aluminum in its formulation. In the case of a two-phase flow, there will be heat and momentum transfer between the two phases wherever there are steep gradients in temperature and velocity. The above outline for the combustion mechanism of a solid propellant rocket motor is sufficiently general to include both double base and composite propellants.

1.2 The Propagation of Pressure Disturbances in Combustion Chambers

A finite amplitude pressure disturbance traveling longitudinally in the combustion chamber of a rocket motor will propagate through the different regions described in Section 1.1 and interact with the gradients in flow properties present in those regions. It is readily shown (see Section 2.4) that a simple pressure disturbance will steepen

into a nonuniform normal shock, a normal shock followed by a rarefaction wave, as it propagates in an adiabatic system. It is a more difficult problem, however, to prove rigorously that a simple pressure disturbance when propagating in a nonadiabatic system will steepen; the rate of either the steepening or flattening of the pressure disturbance is a function of the flow property gradients through which the disturbance is propagating. There is, however, experimental evidence (2)(3) that substantiates the assumption that nonuniform shocks may arise from the interaction of finite amplitude pressure disturbances with the processes occurring in a rocket motor combustion chamber. The subject report does not present a theoretical proof for the formation of a nonuniform shock from a finite amplitude pressure disturbance. Instead, the nonuniform shock is assumed to have been formed, and the interest is in whether or not the amplitude of the normal shock will increase, or amplify, as it propagates through the combustion region.

Theoretical investigations have been made for the propagation of a normal shock through a stationary gas wherein there was only one type of gradient--for example, a density gradient (4)(5)(6)(7). Other theoretical investigations have been concerned with the interaction of a normal shock with some type of discontinuity--for example, a wall or a simplified flame front (7)(8)(9)(10)(11). The results of the aforementioned theoretical investigations are not directly applicable to the conditions in a rocket motor combustion chamber because several gradients are present simultaneously and because the gases in the latter case are flowing through the gradients. Also, the investigations do not include

the rarefaction backside of the nonuniform shock. The results obtained from the simpler analyses should indicate, however, what can be expected to occur when a nonuniform shock interacts with the different regions in a combustion chamber. If there is a density gradient in the combustion chamber, one would expect the nonuniform shock to become amplified as it propagates in the direction of increasing density, and vice versa. Furthermore, the effects of molecular diffusion, viscosity, and heat transfer on amplification or attenuation of the shock will depend upon the sign of the second derivative of the pertinent flow property, while the addition of heat by chemical reaction should cause the nonunfiorm shock to become amplified. In addition, the plane surface at the fore end of a source reigon should act to attenuate the nonuniform shock upon reflection from that surface, and the nonuniform shock should experience attenuation again upon reflection from the nozzle end of the motor.

The analysis of the longitudinal propagation of a nonuniform shock in a rocket motor combustion chamber is a problem in one-dimensional unsteady gas dynamics. The conservation equations for that type of problem, if transport processes have been neglected, are a system of hyperbolic partial differential equations. Such a system of equations sometimes can be solved analytically for an approximate solution for the propagation of the nonuniform shock by employing the technique presented in references (6) and (12). The analysis presented herein will give a method for making a numerical solution for the propagation of a pressure disturbance through a region where gradients in the flow

properties occur and transport processes are present. The method involves transforming the unsteady conservation equations in a manner similar to that employed in method of characteristic solutions and then numerically integrating the transformed equations. The partial derivatives that appear in the transformed equations are approximated by employing their steady state values. The method of obtaining the approximate value is outlined in Section 4.2.

1.3 Physical and Transport Property Data

The application of a nonlinear theory to the study of combustion pressure oscillation introduces greater mathematical complexity than the application of an acoustic theory. In addition, there is the problem of obtaining accurate values for the transport and additional physical properties that appear in the nonlinear equations. The following transport properties must be assigned: thermal conductivity, molecular diffusion coefficient, and second coefficient of viscosity (bulk viscosity). Some of the problems which are encountered that make it difficult to obtain accurate values for those properties are due to the following: (1) the diffusion coefficient is quite complex except for a binary mixture; (2) accurate determinations of the second coefficient of viscosity have been made only for monatomic gases; (3) the rules available for determining the thermal conductivity and viscosity of a mixture of gases are, at best, only approximate; and (4) the flow in the combustion region is turbulent and so requires values for all the transport properties which include turbulent effects.

Evaluation of such physical properties as the specific heats, the specific heat ratio, and the heats of reaction is much less difficult than evaluating the above transport properties; accurate data is not generally available, however, for some of the large molecular weight gases found in the combustion region. Furthermore, the assumption of perfect mixing in evaluating the properties of a gas mixture may be open to question.

The physical properties governing the chemical reaction kinetics (steric factor, frequency factor, and activation energy) must also be evaluated; that is a difficult problem in the case of the combustion of solid and liquid propellants due to the great complexity of the pertinent chemical reactions. The best that can be done is to estimate the value of those properties utilizing the available experimental values for less complex reactions as a guide.

All of the above problems are compounded by the fact that most of the physical and transport properties of the flowing medium are rather strong functions of its temperature. Because the temperatures are high (4000^{o} R and above), it is difficult to obtain accurate values for most of the transport and physical properties. For that reason, the values of the physical and transport properties presented in Appendix B of the subject report should be considered as order of magnitude estimates only of those properties in the combustion region at the surface of a burning solid propellant composed of 80 per cent ammonium perchlorate and 20 per cent polybutadiene-acrylic acid.

1.4 Outline of the Report

The subject report presents the method employed and the results obtained from an investigation of high frequency combustion pressure oscillation employing a nonlinear method of analysis. The interaction of a pressure disturbance, a nonuniform shock, with the combustion region at the surface of an end-burning solid propellant grain is calculated. A description of the models employed for the combustion region and the pressure disturbance is given in Section 2. The mathematics required for solving the interaction is given in Section 3, and the procedure employed to make the numerical solution is contained in Section 4. Section 5 contains the results of investigation as well as related experimental data collected from the literature. A discussion of the results and their comparison with experimental data is contained in Section 6. Suggestions for possible extension of the present program and investigations in related areas are presented in Section 7. Appendix A presents the derivation of the conservation equations for a one-dimensional, two-component, unsteady flow in the presence of heat transfer, molecular diffusion, chemical reaction, and bulk viscosity. Appendix B contains the transport and physical properties employed in the calculations and the assumed process equations. The steady state combustion region profile is also given in that appendix. The information is based on the assumption that the burning propellant is composed of 80 per cent ammonium perchlorate (AP) and 20 per cent polybutadine-acrylic acid (PBAA) by weight. Appendix C contains the characteristic directions and compatibility equations derived from the

conservation equations of Appendix A. Appendix D contains a complete set of the numerical solutions obtained. Appendix E contains experimental data obtained from Rocketdyne by private communication.

2.0 MODEL FOR THE THEORETICAL ANALYSIS

The first step in the theoretical analysis of a problem is to postulate a physical model. Figure 1 is a simple sketch of a rocket motor equipped with a solid propellant end-burning grain. The theoretical analysis requires the calculation of the interaction of a pressure disturbance, assumed to be present in the combustion products region, with the combustion region. That requires the calculation of the propagation of the disturbance from the products region through the combustion region, reflection from the propellant, and propagation back through the combustion region. Therefore, models for the combustion products region, combustion region, propellant, and pressure disturbance have to be postulated.

2.1 Combustion Products Region

The entire region occupied by the products of combustion is assumed to have homogeneous, gradient-free properties under steady state conditions. It is assumed that the pressure disturbance propagates through the combustion products region adiabatically and that the unsteady effects due to the passage of the pressure disturbance do not affect the chemical composition of the gas. Furthermore, the combustion gas is assumed to be an ideal gas mixture obeying the perfect gas law.

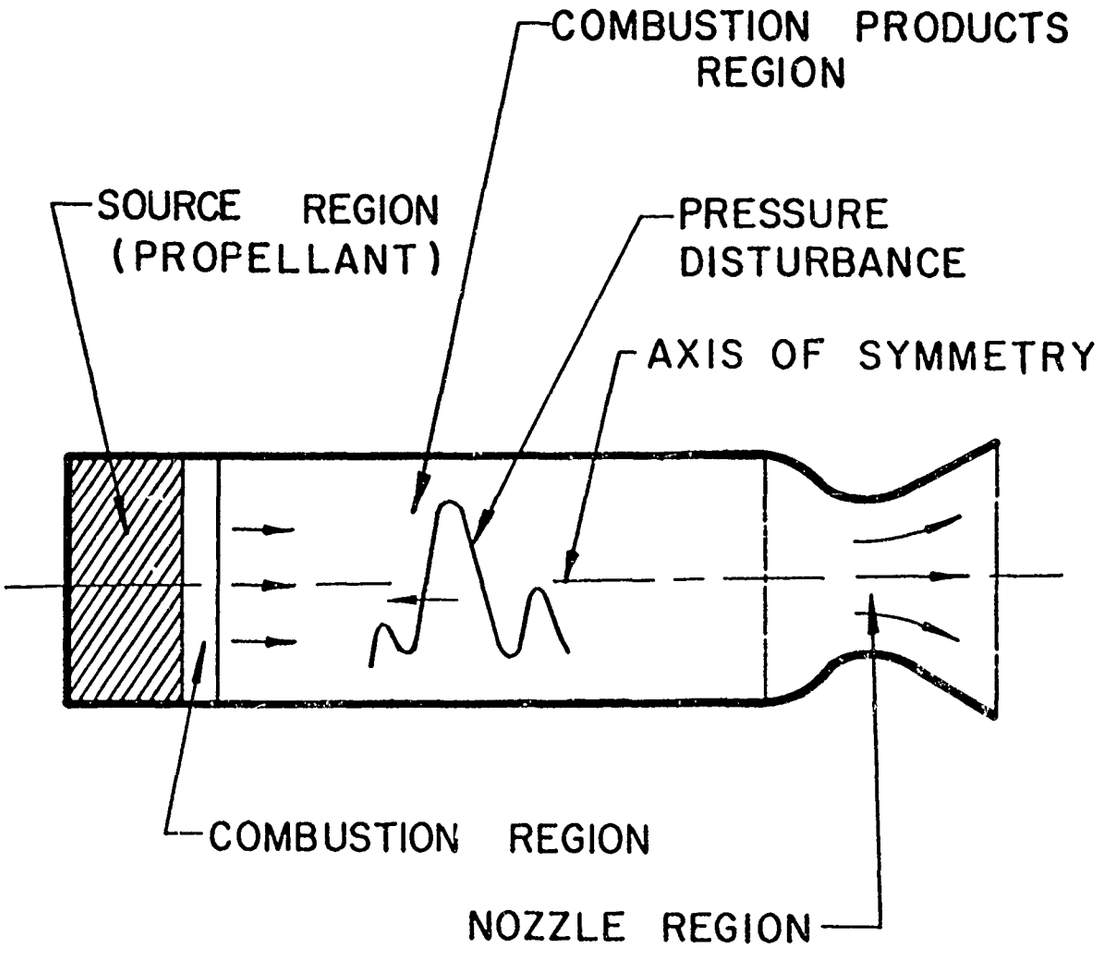

Figure 1 Sketch of a Rocket Motor Equipped with a Solid Propellant End-Burning Grain

2.2 Combustion Region

The combustion region model is by far the hardest to postulate. The model should approximate the actual processes occurring in the combustion region; however, the formulation must be simple enough so that a solution is tenable and can be obtained without an undue loss of mathematical rigor.

Figure 2 shows the scheme suggested in Reference (13) for dividing into zones the combustion region at the surface of a burning composite solid propellant; approximate values for the temperatures and zone widths have also been included. A brief description of each zone taken from the aforementioned reference is as follows:

(1) The unheated propellant--the portion of the propellant which has not yet been affected by the heat transfer.

(2) The heated propellant--the portion of the propellant which has been appreciably heated and in which a temperature gradient exists.

(3) The reacting and phase-change zone--the zone in which phase changes occur with some reaction in the liquid phase and some gasification.

(4) The decomposition zone--the zone in which decomposition reactions occur (can be exothermic in character--depends upon the propellant formulation).

(5) The mixing and induction zone--the zone in which the fuel and the oxidizer mix and some chemical induction reactions occur.

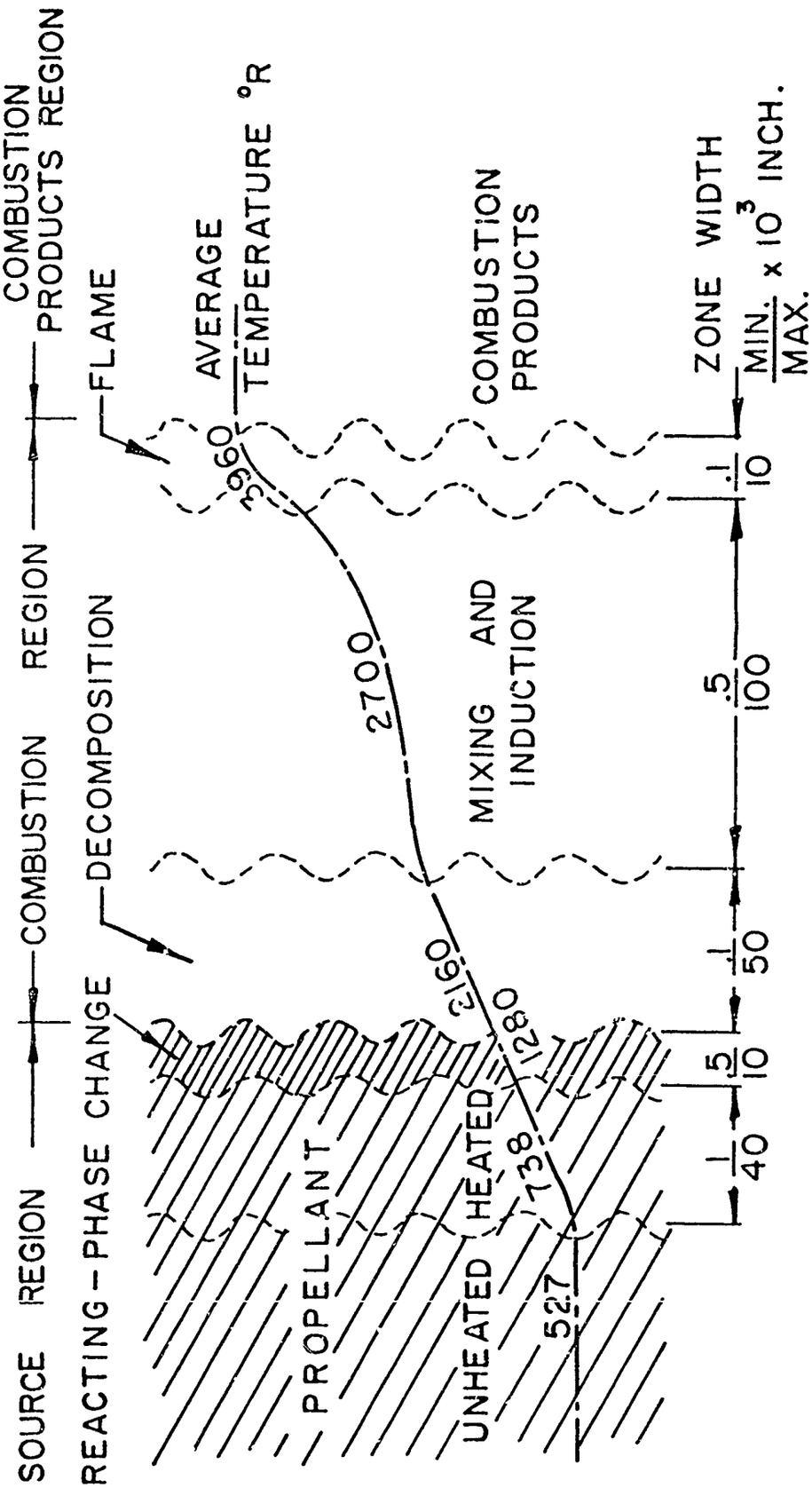

Figure 2 The Combustion Region at the Surface of a Burning Composite Solid Propellant (13)

(6) The flame zone--the zone wherein rapid exothermic chemical reaction takes place.

(7) The combustion products region--the region occupied by the gaseous mixture comprising the products of combustion.

Based upon the information given in Fig. 2, a model for the analysis reported herein was selected and is presented in Fig. 3. The reacting and phase-change zone was omitted because for the propellant employed in the analysis it is probably small or even absent. The oxidizer in the solid propellant changes directly from the solid to the gas phase (14). Although there are actually no distinct lines of demarcation for the different zones, the overall combustion region had to be divided into sharply-defined zones for the purpose of analysis; each zone is determined by the predominant process occurring in that portion of the combustion region. In the analysis there is no distinction made between heated and unheated propellant; the mechanical properties of the propellant are assumed to be unaffected by the heating process.

As can be seen in Fig. 3, the model is composed of a single pressure disturbance in the combustion products region, which will be discussed later in the section; a combustion region divided into a flame zone, induction zone, and decomposition zone; and a solid propellant. The pressure disturbance is assumed to propagate longitudinally upstream with respect to the flow of gaseous products of combustion. Wall effects are assumed to be negligible both with respect to their effect upon the flow and upon the propagation of the disturbance. The analysis is based on the assumption that the flow through the different zones, which are

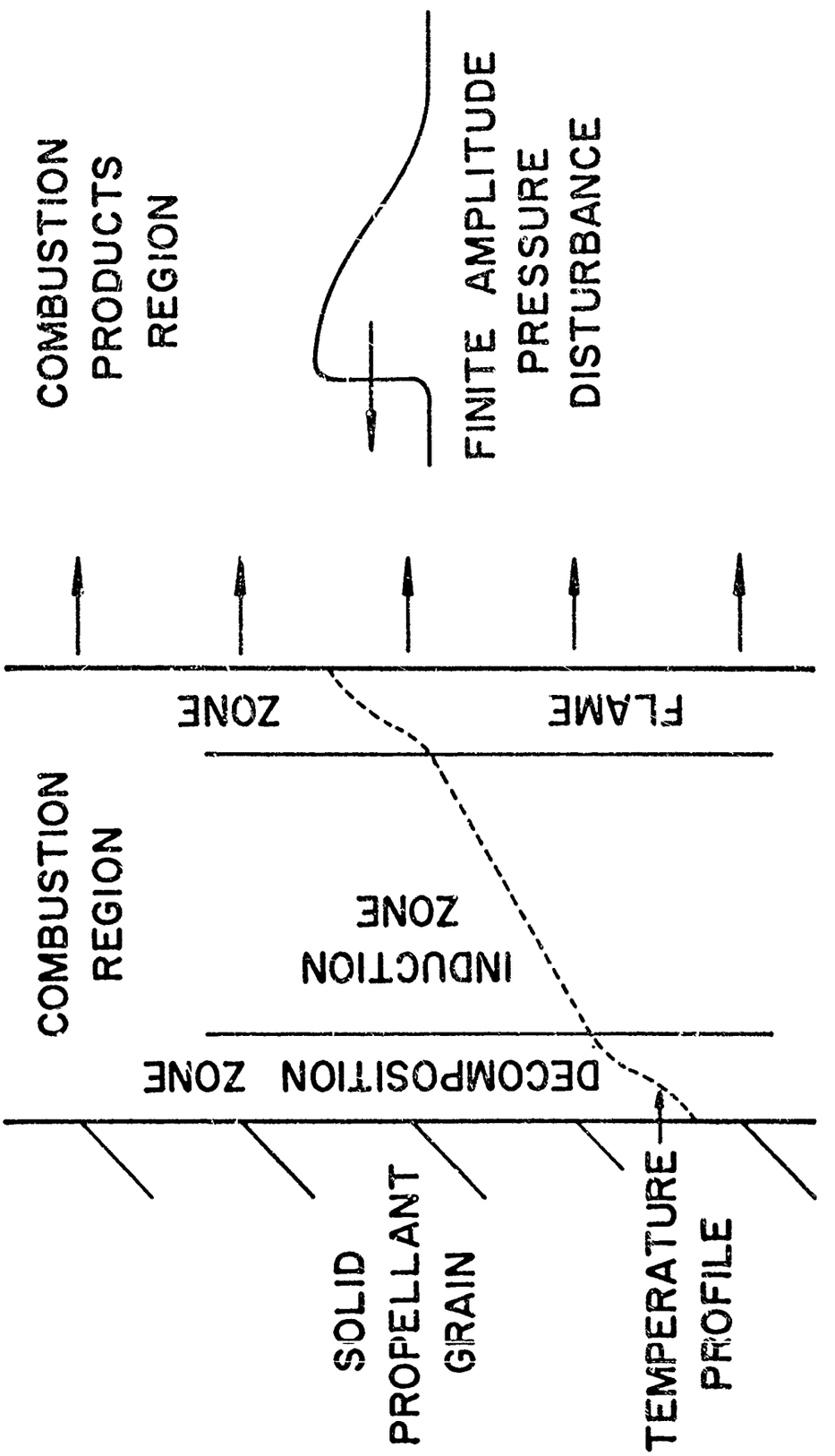

Figure 3 Model of the Combustion Region for the Analysis

separated by parallel planes normal to the axis of the motor, is a one-dimensional flow. Furthermore, the flow is assumed to remain one dimensional during and after the interaction of the pressure disturbance with the combustion region. A detailed description of each zone of the combustion region is given below.

The decomposition zone is located adjacent to the propellant and is considered to be that portion of the combustion region wherein the molecules of the vapors and gases evolved at the propellant surface decompose into lighter molecules; the decomposition process is assumed to be a one-step, exothermic chemical reaction. The temperature rise through the decomposition zone will not, however, be as large as that through the flame zone. The following effects are included in the model for the decomposition zone: (1) heat transfer, (2) change in molecular weight, and (3) change in specific heat. The heat transfer coefficient is assumed to be a function of temperature, but that effect is taken into account only to the extent that the coefficient is evaluated at the local gas temperature when a solution is being made. The medium in the decomposition zone is assumed to be a homogeneous gas that obeys the perfect gas law.

The gases leaving the decomposition zone flow into the induction zone. The induction zone is basically a zone which receives considerable heat from the flame zone. A small amount of exothermic chemical reaction is, however, assumed to occur in the induction zone. The energy added by the aforementioned chemical reaction is assumed to account for approximately three per cent of the enthalpy of combustion. It is further

assumed that the rate of energy release in the induction zone increases linearly with the distance from the burning surface of the propellant (i.e., the rate of energy release due to the chemical reaction is approximately a linear function of time). The only transport process assumed to be present in the induction zone is heat transfer. As in the decomposition zone, the heat transfer coefficient is assumed to be a function of temperature; but that effect is taken into account only to the extent that the coefficient is evaluated at the local flow temperature when a solution is being made. The medium in the induction zone is assumed to have uniform physical properties throughout and to obey the perfect gas law.

The last zone of the combustion region is the flame zone. The flame zone is characterized by a one-step chemical reaction that converts a gaseous "reactant" into a gaseous "product." The following transport processes are assumed to be present in the flame zone: (1) heat transfer due to the temperature gradient, (2) molecular diffusion between the product and reactant, and (3) viscous effects due to the rapid volume change (i.e., effects produced by the second coefficient of viscosity). The transport properties are assumed to be functions of temperature, but again that effect is taken into account only to the extent that the coefficient is evaluated at the local flow temperature when a solution is being made. It is assumed that the physical and transport properties are not materially changed by the chemical reaction that is taking place in the zone. The gas mixture in the flame zone is assumed to obey the perfect gas law.

The process equations defining the transport and chemical processes occurring in each zone are given in Appendix B. Calculated numerical values for all of the physical and transport properties, based on the assumption that the medium in each zone of the combustion region is an ideal gas mixture, are also given in that appendix.

2.3 Solid Propellant

The solid propellant is treated as an elastic solid of semi-infinite extent. A major portion of the energy of the pressure disturbance traveling toward the burning surface (see Fig. 3) is reflected from the surface; however, a small portion of the energy is transmitted into the propellant in the form of a pressure pulse. Since the propellant is assumed to be semi-infinite, the transmitted pressure pulse continues to propagate in through the slab of propellant and will not reflect back and reenter the combustion region. The propellant is assumed to decompose at its surface directly from the solid to the gaseous phase; as a result of that decomposition process, the burning surface recedes (parallel to itself) at a rate which is a function of the pressure acting on the propellant surface. The propellant is assumed to be homogeneous in composition, and its physical properties are assumed to be unaffected by the heating process at its surface.

2.4 Pressure Disturbance

Analytical (15) as well as experimental (3) information reveal that the front of a finite amplitude pressure disturbance can steepen into

a shock front if the pulse is traveling through an appropriate gas medium. Figure 4 illustrates schematically how the steepening of the front of a simple pressure disturbance occurs for adiabatic propagation in a homogeneous gas. The steepening phenomenon arises because each point of the disturbance travels at its own local acoustic speed. At a given time τ_0, the front of a pressure pulse of length Δx is located at the position shown in the figure. The variation in pressure over the length of the pulse is superimposed on the τx plane. Since the gas surrounding point b is at a higher pressure than point c, it will have a correspondingly higher temperature; and, therefore, the portion of the disturbance at point b will propagate with a higher velocity than the portion at point c. At some time τ_1, because the gases behind point c have monatonically increasing propagation velocity, the profile at the front of the disturbance will have steepened from the profile at τ_0. Finally, at some time τ_2 the disturbance which started at point b will have caught up with the front of the disturbance that started at point c and the disturbance will then have deformed into a nonuniform shock. Even if the pressure disturbance is not as simple as that pictured in Fig. 4, the portions of the disturbance with higher local acoustic velocity will catch up with those portions of lower velocity and the net result will be the same as that pictured in Fig. 4. The deformation process of the disturbance will, however, be more complicated than that shown in Fig. 4.

Because of the aforementioned phenomenon, it is assumed in the subject report that the pressure disturbance which propagates through

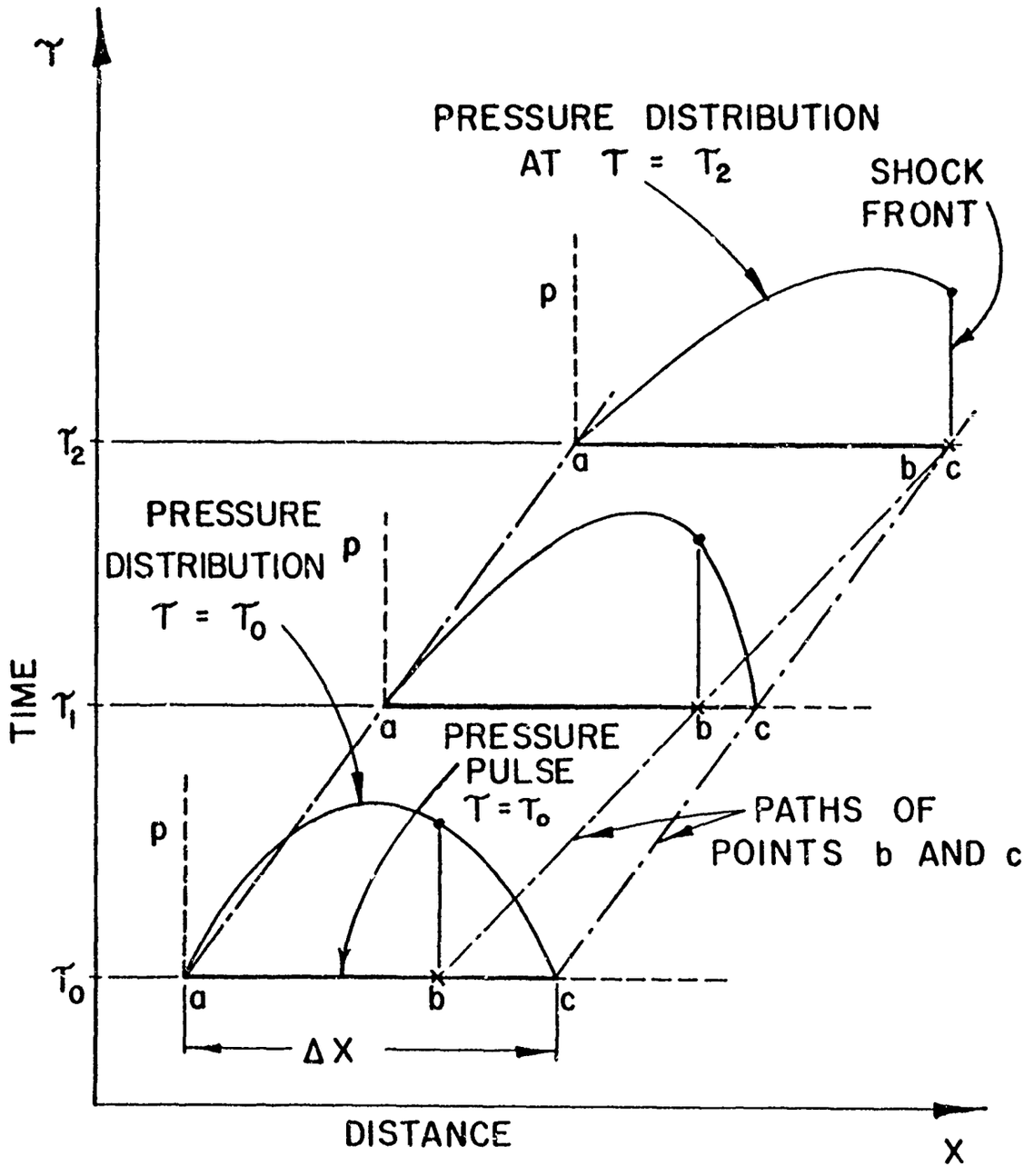

Figure 4 The Steepening of the Front of a Simple Pressure Disturbance during Adiabatic Propagation

the combustion region is a nonuniform shock and that its propagation can be treated as that of a weak normal shock. The effect of the rarefaction backside of the nonuniform shock on its shock front is neglected. The effect of the rarefaction backside is assumed to be that of returning the combustion region to its previous steady state condition after passage of the shock front and the calculations for the presence of the rarefaction wave are not performed. The assumption that the pressure disturbance is a nonuniform shock greatly decreases the amount of work required to obtain a numerical solution.

3.0 ANALYSIS

Two effects that are interdependent occur simultaneously as the nonuniform shock, treated as a normal shock for calculation purposes, propagates through the combustion region where gradients in the flow properties and chemical reactions are present. (1) The amplitude of the nonuniform shock becomes modified as it travels through the region. (2) Waves are shed from the back of the nonuniform shock which cause the region immediately behind the pulse to become unsteady. Figure 5 illustrates qualitatively the above phenomenon on a time-distance diagram. The lower portion of the diagram represents the combustion region before the passage of the shock. The region is under steady state conditions and the processes occurring therein are functions only of distance. This condition is illustrated in the figure by the double lines marking the boundary between zones A-A', B-B', and C-C' which are vertical and, therefore, independent of time. At some given time a nonuniform shock is assumed to appear at the right in the combustion products region and to propagate to the left through the flame, induction, and decomposition zones. While the shock propagates through the uniform, gradient-free, combustion products region, the flow behind the shock is also uniform and gradient free and the amplitude of the shock does not change. However, as the shock propagates through the flame zone, and later the induction and decomposition zones where there are gradients and chemical

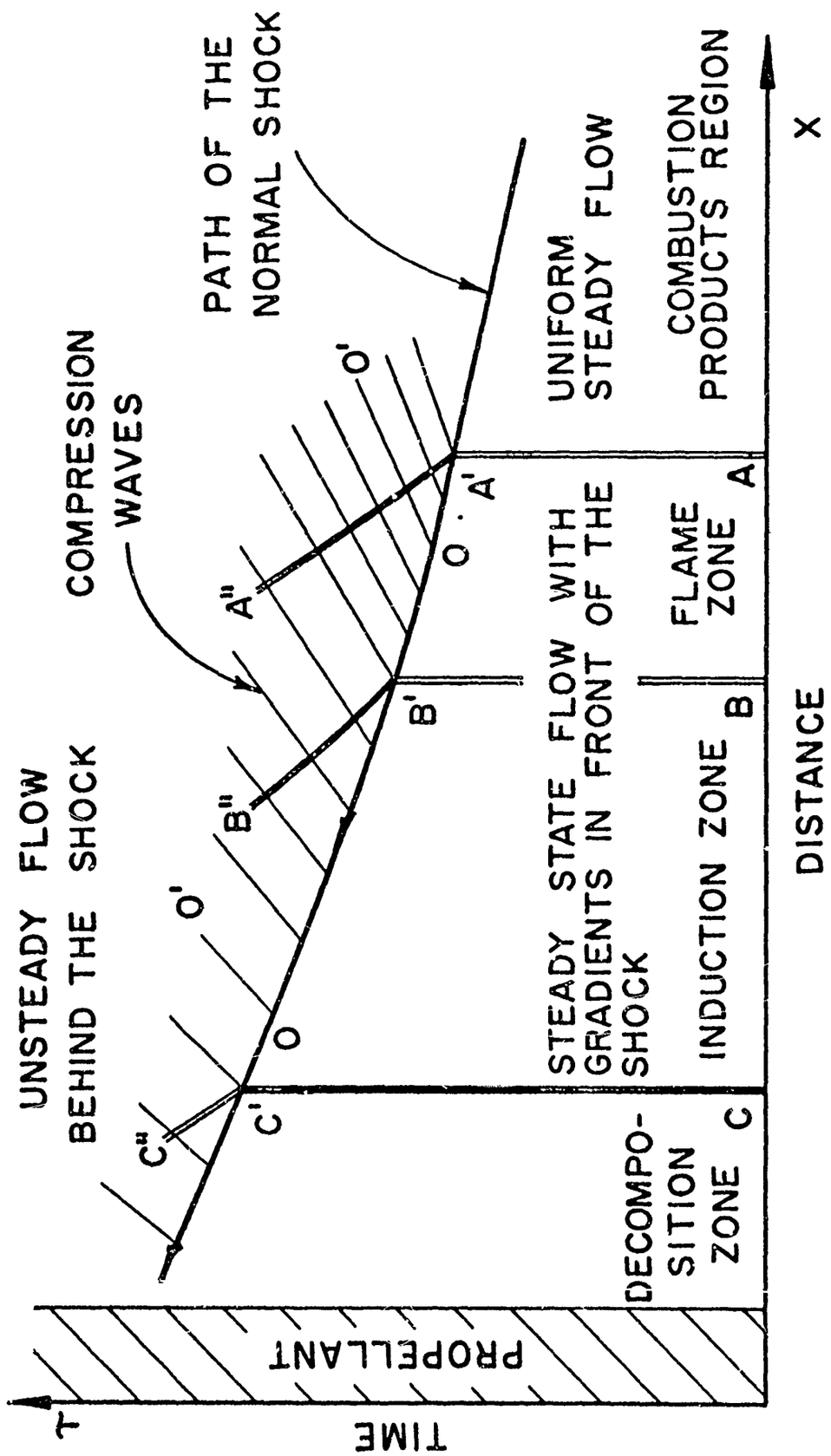

Figure 5 The Propagation of the Nonuniform Shock through the Postulated Combustion Region

processes occurring, the amplitude of the shock changes and the flow behind the shock becomes unsteady. The unsteady nature of the flow behind the shock is indicated in Fig. 5 by the lines slanting to the right which indicate waves shed from the back of the shock; two of the lines are marked 0-0'. The gas flow through the zones is to the right into the combustion products region before passage of the shock. The shock propagating toward the left causes the flow velocity behind it to be decreased; or if the shock is strong enough, the flow velocity is reversed and to the left. The effect of the passage of the shock on the zone boundaries is to make them functions of time; the boundaries between the zones A'-A", B'-B", and C'-C" move to the left after passage of the shock.

When the shock reaches the propellant surface, it is reflected as another normal shock. The reflection of the shock from the propellant surface is covered in detail in Section 3.3. The rarefaction backside of the nonuniform shock is assumed to have returned the combustion region to steady state conditions before the reflected shock front propagates back through it; therefore, the propagation of the shock back through the combustion region will be similar to that presented for the forward passage of the shock.

3.1 Mathematical Description

A solution for the change in amplitude of the normal shock front of the nonuniform shock as it propagates through the combustion region requires a solution of the unsteady flow field immediately behind the shock, the upper portion of Fig. 5. Before a solution to the unsteady

flow field behind the normal shock can be obtained, boundary conditions must be given along the distance and time axes. The boundary condition along the distance axis is the steady state solution for the flow properties in the combustion region. The steady state solution is not, however, matched directly to the unsteady solution; it must be matched across the normal shock. In the process of matching the two solutions together across the shock, the amplitude for the shock required to make the two solutions fit continuously along the shock's path is determined. Because of the nature of the problem, the boundary condition along the time axis requires only that the strength of the shock as it enters the combustion region and the steady state values for the flow properties in the combustion products region be given.

The initial portion of the net employed to calculate the interaction of the normal shock with the combustion region is plotted in Fig. 6. Figure 6 is a "blowup" of the area around point A' in Fig. 5. As noted in the previous section, the shock travels from right to left and enters the flame zone at point A'. Prior to entering the flame zone the shock is traveling in the gradient-free combustion products region so the amplitude of the shock remains constant and the flow behind the shock, region B, remains gradient free. As the shock enters the flame zone where gradients in the flow properties and chemical reactions are present, the amplitude of the shock changes and waves are shed from the back of the shock. Line A'-E is the path of the very first wave shed from the back of the shock. The line A'-E is a characteristic line with a slope $dt/dx=1/(u+a)$ and marks the division between

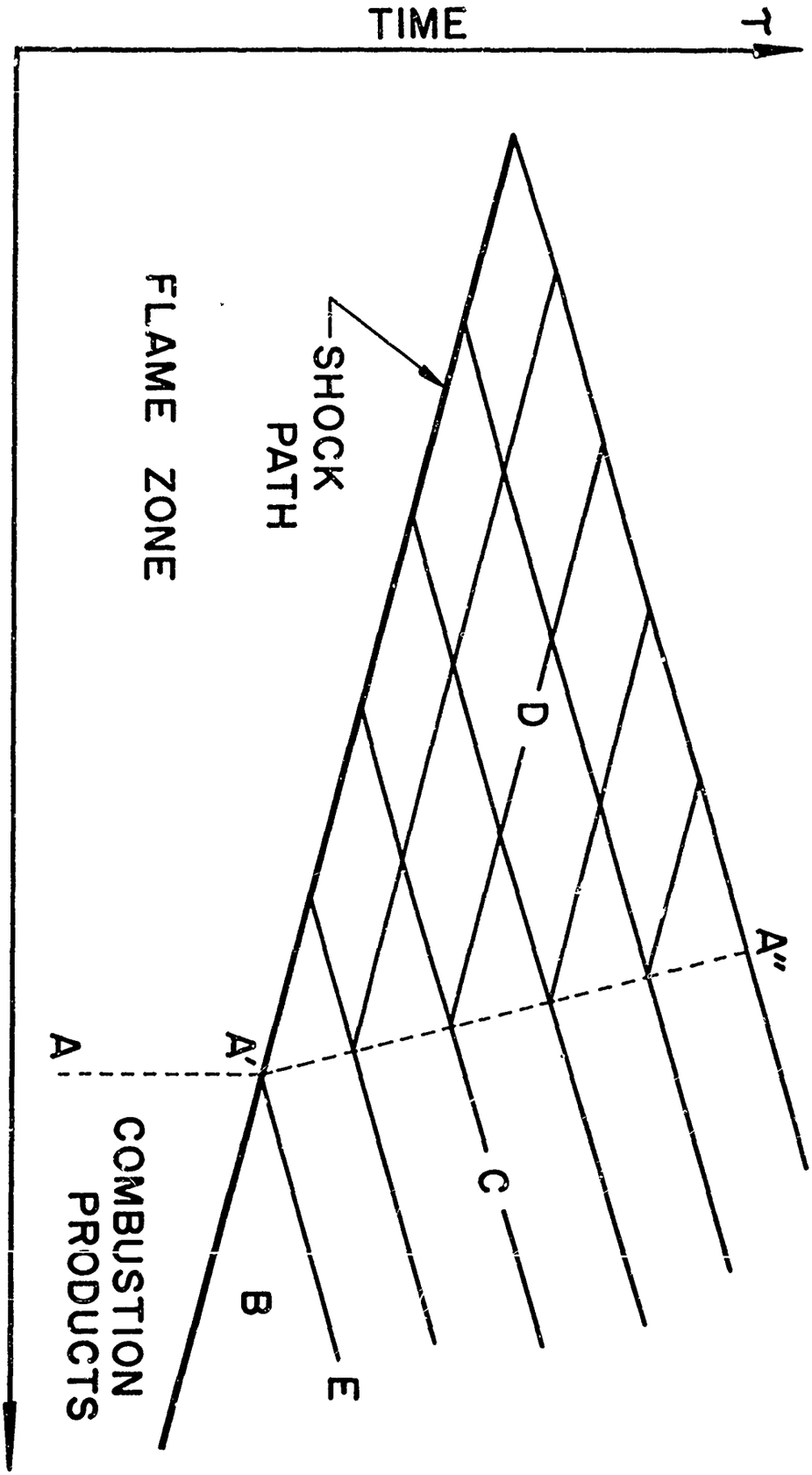

Figure 6 Initial Portion of the Net for the Interaction Calculation

the steady flow region behind the shock, region B, and the unsteady flow region, region C. It can be shown (11) that a region bordering on a gradient-free region, simple region, can have waves propagating in only one direction, waves of only one family present; and the boundary between the two regions is a characteristic curve. Therefore, since region C borders on a gradient-free region, the region must contain only waves of one family. It can be shown further (11) that where only one family of waves are present, as in region C, the flow properties along the characteristic curves in the direction of wave propagation are constant. The characteristic curves are actually the paths along which the waves propagate.

The path line characteristic curve A'-A" with slope dt/dx=1/u separates the region C, where one family of waves are present, from region D, where both families of waves are present. As the shock propagates deeper into the flame zone, the waves shed from the back of the shock and traveling to the right interact with the gradients and chemical processes present in the flow and are altered in shape and amplitude and cause other waves to arise that travel to the left. The new waves traveling to the left are altered and cause still another set of waves to be formed which travel to the right. The aforementioned process continues until a very complex wave flow is present in region D. The net effect of all of the wave interactions can be determined numerically by solving the unsteady conservation equations applicable to the flame zone. The complexity of the numerical solution is reduced if the conservation equations are first transformed into a system of

compatibility equations satisfied along characteristic curves. Also the physics of the problem is more easily satisfied if the equations are in characteristic form.

3.2 Characteristic Equations and Compatibility Equations

The complex nature of the problem being studied prevents obtaining any other than numerical solutions. As outlined in the previous section, the calculation of the change in amplitude of the normal shock as it propagates through the combustion region requires that a solution be made for the unsteady flow region just in back of the shock. That means the unsteady conservation equations with appropriate boundary conditions must be solved. The task of making the numerical solution is reduced if the equations are first transformed into a set of compatibility equations, total differential equations, satisfied along characteristic curves. The equations cannot be transformed completely in a rigorous mathematical sense because of the second derivatives with respect to distance and squares of derivatives appearing in the transport process terms. However,if those derivatives can be approximated in some fashion the transformed equations can be solved as a regular set of total differential equations.

The model for the combustion region through which the normal shock propagates has been given in detail in Section 2.2. The processes that will be occurring in the different zones of the combustion region are heat transfer, molecular diffusion, bulk viscosity effects, and chemical

heat release; and the physical and transport properties may be a function of the composition of the medium. The unsteady conservation equations for a system in which all of the above processes are occurring are derived in Appendix A and the results are presented below.

conservation of mass

specie 1

$$\frac{\partial Y}{\partial \tau} + u \frac{\partial Y}{\partial x} = - \alpha \; Y \, e^{-E/R_o T} + \frac{D}{\rho} \frac{\partial}{\partial x} \left(\rho \frac{\partial Y}{\partial x}\right) \qquad (1)$$

mixture

$$\rho \frac{\partial u}{\partial x} + \frac{\partial \rho}{\partial \tau} + u \frac{\partial \rho}{\partial x} = 0 \qquad (2)$$

where

ρ = density,

u = velocity,

τ = time,

x = distance measured along the longitudinal axis of the combustion chamber,

Y = ρ_1/ρ concentration of species 1 (reactant),

α = combination frequency and steric factor,

E = activation energy,

R_o = universal gas constant, and

D = diffusing coefficient.

conservation of momentum

$$\rho R \frac{\partial T}{\partial x} + \rho \frac{\partial u}{\partial \tau} + \rho u \frac{\partial u}{\partial x} + RT \frac{\partial \rho}{\partial x} = - \rho T \frac{\partial R}{\partial x} + \eta \frac{\partial^2 u}{\partial x^2} \tag{3}$$

where

R = gas constant,

T = static temperature, and

η = second coefficient of viscosity.

conservation of energy

$$\rho c_v \frac{\partial T}{\partial \tau} + \rho u c_v \frac{\partial T}{\partial x} + \rho RT \frac{\partial u}{\partial x} = \alpha U \rho Y e^{-E/R_o T} + \eta \left(\frac{\partial u}{\partial x}\right)^2 + k \frac{\partial^2 T}{\partial x^2} + D\eta \frac{\partial}{\partial x} \left[\left(\frac{1}{1-Y} - \frac{1}{Y}\right) \frac{\partial Y}{\partial x} \frac{\partial u}{\partial x}\right] \tag{4}$$

where

c_v = specific heat at constant volume,

U = heat of reaction, and

k = heat transfer coefficient.

Equation 1 for the conservation of species 1 (reactant) is in a form such that its characteristic direction and compatibility equation can be obtained by inspection. The characteristic directions and compatibility equations for the other three conservation equations are obtained in Appendix C and all four compatibility equations are presented below.

As previously noted, the second derivative with respect to distance and squares of derivatives are assumed to be known functions and will be evaluated in some other way.

(1) For the characteristic direction $d\tau/dx = 1/(u+a)$

$$\frac{\delta+p}{\delta\tau} + a\rho \frac{\delta+u}{\delta\tau} = \rho T \frac{DR}{D\tau} + a\eta \frac{\partial^2 u}{\partial x^2} + (\gamma-1) \{\alpha \rho Y U e^{-E/R_o T} + \eta \left(\frac{\partial u}{\partial x}\right)^2 + k \frac{\partial^2 T}{\partial x^2} + D \frac{\partial}{\partial x} \left[\left(-\frac{\eta_1}{Y} + \frac{\eta_2}{1-Y}\right) \frac{\partial Y}{\partial x} \frac{\partial u}{\partial x}\right]\} \tag{5}$$

(2) For the characteristic direction $d\tau/dx = 1/(u-a)$

$$\frac{\delta-p}{\delta\tau} - \rho a \frac{\delta-u}{\delta\tau} = \rho T \frac{DR}{D\tau} - a\eta \frac{\partial^2 u}{\partial x^2} + (\gamma-1) \{\alpha \rho Y U e^{-E/R_o T} + k \frac{\partial^2 T}{\partial x^2} + D \frac{\partial}{\partial x} \left[\left(-\frac{\eta_1}{Y} + \frac{\eta_2}{1-Y}\right) \frac{\partial Y}{\partial x} \frac{\partial u}{\partial x}\right]\} \tag{6}$$

and

(3) and (4) For the characteristic direction $d\tau/dx = 1/u$

$$\rho c_v \frac{DT}{D\tau} - RT \frac{D\rho}{D\tau} = \alpha \rho Y U e^{-E/R_o T} + \eta \left(\frac{\partial u}{\partial x}\right)^2 + k \frac{\partial^2 T}{\partial x^2} + D \frac{\partial}{\partial x} \left[\left(-\frac{\eta_1}{Y} + \frac{\eta_2}{1-Y}\right) \frac{\partial Y}{\partial x} \frac{\partial u}{\partial x}\right] \tag{7}$$

$$\frac{DY}{D\tau} = \frac{D}{\rho} \frac{\partial}{\partial x} \left(\rho \frac{\partial Y}{\partial x}\right) - \alpha Y e^{-E/R_o T} \tag{8}$$

where the following operators are defined

$$\frac{\delta_+}{\delta t} \equiv \frac{\partial}{\partial t} + (u+a)\frac{\partial}{\partial x}$$

$$\frac{\delta_-}{\delta t} = \frac{\partial}{\partial t} + (u-a)\frac{\partial}{\partial x}$$

$$\frac{D}{Dt} = \frac{\partial}{\partial t} + u\frac{\partial}{\partial x}$$

The four compatibility equations are in a general form applicable to any of the three zones of the combustion region. As the equations are applied to each zone of the combustion region those phenomena which are considered to be higher order effects in that zone can be dropped from the equations. The aforementioned compatibility equations with an equation of state are sufficient to solve the unsteady flow field behind the shock when given a set of boundary and initial conditions. The necessary equation of state is

$$p = \rho R_o T \left(\frac{\gamma (M_2 - M_1) + M_1}{M_1 M_2}\right) \tag{9}$$

where M_1 and M_2 are the molecular weights of the two gas species.

3.3 Reflection of the Nonuniform Shock from the Propellant Surface

The reflection of the nonuniform shock from the burning propellant surface of a solid propellant is considered in this section. All motion

is assumed to be longitudinal; that is, perpendicular to the propellant surface. When the nonuniform shock strikes the burning surface, a portion of its energy is transmitted through the surface into the solid propellant; the remainder of the energy is reflected from the surface. The object of this section is to derive the equations for determining the amplitude of the reflected pressure disturbance. The transmitted and reflected pressure disturbances are assumed to be normal shocks.

Figure 7 presents the τx-diagram for the interaction of a normal shock with the burning surface of a solid propellant of semi-infinite extent. The steps which occur in the interaction are as follows:

(1) An incident normal shock of some given strength travels to the left through flow field 1 and strikes the propellant surface.

(2) A portion of the energy of the incident shock is transmitted through the burning surface and propagates into the solid propellant as a normal shock. The shock compresses the propellant as it propagates which causes the propellant behind the shock to have a small velocity in the direction of propagation.

(3) The remaining portion of the energy of the incident shock is reflected back from the burning surface as another normal shock.

(4) A contact discontinuity (a surface across which the flow properties of pressure and velocity are continuous but the

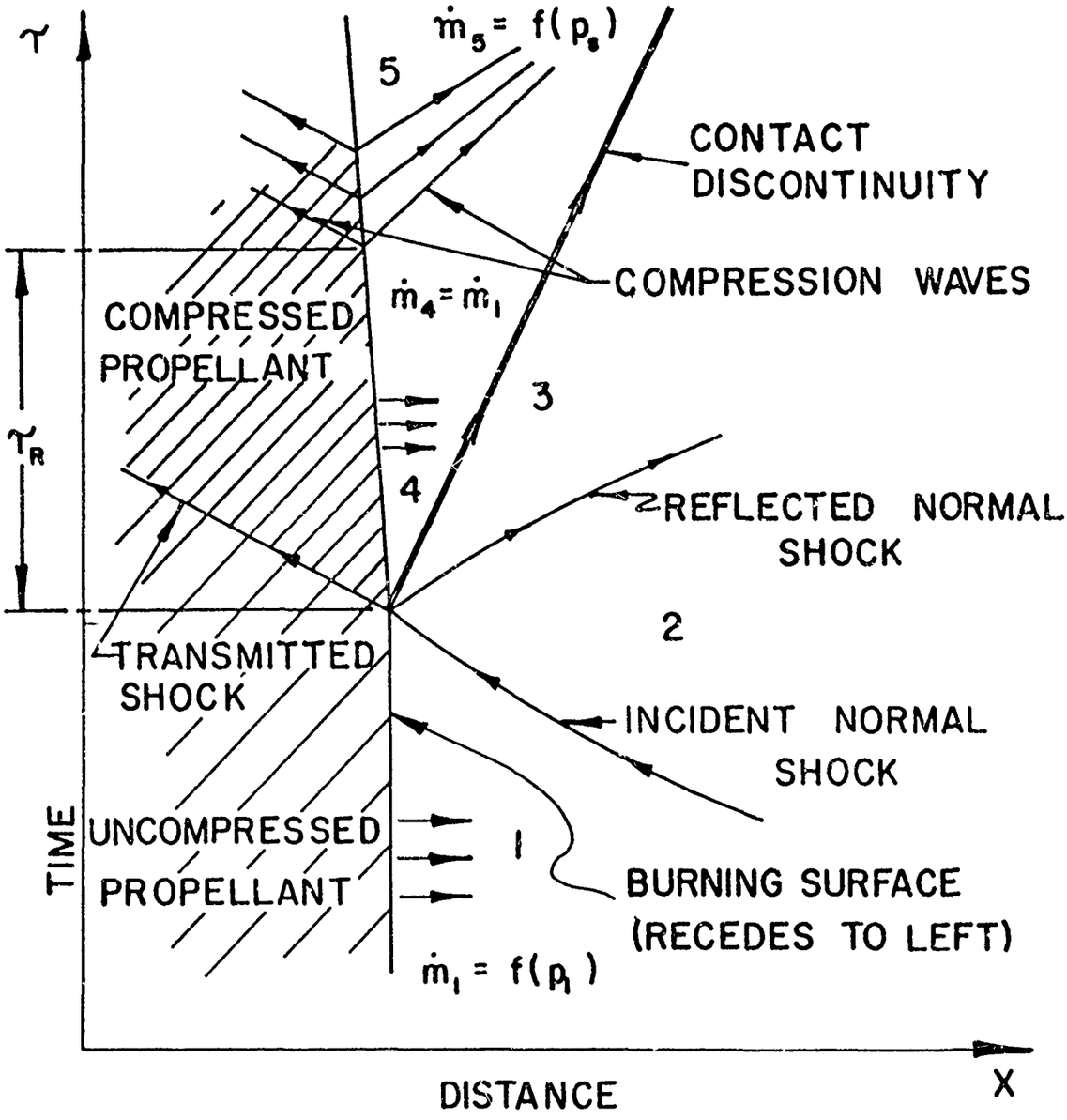

Figure 7 The Reflection of the Nonuniform Shock from the Surface of the Postulated Propellant

density is discontinuous) appears in the flow field simultaneously with the transmission and reflection of the incident shock. The discontinuity separates the flow field behind the reflected shock into two parts: (a) gases which were released from the uncompressed propellant burning surface and then were compressed by the incident and reflected shocks (flow field 3), and (b) gases that were released from the compressed propellant surface (flow field 4).

(5) The propellant starts burning at an increased rate after some relaxation time τ_R has elapsed due to the pressure increase at the propellant burning surface. The increased burning rate further raises the pressure at the propellant surface and produces compression waves which propagate into the compressed propellant and into flow field 4. The burning rate continues to increase until a new equilibrium rate is reached (flow field 5).

The limiting cases for the relaxation times (namely, zero and infinite) are readily calculated. If the relaxation time is infinite, the compression waves and flow field 5 do not appear in Fig. 7, because the burning rate does not increase after the shock wave interacts with the burning surface. If the relaxation time is zero, the compression waves in Fig. 7 are integral with the transmitted and reflected shocks, and the flow field 4 does not appear in the interaction. The relaxation processes at the burning surface of the propellant must be defined if an intermediate case is to be solved.

3.3.1 Derivation of the Mathematical Equations

The problem is to determine the strength of the reflected shock when given the following information: (1) the strength of the incident shock immediately before contact with the propellant surface, (2) the flow properties of the gas between the incident shock and the propellant surface (flow field 1), (3) the resulting burning rate of the propellant as a function of surface pressure and the modulus of elasticity of the semi-infinite propellant, and (4) the assumption that zero relaxation time is required for adjustment of the burning rate to the new pressure at the surface of the propellant; in that case flow field 4 and the compression waves are omitted from the Fig. 7. In this section, the numerical subscript attached to each flow variable denotes the flow region to which the variable applies (see Fig. 7); subscript 4 will not appear because it is assumed hereafter that $\tau_R = 0$.

The procedure for obtaining the equations for determining the strength of the reflected shock is as follows (refer to Fig. 7): (1) equations are written for the flow velocity in flow fields 5 and 1, (2) the normal shock relations are employed for calculating the flow properties in flow fields 2 and 3 in terms of properties in flow field 1 and the pressure ratios across the incident and reflected shocks, and (3) the static pressure and velocity in flow field 5 are equated to the respective flow properties in flow field 3 in front of the contact discontinuity. The strength of the reflected shock is determined by the change in the flow properties across the shock that is required to match pressure and velocity across the contact discontinuity.

The equation for the velocity of the gas in flow field 5 is obtained from the relative velocity of the gas leaving the propellant surface; the relative velocity is converted to absolute velocity by subtracting the velocity at which the burning surface recedes parallel to itself. The propellant surface recedes to the left because of two effects: (1) removal of material by combustion and (2) compression of the propellant by the transmitted shock. The latter effect on the velocity of the propellant surface will be determined first.

The velocity of the burning surface due to compression of the propellant by the transmitted shock is given by the equation (16)

$$u_p = a_p \Delta\varepsilon \tag{10}$$

where

a_p = the velocity of propagation of the shock in the solid propellant and

$\Delta\varepsilon$ = the strain, the amount the propellant is compressed per unit length by a pressure increase equal to the pressure rise at the surface of the propellant.

The velocity of propagation of the normal shock through the solid propellant is given by (16)

$$a_p = (S/\rho_p)^{\frac{1}{2}} \tag{11}$$

where

ρ_p = the density of the propellant and

S = the slope of the stress-strain curve for the propellant at the level of stress (pressure) present in the propagating wave.

The strain in the propellant $\Delta\epsilon$ due to increasing the stress from p_1 to p is given by

$$\Delta\epsilon = \int_{p_1}^{p} \frac{dp}{S} \tag{12}$$

If the portion of the stress-strain curve for the propellant between pressures p_1 and p is replaced by a straight line of slope $\overline{S}$ then

$$\Delta\epsilon = \frac{p - p_1}{\overline{S}} \tag{13}$$

Substituting equations 11 and 13 into equation 10, yields

$$u_p = (p - p_1) \left(\frac{1}{\overline{S}\ \rho_p}\right)^{\frac{1}{2}} \tag{14}$$

The stress (or pressure) p is equal to $p_3 = p_5$ (see Fig. 7) when the relaxation time is either zero or infinite.

The rate at which the burning surface of the propellant recedes is given by Saint-Robert's Law. Thus (17)

$$r = bp^n \tag{15}$$

where

b and n are constants and

r = the burning rate of the propellant in feet per second.

The mass flow rate for the material leaving the burning surface of the propellant is given by

$$\dot{m} = r\rho_p \tag{16}$$

The relative velocity of the gases leaving the propellant is given by

$$u_{rp} = \frac{\dot{m}}{\rho} = \frac{\dot{m}\ RT}{p} \tag{17}$$

Substituting equation 16 and 17, yields

$$u_{rp} = \frac{r\ \rho_p\ RT}{p} \tag{18}$$

The equation for the absolute velocity of flow in flow field 5 (see Fig. 7) is

$$u_5 = u_{rp5} - r_5 - u_{p5} \tag{19}$$

Substituting equations 14 and 18 into 19, gives

$$u_5 = r_5 \left[\frac{\rho_p\ R\ T_5}{p_5} - 1\right] - (p_5 - p_1)\left(\frac{1}{\bar{S}\ \rho_p}\right)^{\frac{1}{2}} \tag{20}$$

In flow field 1 the burning surface recedes due to combustion only; therefore, the equation for the velocity of flow in field 1 is

$$u_1 = u_{rp_1} - r_1 \tag{21}$$

Substituting equation 18 into 21,

$$u_1 = r_1 \left[\frac{\rho_p R T_1}{p_1} - 1\right] \tag{22}$$

Matching the velocities across the contact discontinuity gives the following relation:

$$u_5 = u_3 = u_1 + {}_1\Delta u_2 + {}_2\Delta u_3 \tag{23}$$

Substituting equations 20 and 22 into 23, yields

$$r_5 \left[\frac{\rho_p R T_5}{p_5} - 1\right] - (p_5 - p_1)\left(\frac{1}{\bar{S}\rho_p}\right)^{\frac{1}{2}} = r_1 \left[\frac{\rho_p R T_1}{p_1} - 1\right] + {}_1\Delta u_2 + {}_2\Delta u_3 \tag{24}$$

where

${}_1\Delta u_2$ and ${}_2\Delta u_3$ are the change in velocity across the incident and reflected shocks, respectively.

Employing equation 47 to evaluate the change in velocities across the shocks, and noting that $p_3 = p_5$ (therefore $r_3 = r_5$) across the contact distontinuity, equation 24 becomes

$$r_3 \left[\frac{\rho_p R T_5}{p_3} - 1\right] - (p_3 - p_1)\left(\frac{1}{\bar{S}\rho_p}\right)^{\frac{1}{2}} = r_1 \left[\frac{\rho_p R T_1}{p_1} - 1\right]$$

$$- \left(\frac{p_2}{p_1} - 1\right)\left[\frac{2g R T_1}{(\gamma+1)\, p_2/p_1 + (\gamma-1)}\right]^{\frac{1}{2}} + \left(\frac{p_3}{p_2} - 1\right)\left[\frac{2g R T_2}{(\gamma+1)\, p_3/p_2 + (\gamma-1)}\right]^{\frac{1}{2}} \tag{25}$$

where the subscripts denote the different flow fields in Fig. 7.

The flow properties in field 1 and the strength of the incident shock are assumed to be known. The temperature T_2 can, therefore, be calculated by employing equation 44; similarly, T_3 can be expressed in terms of p_3 and known quantities by employing the latter equation. Furthermore, the burning rate r_3 can be expressed in terms of p_3 by employing equation 15. In equation 25 the only unknown flow properties are T_5 and p_3. There is a difference between T_3 and T_5 -- the gases in flow field 3 were released from the uncompressed propellant surface and were then compressed by the incident and reflected shocks; on the other hand, the gases in flow field 5 were released from the compressed propellant. The total enthalpy of the propellant after compression does not differ markedly from the enthalpy before compression, since only a small amount of energy is required to compress the solid. For a demonstration of that fact see reference (18). Therefore, T_5 should not differ markedly from T_1. The assumption is made that $T_5 = T_1$, and then p_3 is the only unknown in equation 25. Because of the nature of equation 25, p_3 can only be determined by trial and error. Once p_3 is obtained, the amplitude of the reflected shock can be calculated.

If the relaxation time is infinite, the condition $r_1 = r_3$ is substituted into equation 25, the subscript 4 is substituted for 5, and the procedure described above is employed to determine p_3.

At first glance it may appear that excluding the rarefaction backside of the nonuniform shock from the calculations for the reflection would make the solution presented above a very poor approximation.

However, upon further investigation it is seen that the presence of the rarefaction in the reflection process is a higher order effect. If the rarefaction backside of the nonuniform shock is included in the reflection, the above calculation is performed to determine the amplitude of the front of the nonuniform shock and then the interaction of that reflected shock with the rarefaction must be made. The interaction is handled in the same way as the head-on collision of a normal shock and a rarefaction wave except the boundary condition at the surface of the propellant must be maintained. The effect of including the rarefaction is to increase the amplitude of the shock. However, the gradient present in the flow due to the rarefaction with which the shock interacts will be very small compared to the gradients present due to the combustion process; so the net effect of the rarefaction will be negligible when considering the overall interaction of the nonuniform shock with the combustion region.

The interaction of a nonuniform shock with the propellant was calculated for a 500 psia combustion pressure and at shock amplitudes of 5 and 75 psi. To simplify the calculation the gases near the surface of the propellant were assumed to be at a uniform temperature and pressure. A tolerance of 0.6 percent was set on the iterations required to calculate the pressure ratio across the shock. The effect of the presence of the rarefaction wave was evident but was less than the tolerance set upon the iteration.

4.0 NUMERICAL PROCEDURE

The four compatibility equations (equations 5 through 8) and the equation of state (equation 9) are a system of five independent equations containing five dependent variables. The only way that the equations can be solved for the five variables is to write the differential equations as finite-difference equations so that a system of five algebraic equations is obtained. A net solution similar to that shown in Fig. 6 can then be calculated. The location of the net on the time-distance plane is obtained by making geometric calculations. The procedure for making the solution is given in detail in the latter part of this section.

4.1 Compatibility Equations in Finite-Difference Form

As mentioned above, the compatibility equations must first be written in finite-difference form before a solution can be obtained. The compatibility equations will be different for each zone; however, the characteristic curves along which the compatibility equations must be satisfied will be the same for each zone. The compatibility equations in finite-difference form for the combustion products region and for each zone of the combustion region are given below. The equation of state is also given for each zone and for the combustion products region.

4.1.1 Combustion Products Region

The combustion products region is assumed to be gradient free and reversibly adiabatic. Under those conditions the right sides of equations 5 and 6 are equal to zero and equations 7 and 8 are not applicable. The two compatibility equations in finite-difference form and the equation of state for the combustion products region are as follows:

along characteristic curve $d\tau/dx = 1/(u+a)$

$$\text{⨭}p + (\overline{a\rho})_{+} \text{⨭}u = 0 \tag{26}$$

along characteristic curve $d\tau/dx = 1/(u-a)$

$$\text{⨪}p - (\overline{a\rho})_{-} \text{⨪}u = 0 \tag{27}$$

the equation of state

$$p = \rho RT \tag{28}$$

The notation employed in the above equations is as follows:

⨭H = an incremental change in H (where H represents one of the variables p, u, t, Y, R, τ or x) along the characteristic curve $d\tau/dx = 1/(u + a)$,

⨪H = an incremental change in H along the characteristic curve $d\tau/dx = 1/(u - a)$,

△H = an incremental change in H along the characteristic curve $d\tau/dx = 1/u$,

$\overline{(HG)}_{+}$ = average values of HG (where HG represents groups of the variables and constants) along an increment of the characteristic curve $d\tau/dx = 1/(u + a)$,

$\overline{(HG)}_-$ = average value of HG along an increment of the characteristic curve $d\tau/dx = 1/(u - a)$, and

$\overline{(HG)}$ = average value of HG along an increment of the characteristic curve $d\tau/dx = 1/u$.

The average value for an expression is obtained by summing its values at each end of the increment and dividing by two.

4.1.2 Flame Zone

In the flame zone chemical reaction, heat transfer, molecular diffusion, and bulk viscosity effects are assumed to be present. The physical properties, however, are assumed to be affected very little by the chemical reaction taking place in the zone. The compatibility equations will be the same as equations 5 through 8 except that the mass change terms will not be present. The equation of state will reduce to equation 33 given below. The compatibility equation in finite-difference form and the equation of state for the flame zone are as follows:

along characteristic curve $d\tau/dx = 1/(u + a)$

$$\Delta p + (\overline{a\rho})_+ \Delta u = \left(a\eta \frac{\partial^2 u}{\partial x^2}\right)_+ \Delta\tau + (\gamma-1)\,\Delta\tau \left\{ \left(\alpha \rho Y U e^{-E/R_o T}\right)_+ + \left[\eta \left(\frac{\partial u}{\partial x}\right)^2\right]_+ + \left(k \frac{\partial^2 T}{\partial x^2}\right)_+ + D\eta \frac{\partial}{\partial x}\left[\left(\frac{1}{1-Y} - \frac{1}{Y}\right) \frac{\partial Y}{\partial x} \frac{\partial u}{\partial x}\right]_+ \right\} \tag{29}$$

along characteristic curve $d\tau/dx = 1/(u - a)$

$$\Delta p - (\overline{a\rho})_- \Delta u = -(a\eta \frac{\partial^2 u}{\partial x^2})_- \Delta\tau + (\gamma-1)\Delta\tau \{ (\alpha \rho Y U e^{-E/R_o T})_- + [\eta(\frac{\partial u}{\partial x})^2]_- + (k \frac{\partial^2 T}{\partial x^2})_- + Dn \frac{\partial}{\partial x} [(\frac{1}{1-Y} - \frac{1}{Y}) \frac{\partial Y}{\partial x} \frac{\partial u}{\partial x}]_- \} \quad (30)$$

along characteristic curve $d\tau/dx = 1/u$

$$(\overline{\rho c_v}) \Delta T - (\overline{RT}) \Delta\rho = \{(\alpha \rho Y U e^{-E/R_o T}) + [\eta (\frac{\partial u}{\partial x})^2] + (k \frac{\partial^2 T}{\partial x^2}) + Dn \frac{\partial}{\partial x} [(\frac{1}{1-Y} - \frac{1}{Y}) \frac{\partial Y}{\partial x} \frac{\partial u}{\partial x}] \} \Delta\tau \quad (31)$$

$$\Delta Y = [\frac{D}{\rho} \frac{\partial}{\partial x} (\rho \frac{\partial Y}{\partial x}) - (\alpha Y e^{-E/R_o T})] \Delta\tau \quad (32)$$

the equation of state

$$p = \rho RT \quad (33)$$

4.1.3 Induction Zone

In the induction zone only chemical reaction and heat transfer are assumed to be present. The expression for the chemical reaction rate is simplified and written as a linear function of the distance coordinate. The induction zone is assumed to be of uniform chemical composition; therefore, the concentration equation (equation 8) is not applicable in the zone. The compatibility equations in finite-difference form for the induction zone are as follows:

along characteristic curve $d\tau/dx = 1/(u + a)$

$$\triangle p + \overline{(a\rho)}_{+} \triangle u = (\gamma-1) \triangle \tau \left[\overline{\left(k \frac{\partial^2 T}{\partial x^2}\right)}_{+} + \overline{(Q_{cc})}_{+}\right] \tag{34}$$

along characteristic curve $d\tau/dx = 1/(u-a)$

$$\triangle p - \overline{(a\rho)}_{-} \triangle u = (\gamma-1) \triangle \tau \left[\overline{\left(k \frac{\partial^2 T}{\partial x^2}\right)}_{-} + \overline{(Q_{cc})}_{-}\right] \tag{35}$$

along characteristic curve $d\tau/dx = 1/u$

$$(\overline{\rho\ c_v})\ \Delta T - (\overline{RT})\ \Delta\rho = \left[\overline{(Q_{cc})} + \overline{\left(k \frac{\partial^2 T}{\partial x^2}\right)}\right]\ \Delta\tau \tag{36}$$

The linear heat addition term is

$$Q_{cc} = \frac{2\ \dot{m}\ Q}{x_o} \left(\frac{x}{x_o}\right) \tag{37}$$

where

x = distance from the fore end of the induction zone to the point of interest and

Q = heat released per pound of mass flowing through the induction zone.

The equation of state reduces to

$$p = \rho\ RT \tag{38}$$

4.1.4 Decomposition Zone

In the decomposition zone chemical reaction and heat transfer are assumed to be present. Unlike the other two zones the chemical reaction is assumed to affect the chemical composition of the zone. The compatibility equations in finite-difference form and the equation of state for the induction zone are as follows:

along characteristic curve $d\tau/dx = 1/(u + a)$

$$\oplus p + (\overline{a\rho})_{+} \oplus u = \overline{(\rho\, T \frac{\Delta R}{\Delta \tau})}_{+} \oplus \tau + (\overline{\gamma-1})_{+} \oplus \tau \left[\overline{(\alpha\, \rho\, Y\, U\, e^{-E/R_o T})}_{+} + \overline{(k \frac{\partial^2 T}{\partial x^2})}_{+} \right] \tag{39}$$

along characteristic curve $d\tau/dx = 1/(u - a)$

$$\ominus p - (\overline{a\rho})_{-} \ominus u = \overline{(\rho\, T \frac{\Delta R}{\Delta \tau})}_{-} \ominus \tau + (\overline{\gamma-1})_{-} \ominus \tau \left[\overline{(\alpha\, \rho\, Y\, U\, e^{-E/R_o T})}_{-} + \overline{(k \frac{\partial^2 T}{\partial x^2})}_{-} \right] \tag{40}$$

along characteristic curve $d\tau/dx = 1/u$

$$(\overline{\rho c_v}) \Delta T - (\overline{RT}) \Delta \rho = \left[\overline{(\alpha\, \rho\, Y\, U\, e^{-E/R_o T})} + \overline{(k \frac{\partial^2 T}{\partial x^2})} \right] \Delta \tau \tag{41}$$

$$\Delta Y = - \overline{(\alpha\, Y\, e^{-E/R_o T})} \Delta \tau \tag{42}$$

the equation of state

$$p = R_o T \left(\frac{Y\,(M_2 - M_1) + M_1}{M_1\, M_2} \right) \tag{43}$$

where M_1 and M_2 are the molecular weights of the first and second species respectively.

4.2 Evaluation of the Partial Derivatives

The partial derivatives with respect to distance that appear in the difference equations of Section 4.1 cannot be evaluated directly, and their presence in those equations prevents obtaining a mathematically rigorous solution. If, however, reasonably accurate numerical values can be assigned to the partial derivatives, an approximate solution can be obtained. A method for obtaining approximate values for the partial derivatives is illustrated in Fig. 8. It is assumed that each partial derivative with respect to distance at an arbitrary point A in the unsteady flow field, behind the normal shock, is equal to the corresponding total drivative that applied to a small mass of fluid surrounding point A just prior to the instant when the shock traversed the aforementioned mass. The location of the mass in the steady flow field is obtained by determining where the path line from point A in the unsteady flow field intersects the shock; the point of intersection is denoted by A_{fs}. The total derivatives with respect to distance at point A_{fs} are assumed to be equal to their corresponding partial derivatives at point A.

The method for obtaining the partial derivatives presented above should be a good approximation provided that the strength of the normal shock does not change too rapidly and the point A is not removed too far in time from the passage of the shock.

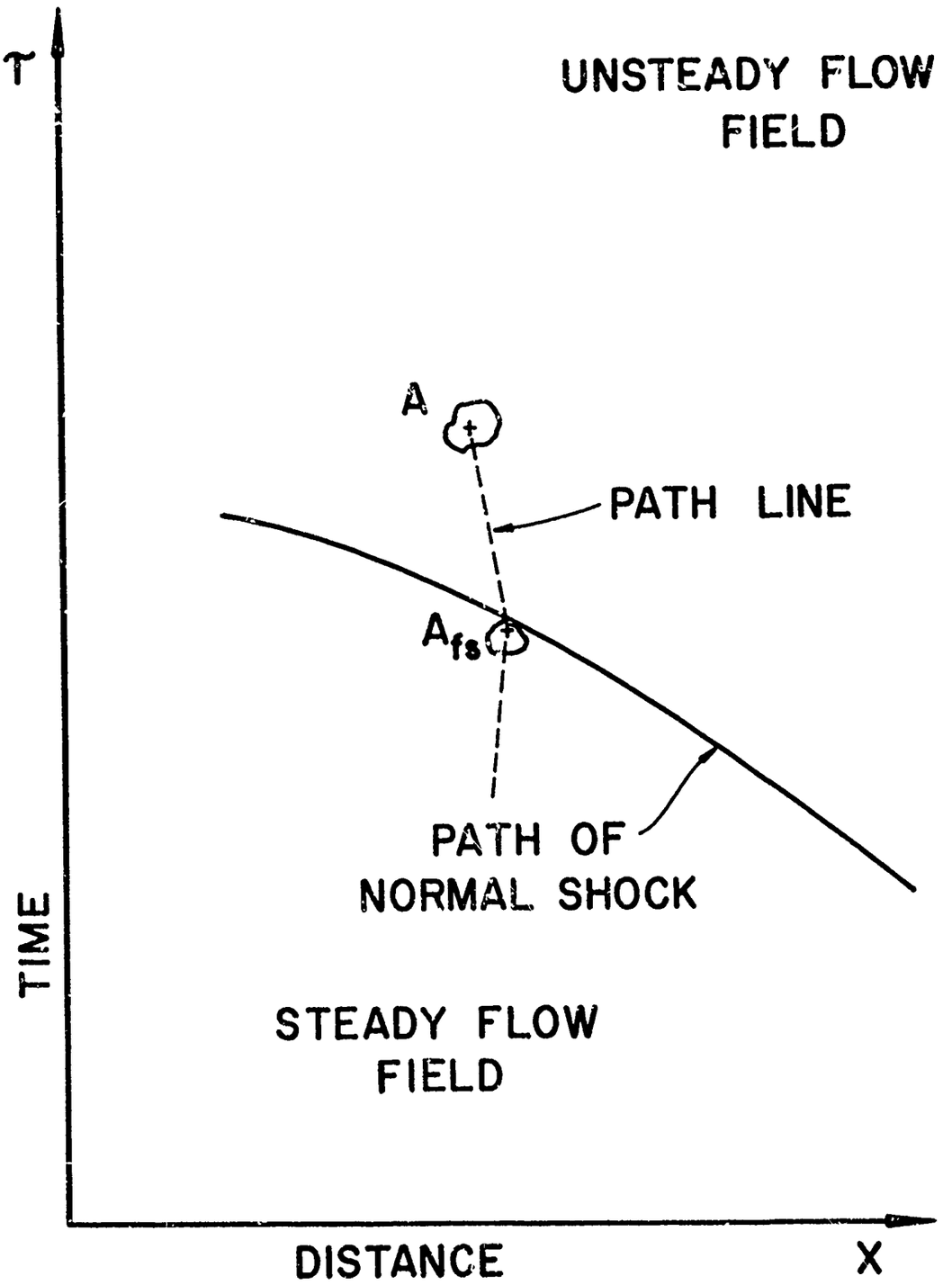

Figure 8 Method of Approximating Partial Derivatives

4.3 Application of the Difference Equations

The application of the finite-difference equations is described for a point located in the flame zone; however, the application of the equations to find a solution in any of the other zones or in the combustion products region is quite similar. Consider the flow properties to be given either along a curve which is not a characteristic or at closely-spaced discrete points along such a curve. It is desired to extend the solution of the flow field beyond the given curve. The field is extended by employing equations 29 through 33, a system of five algebraic equations in five unknowns (the partial derivatives are assumed to be known functions and are evaluated as outlined in Section 4.2). Figure 9 illustrates the geometry involved in solving equations 29 through 33 in the τx plane. Curve S is a portion of a curve along which the flow properties of a system are given, and points B and D are two points Δx apart on curve S.

The solution is extended into the flow field by performing the following operations:

(1) Draw a line from point D in a direction $d\tau/dx = 1/(u + a)$ and a line from B in direction $d\tau/dx = 1/(u - a)$ until they intersect at point A. The line from D is called a plus characteristic and the line from B is called a minus characteristic. Mean values of u and a are employed for determining the approximate direction of the characteristics.

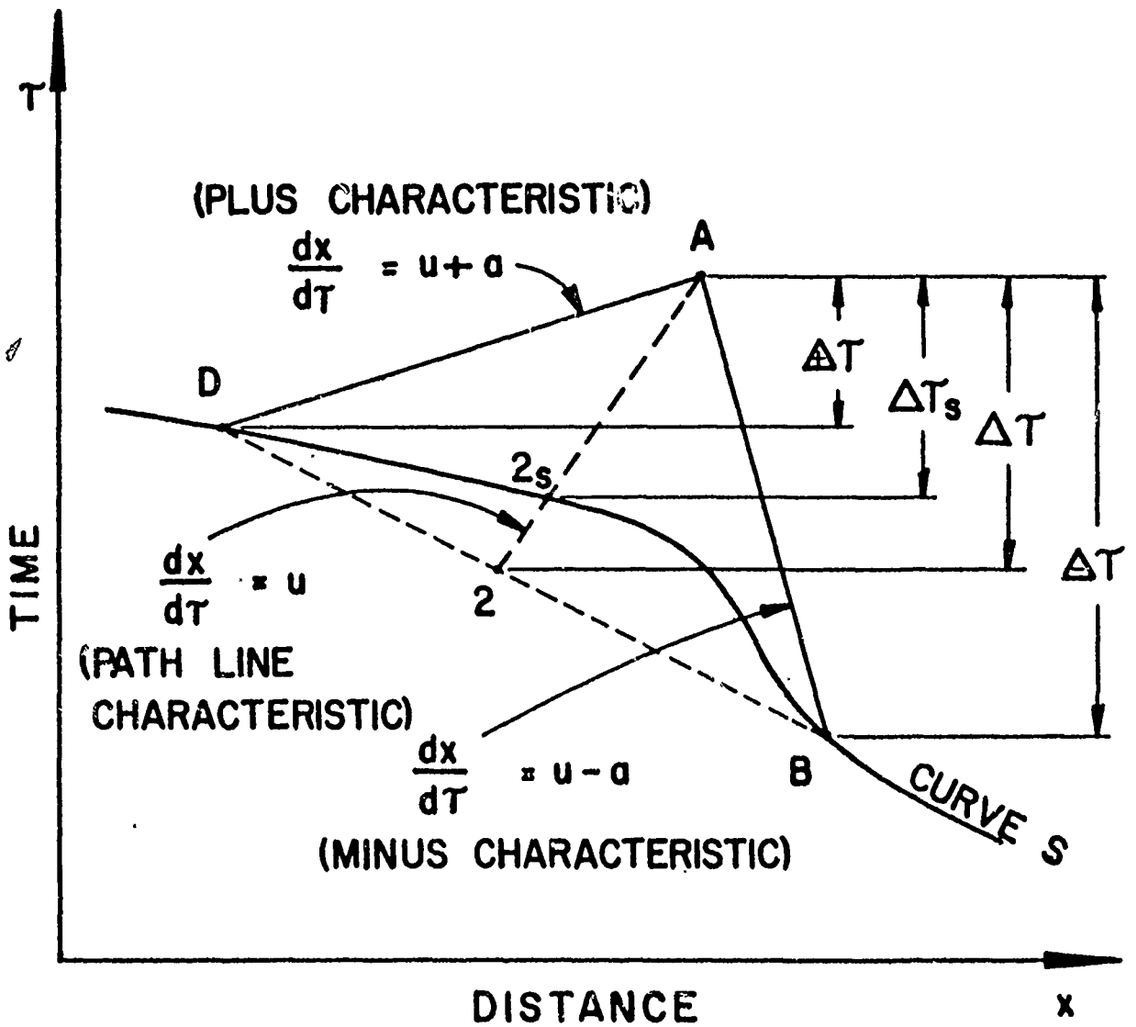

Figure 9 Determination of the Flow Properties at Point A

(2) A line, termed a path line characteristic, is drawn back from point A with direction $d\tau/dx = 1/u$. The mean value of u along the path line characteristic A-2 determines its direction; the mean value is obtained by iteration in steps between points A and 2.

(3) The flow properties at point A are estimated employing the known flow properties at points B and D as a guide. By trial and error the correct values for the flow properties at point A are determined; that is, iteration is continued until equation 29 is solved identically between points D and A, equation 30 between points B and A, and equations 31 and 32 between points A and either 2 or 2_s (depending on the boundary condition that is given). If only the flow properties at points B and D were given initially, the flow properties at point 2 are determined by linear interpolation between points B and D. The time increments ($\Delta\tau$, $\triangleq\tau$, and $\triangle\tau$) to be employed in solving the equations are presented at the right side of Fig. 9. The numerical values of the $\Delta\tau$'s are obtained from the geometry calculations of the three characteristic lines and the given points D and B.

(4) The steps presented in 1, 2, and 3 above are repeated until the desired accuracy for the properties at point A is obtained. If an electronic computer is employed to make the calculations, an iterative procedure may be employed

for correcting successive estimates for the flow properties at point A. The process is continued until the desired accuracy is obtained.

The numerical calculations in each zone of the combustion region are performed in the manner described above employing the difference equations pertinent to each zone.

4.4 Normal Shock

The normal shock propagating through the combustion region represents a discontinuity between the steady and unsteady flow fields (see Fig. 5). The steady state flow properties cannot, therefore, be employed directly to start the mapping of the net outlined in Section 4.3; but adjustments must first be made for the effect of the shock discontinuity between the two flow fields.

The equations for the change in flow properties across a normal shock in terms of the pressure ratio r_p across the shock are as follows (19):

$$\frac{T_2}{T_1} = \frac{r_p \left[(\gamma+1) + r_p (\gamma-1)\right]}{(\gamma+1) r_p + (\gamma-1)} \tag{44}$$

$$\frac{\rho_2}{\rho_1} = \frac{r_p (\gamma+1) + (\gamma-1)}{(\gamma+1) + r_p (\gamma-1)} \tag{45}$$

$$Ma^2 = \frac{\gamma+1}{2\gamma} r_p + \frac{\gamma-1}{2\gamma} \tag{46}$$

$$u_2 - u_1 = (r_p - 1) \left[\frac{2 g R \bar{T}_1}{(\gamma+1)\, r_p + (\gamma-1)} \right]^{1/2} \qquad (47)$$

where

Ma = Mach number of the gases entering the shock relative to the shock,

1 = static properties in front of the shock, and

2 = static properties behind the shock.

Figure 10 illustrates, on the τx plane, the propagation of the normal shock through an increment of distance Δx in the combustion region. It is assumed that the strength of the shock at point E, the flow properties in front of the shock (points E_{fs} and B_{fs}) and the flow properties at points E and D are given (points E and D lie on the same minus characteristic). The aforementioned information will be given either as initial and boundary condition data or will be available from the calculation of the previous increment of travel of the shock in the combustion region.

The strength of the shock changes as it travels from point E to B due to the gradients in the flow properties and the chemical reaction present in the steady flow field. The new strength of the shock will be such that it gives flow properties at point B that satisfy identically the plus characteristic compatibility equation between points B and C, where the flow properties at point C are obtained by linear interpolation between points D and E.

For an outline of the step-by-step procedure involved in employing the boundary condition for calculating numerically the propagation of

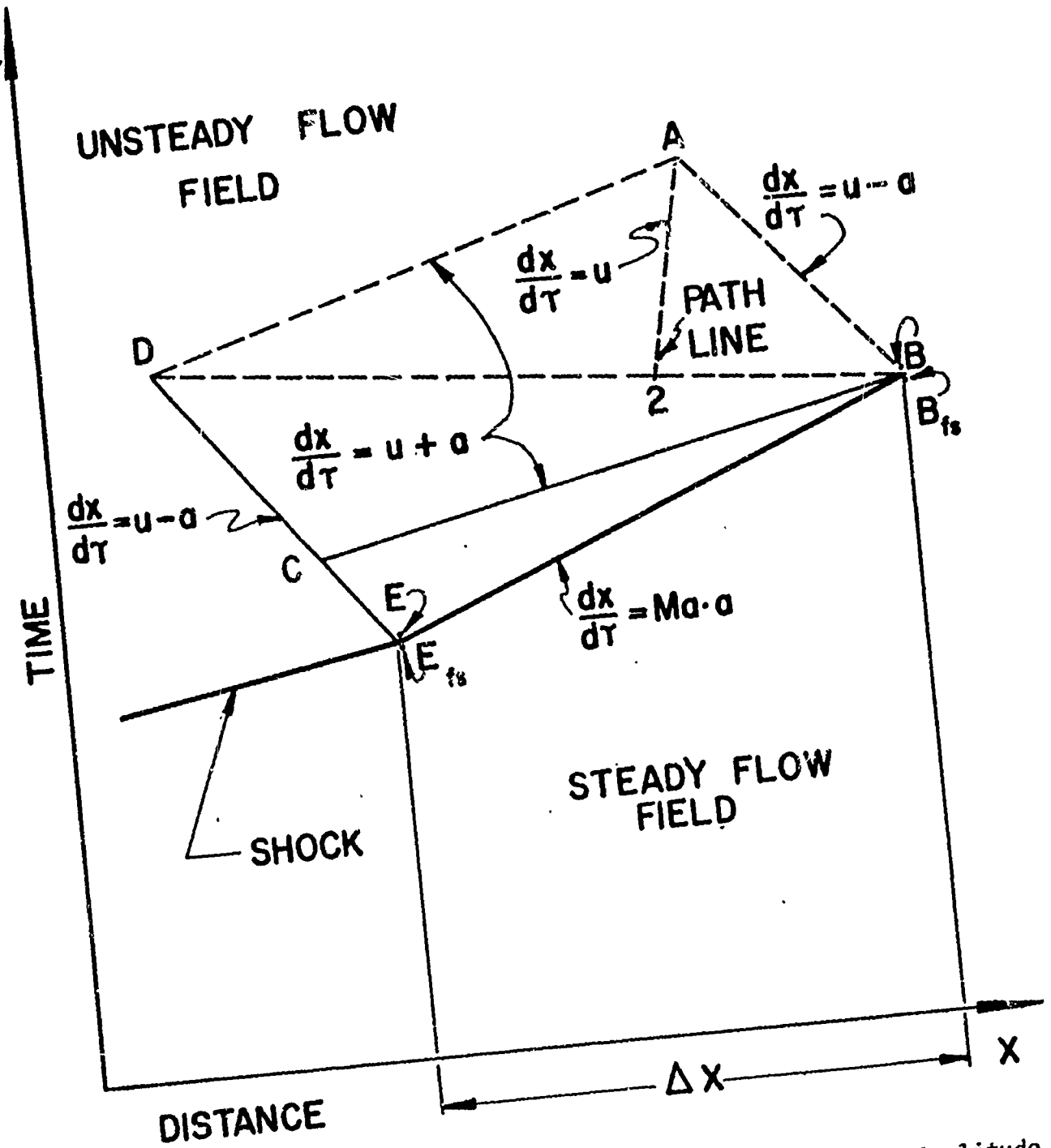

Figure 10 Determination of the Incremental Change in the Amplitude of the Nonuniform Shock

the normal shock, consider the case where the increment illustrated in Fig. 10 is located in the flame zone. Similar calculations are applicable to each of the other zones.

The propagation of the shock is determined by solving five equations in five unknowns, equations 29, 33, 44, 45 and 47. Those equations cannot be solved explicitly for the flow properties, but a trial and error procedure may be employed. The procedure is as follows:

(1) Select a value for the strength of the shock at point B_{fs}, employing as a guide the strength of the shock at point E, and calculate the flow properties at point B.

(2) Calculate a mean value for a and Ma between points B_{fs} and E_{fs} and determine the time coordinate of point B_{fs} (Δx is assumed to have a preassigned value).

(3) Locate point C by employing mean values for u and a between points B and the estimated location of point C.

(4) Insert the flow properties from points C and B into the plus characteristic compatiblity equation (equation 29) and check for identical solution of the equation.

(5) Correct the selected value for the strength of the shock at point B_{fs}, and repeat the above steps. An iterative approach may be employed for correcting the selected values for the shock strength in a systematic manner.

Once the correct strength of the shock has been determined, the flow properties at point A may be obtained by employing the procedure outlined in Section 4.3. The propatation of the shock can be extended

one more increment once the flow properties at points A and B and the strength of the shock are known. The above procedure is repeated until the propellant surface is reached.

4.5 Increment Size

The selection of proper increment size is important when making a numerical solution. A small increment size does not necessarily mean that the solution will be approaching the solution to the differential equations. As the size of the increment is decreased, the number of significant figures required to make accurate calculations increases because numerous subtractions occur in the calculations. The size of the increment must be kept large enough so that the capabilities of the computer will not be exceeded.

An increment size study was made for the flame zone where the steepest gradients occur. The results of the analysis are presented in Fig. 11. The amplitude of the normal shock after propagating through the flame zone P_f is plotted as a function of the number of increments employed in making the calculation. Two curves are plotted--the upper one is for an initial shock amplitude P_1 entering the flame zone of 75 psi and the lower one for an initial amplitude of 10 psi. The combustion pressure is 500 psia. As can be seen, the amplitude of the shock after propagating through the flame zone is correct to four significant figures even when employing only two increments, and the precision increases to five figures if ten or more increments are employed. The high precision obtained with only a small number of increments is probably due to the fact that in

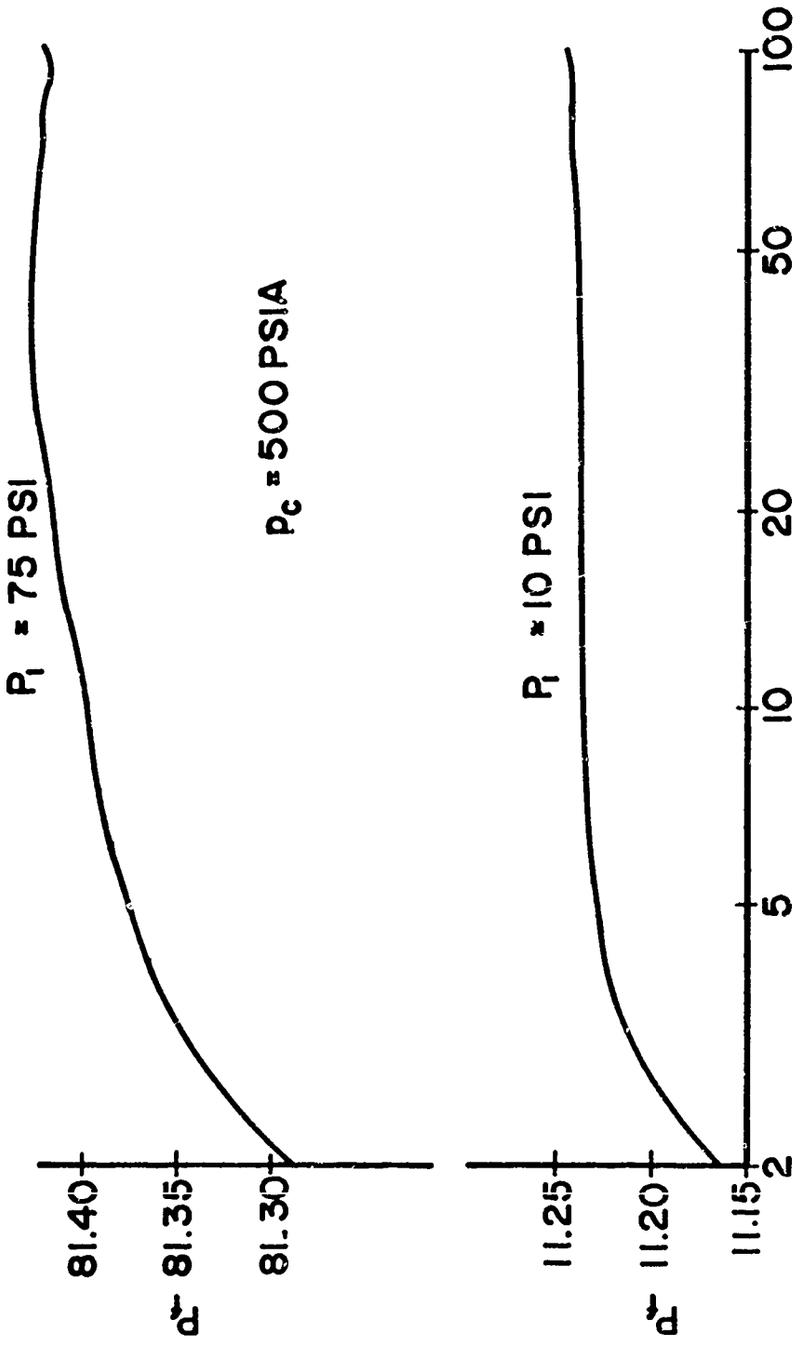

Figure 11 The Effect of Increment Size upon the Precision of the Numerical Calculations

calculating the amplitude of the shock only the unsteady solution near the distance boundary was required. If the solution for the amplitude of the pulse required a solution of the unsteady field far from the boundary, the effect of increment size would probably have been more significant. The curves do not approach some limiting value because as the increments are made very small the computer does not employ enough significant figures to maintain the precision of the calculation.

The problem being numerically solved will require that the amplitude of the shock be known to about four significant figures. Therefore, if ten or more increments are employed to make the calculation the required precision will be obtained. The use of the same number of increments will apply to the other two zones. The number of increments employed in the numerical solution is as follows: flame zone, 15 increments; induction zone, 40 increments; and decomposition zone, 12 increments. The reason for the various numbers of increments in each zone was that it facilitated matching the zones at their boundaries.

5.0 RESULTS

The interaction of the nonuniform shock with the combustion region was calculated for three combustion pressures: 250, 500, and 1000 psia. Interactions were calcuated for initial shock pressure ratios of 1.01, 1.02, 1.05, 1.10, and 1.15 at each of the three combustion pressures. In addition, interactions for pressure ratios of 1.002 and 1.005 were calculated at 1000 psia combustion pressure and a pressure ratio of 1.005 at 500 psia combustion pressure. The heat addition in each zone by the chemical reactions was the same for all cases studied; however, the rate of heat addition and the width of the steady state combustion region were assumed to be functions of the combustion pressure. The profile of the steady state combustion region assumed for each combustion pressure is given in the latter part of Appendix B. The results of the calculations showed smooth trends for the variation of the amplification of the shock as a function of combustion pressure and as a function of initial shock pressure ratio.

5.1 Shock Amplified by the Combustion Region

The value of the initial pressure ratio across the shock and the combustion pressure will determine whether the shock is amplified or attenuated by the combustion region. A typical set of calculated results for a nonuniform shock amplified by the combustion region

is presented in Fig. 12. The variation in shock amplitude rather than pressure ratio across the shock is plotted as a function of location in the combustion region. In the lower portion of the figure the steady state temperature profile in the combustion region is plotted. The horizontal distance coordinate for each zone is plotted to a different scale to give a better presentation of the data. In the upper portion of the figure the amplitude of the shock, P, in psi above the mean combustion pressure is plotted as a function of position in the combustion region. The plot is for a shock with an initial amplitude of 5 psi interacting with a combustion region that has a 250 psia combustion pressure (initial shock pressure ratio of 1.02).

The line A-B is a plot of the amplitude of the shock as it propagates through the combustion region from right to left toward the burning propellant surface. The point C is the amplitude of the shock after reflection from the burning surface. The line C-D is the amplitude of the shock as it propagates back through the combustion region to the combustion products region at the right.

The phenomena which contribute to a change in amplitude of the shock are chemical heat addition, heat transfer, velocity gradient, viscosity, molecular weight change, and molecular diffusion. The contribution of each of the aforementioned phenomena toward changing the amplitude of the shock is discussed in detail in Section 5.4. However, a few brief qualitative statements will be made at this time so that Figs. 12 and 13 can be discussed. The heat addition due to chemcial reaction, the change in molecular weight of the flowing

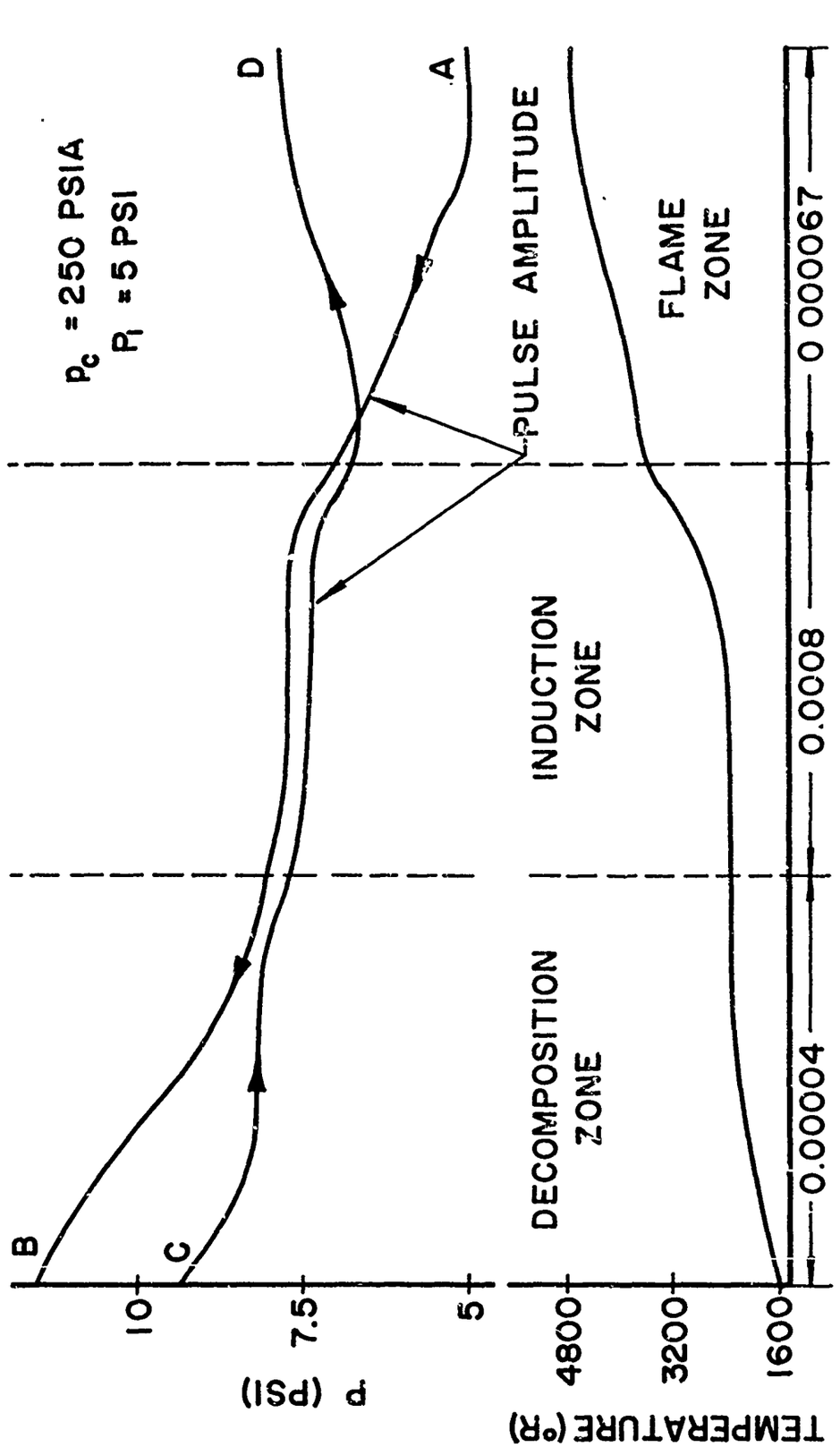

Figure 12 Amplitude of the Nonuniform Shock as a Function of Combustion Region Position (Amplification)

gases due to the reaction, and the velocity gradient in the combustion region all have a marked effect upon changing the amplitude of the shock. The chemical heat addition amplifies the shock. A decrease in molecular weight during chemical reaction and a decreasing velocity gradient in the direction of shock propagation both lead to amplification of the shock and vice versa. The contribution of molecular diffusion and viscosity toward changing the amplitude of the shock are of higher order. Heat transfer is important near the propellant surface where a large amount of heat is transported into the propellant and leads to an attenuation of the shock, but in the other parts of the combustion region its effect upon changing the amplitude of the shock is small.

As mentioned above, the nonuniform shock starts at point A and travels toward point B. As the shock travels through the flame zone its amplitude is increased as a result of the large amount of heat released in that zone. The decreasing steady state velocity gradient also helps to amplify the shock. At the start of the induction zone the shock is further amplified by the decreasing velocity gradient. Toward the end of the zone the velocity gradient is small as is the heat release through the whole zone so the shock travels along with an almost constant amplitude. As the shock enters the decomposition zone there is a sharp rise in amplitude due to the discontinuity in physical properties assigned in the model for the induction and decomposition zones. In the decomposition zone the amplitude of the shock rapidly increases due to heat addition, molecular weight decrease of the gas, and decreasing velocity gradient. The shock is amplified more in the

decomposition zone than the flame zone during its forward propagation because of the larger amplification in the decomposition zone by the velocity gradient. In the flame zone the velocity changes only as a result of temperature change. In the decomposition zone the velocity changes as a result of temperature change and molecular weight change.

Upon reflection from the burning propellant surface the shock has an amplitude indicated by point C. A small amount of the attenuation is due to the momentary decrease in the velocity with which the gases leave the propellant surface. The decrease in velocity is caused by the increased pressure at the surface of the propellant. The major portion of the attenuation of the shock is, however, due to the compression of the propellant by the shock.

The calculation for the rate at which the propellant is compressed should employ the "effective" modulus of elasticity of the propellant, i.e., the modulus of elasticity that would be measured under the rapid loading condition such as imposed by the pressure shock. Since a representative value for the "effective" modulus of elasticity was not readily available for the propellant, the static modulus of elasticity was employed for the calculation. Employing this lower value for the modulus rather than the "effective" modulus required yields an attenuation of the shock larger than the amount that would normally occur. Therefore, point C is the lower limit for the amplitude of the shock after reflection from the burning surface.

Line C-D is the variation in shock amplitude as the shock propagates back through the combustion region away from the burning

surface. Upon reflection of the shock the velocity gradient which was negative in the direction of shock propagation becomes positive. Therefore, as the shock returns through the combustion region the velocity gradient exerts an attenuating influence upon the shock. The heat that is added and the decrease in molecular weight due to chemical reaction exert amplifying influences upon the shock independent of the direction of propagation. The velocity gradient and chemical reaction effects upon the shock are, therefore, opposite and whether the shock amplifies or attenuates as it propagates depends upon which effect is larger at the given location. As can be seen, the shock is initially attenuated as it leaves the propellant surface; however, later in the decomposition zone the heat addition and molecular weight change about compensate for the attenuating effect of the velocity gradient. In the induction zone where the shock had been previously amplified by the velocity gradient on its forward propagation, the shock is now attenuated by about the same magnitude. In the flame zone the large amount of heat release is enough to overcome the attenuating effect of the velocity gradient and a net amplification of the shock is obtained. Numerical values for the effects upon the amplification of the shock of the various phenomenon discussed above are tabulated in Section 5.4 and Appendix D.

5.2 Shock Attenuated by the Combustion Region

Figure 13 is similar to Fig. 12 except that the initial shock amplitude and combustion pressure are such that the shock is attenuated

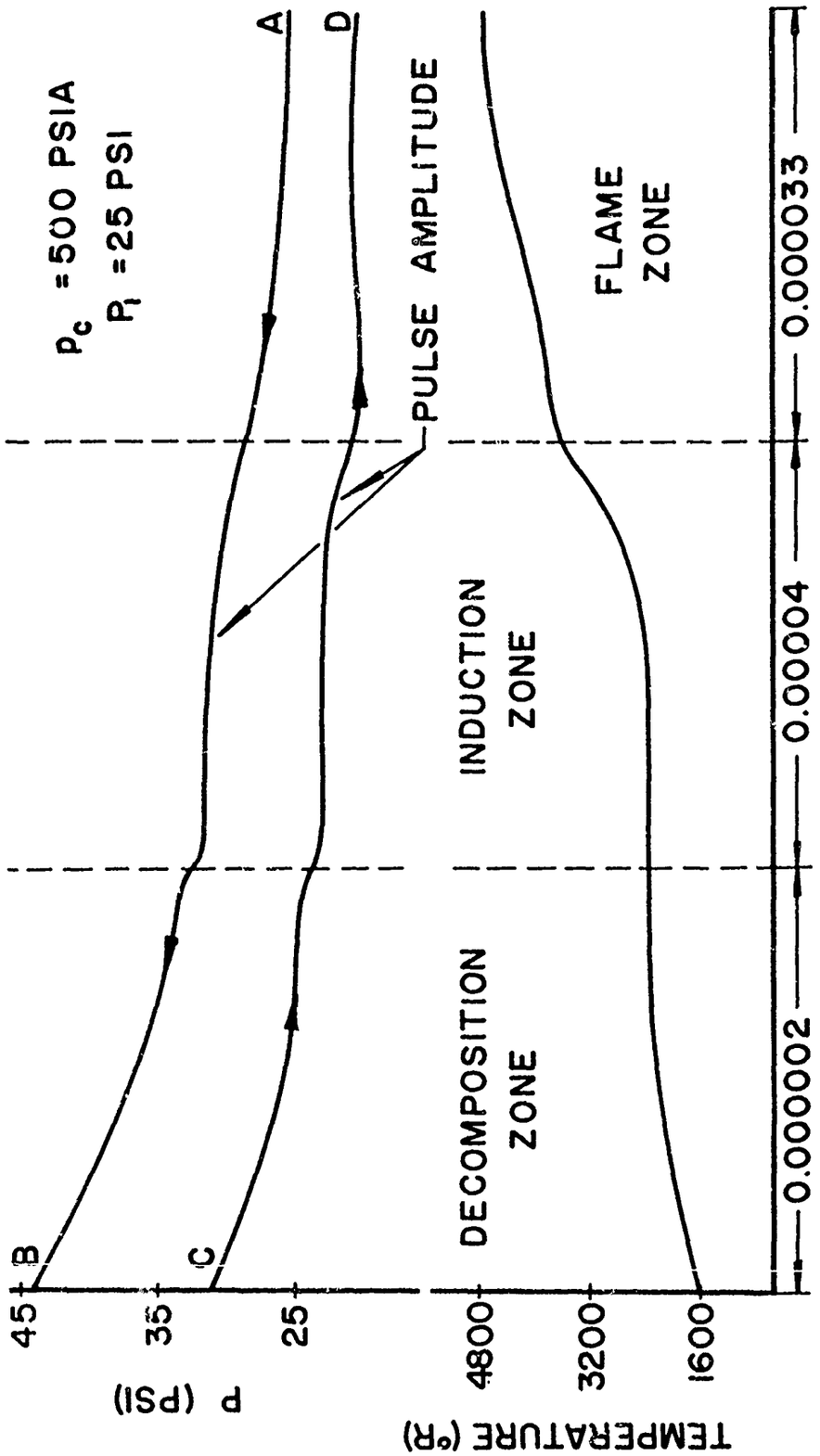

Figure 13 Amplitude of the Nonuniform Shock as a Function of Combustion Region Position (Attenuation)

by the combustion region. The figure is representative of the results obtained for shocks that were attenuated by the combustion region. The shock amplitude, P, is plotted as a function of combustion zone location in the upper portion of the figure and the steady state temperature profile is plotted in the lower portion. The horizontal distance coordinate is again plotted to different scales for each zone to give a better representation. The plot is for a shock with an initial amplitude of 25 psi propagating through a combustion region that has a combustion pressure of 500 psia (an initial pressure ratio across the shock of 1.05). The horizontal scales are twice as large as those employed in Fig. 12.

As in the previous figure, the line A-B is the amplitude of the shock as it propagates to the burning surface; point C is the amplitude of the shock after reflection from the burning surface; and line C-D is the amplitude of the shock as it propagates back through the combustion region away from the burning surface.

As the shock propagates from right to left toward the burning surface (line A-B), the amplitude of the shock increases due to the amplifying effect of the decreasing velocity gradient in the direction of shock propagation, the chemical heat release, and in the decomposition zone the decreasing molecular weight--as mentioned before, the molecular diffusion, heat transfer, and bulk viscosity effects upon the amplification of the shock are small. The shock is reflected from the burning surface with an amplitude indicated by point C. The line C-D is a plot of the variation in shock amplitude as it propagates back through the

combustion region away from the burning surface. The gradients in the combustion region increase with increasing combustion pressure so that the attenuating effect of the increasing velocity gradient in the direction of shock propagation for 500 psia combustion pressure is larger than the amplifying effect of the chemical heat addition and decreasing molecular weight along almost the entire return path. Only in a portion of the flame zone is the attenuating effect of the velocity gradient overcome by the heat addition, but it is not enough to give a net amplification of the shock.

As in the aforementioned case of shock amplification, the static modulus of elasticity for the propellant was employed in the calculation for the amplitude of the shock upon reflection from the burning surface; therefore, point C represents the maximum attenuation the shock would exeprience upon reflection from the propellant surface.

5.3 Shock Amplification as a Function of Combustion Pressure and Initial Shock Amplitude

The results of all of the numerical calculations are presented in Fig. 14. The ratio of the amplitude of the shock after interaction with the combustion region P_2 divided by the initial amplitude of the shock P_1 is plotted as a function of initial amplitude of the shock for combustion pressures p_c of 250, 500, and 1000 psia. The figure shows that the combustion pressure influences the amplification of the shock by the combustion region. The higher the combustion pressure the less the amplifying effect of the combustion region. The results cannot be considered too quantitative, however,

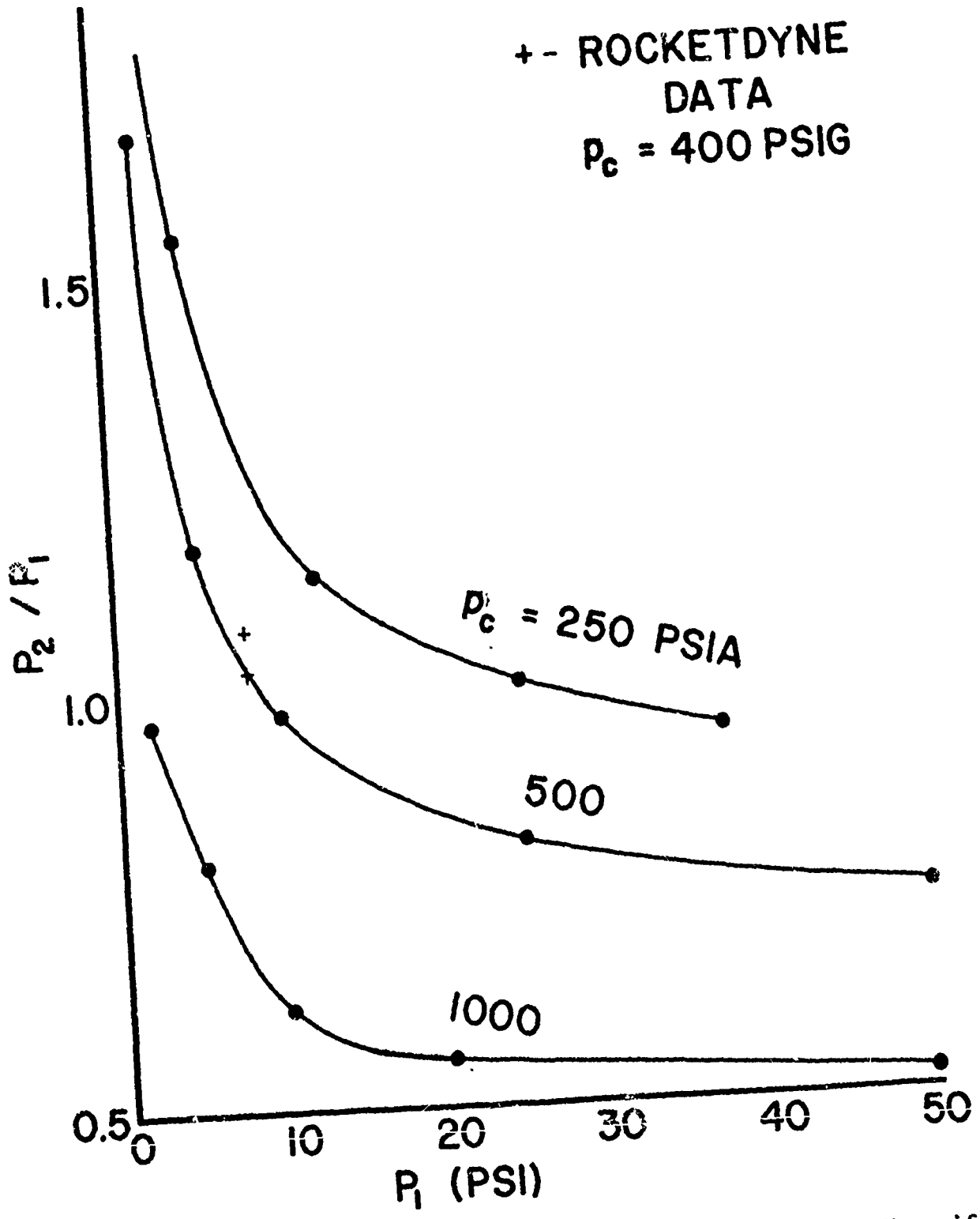

Figure 14 Amplification Ratio P_2/P_1 as a Function of Initial Nonuniform Shock Amplitude P_1 and Combustion Pressure p_c

because a rough approximation was employed for the effect of combustion pressure on steady state zone widths (see Appendix B). The figure also shows that very small amplitude shocks show large relative amplification at all combustion pressures. The large relative amplification rapidly decreases with increased initial shock amplitude, P_1.

The two crosses indicate experimental data obtained at Rocketdyne (see Appendix E)(21). The data points were obtained from pressure-time traces for a nonuniform shock impinging on and reflecting from a burning propellant surface. The combustion pressure was 400 psig and the initial shock amplitude was 8 psi. The propellant grain was non-metal bearing and approximated a propellant composition of 80 per cent ammonium perchlorate and 20 per cent polybutadiene-acrylic acid as employed in the analysis reported herein.

5.4 Amplification Parameters

The previous section contained the results for the overall amplification of the nonuniform shock by the combustion region. This section presents the effect of each of the various processes assumed to be present in the combustion region upon the amplification of the nonuniform shock.

The influence of the various effects upon the amplification of the shock can be studied by noting which phenomena influence the change in pressure along a plus characteristic curve in the unsteady flow field. That fact becomes evident from a study of Fig. 10. In that figure the line B-C is a plus characteristic and the line E-B is the path of propagation of the shock. Except for a very strong shock the two lines

will have nearly the same slopes, and the point C will have about the same properties as point E. The steady state pressure in front of the shock was assumed to be constant; and since the pressures at C and E are approximately equal, a variation in pressure along plus characteristic B-C will be very nearly equal to the variation in pressure of the amplitude of the shock. Therefore, an investigation of the factors which influence the change in pressure along the plus characteristic B-C will reveal the phenomena which produce amplification or attenuation of the shock. The finite-difference form of the plus characteristic equation (equation 5) with all effects included is given below.

$$\begin{aligned}\Delta p = &- \underbrace{(\overline{a\rho})_+ \Delta u}_{\text{velocity increment}} + \underbrace{\overline{(\rho T \frac{\Delta R}{\Delta \tau})_+} \Delta \tau}_{\substack{\text{molecular weight}\\ \text{change rate}}} \\ &+ \underbrace{\overline{(a\eta \frac{\partial^2 u}{\partial x^2})_+} \Delta \tau}_{\text{viscosity}} + \underbrace{\overline{(\gamma-1)_+ \{ (\alpha \rho Y U e^{-E/R_o T})_+}}_{\text{heat addition}} \\ &+ \overline{(k \frac{\partial^2 T}{\partial x^2})_+} + \overline{[\eta (\frac{\partial u}{\partial x})^2]_+} + \overline{D\eta \frac{\partial}{\partial x} [(-\frac{1}{Y} + \frac{1}{1-Y}) \frac{\partial Y}{\partial x} \frac{\partial u}{\partial x}]_+ \} \Delta \tau}\end{aligned} \qquad (48)$$

heat transfer; viscous dissipation; diffusion

The physical significance of the first term on the right side of equation 48, the velocity increment term, can best be understood by considering the following two examples. Consider first the example where the strength of the shock does not change very rapidly; the incremental velocity change behind the shock Δu will then be approximately equal to the Δu in front of the shock. Under the aforementioned conditions, any decrease in the steady state velocity gradient will produce an amplification of the shock and vice versa. Now consider the case where the steady state velocity is approximately constant but the strength of the shock is changed by some means. An increase in shock strength will cause a positive increment in velocity behind the shock and vice versa. Since there is a minus sign in front of the Δu term in equation 48, the effect of that term will be to oppose any change in amplitude of the shock. From the two aforementioned examples, it is evident that the velocity increment term represents the effect of the steady state velocity gradient upon the amplification of the shock and a nonlinear effect that is related to the rate of change of amplitude of the shock. The numerical value of the velocity increment term will represent the algebraic sum of the two effects.

The second term on the right hand side of equation 48 is the change in molecular weight effect. The portion of the term $\Delta R/\Delta\tau$ is the rate of change of the gas constant or rate of change of the molecular weight of the mixture due to the chemical reaction. If the gas constant increases, which means that the molecular weight is

decreasing during the chemical reaction, that chemical reaction will contribute to amplifying the shock. The reverse is true if the molecular weight of the mixture decreases as a result of the chemical reaction. The term will be zero if the molecular weight is assumed not to change during the chemical reaction.

There are two terms on the right hand side of equation 48 that are due to the presence of bulk viscosity. The first term can be considered a type of transport of momentum effect and its amplifying or attenuating effect will depend upon the second derivative of velocity with respect to distance. The second viscosity term is a type of dissipation term; it will always have an attenuating effect upon the shock because the second coefficient of viscosity is negative.

There are two heat terms; one is the heat addition due to chemical reaction and the other is heat transfer in the flow direction. The chemical heat addition term is always positive and is the main amplifying effect in the combustion region. The heat transfer acts to redistribute the heat released by the chemical reaction. If no heat were to leave the gases, the net effect of the heat transfer would be zero. However, a portion of the energy released in the combustion region is transferred into the propellant by heat transfer. Because of the heat transferred to the propellant, the net effect of heat transfer in the combustion region will be to attenuate the shock.

The last term on the right hand side of equation 48 is the effect of diffusion upon the amplification of the shock. The effect of diffusion will depend upon the sign of the derivatives of velocity and concentration.

Tables 1, 2, and 3 are presented below to show the order of magnitude of the different terms in equation 48. The tables contain only a representative portion of the data calculated. The complete set of data calculated is presented in Appendix D. The numbers in the tables are the sum over the whole zone width of the incremental values for each of the terms. Since the terms are evaluated on the plus characteristic immediately behind the shock, the net amplification obtained from summing all of the individual effects listed in the tables will vary slightly from the results given for the amplification calculated along the shock path. The tables present values for an initial shock amplitude of 5 psi and combustion pressures of 250, 500, and 1000 psia; and for an initial shock amplitude of 25 psi and a combustion pressure of 250 psia. The results for the forward and return propagation of the shock through the zone are given separately. Table 1 contains the results for the flame zone, Table 2 the results for the induction zone, and Table 3 the results for the decomposition zone. The amplification effect upon the shock of each of the parameters listed at the top of the columns is given in psi. The numbers indicate how much the amplitude of the shock is altered by each effect.

Table 4 is presented below and contains the total effect of each parameter upon the amplification of the shock for the entire combustion region. It represents a summation of Tables 1, 2, and 3. The viscosity and diffusion effects were combined under the title "Miscellaneous."

Table 1

Flame Zone

Numerical Values for the Amplification Parameters*

P_1	Velocity Increment	Viscosity	Heat Addition	Viscous Heat	Heat Transfer	Diffusion	Shock Direction
250 psia Combustion Pressure (p_c)							
5	-1.407	0.099	3.810	-0.002	-0.383	-0.004	Forward
5	-2.354	0.097	3.744	-0.002	-0.378	-0.003	Return
25	-0.345	0.095	4.517	-0.002	-0.368	-0.004	Forward
25	-3.986	0.094	4.405	-0.002	-0.365	-0.002	Return
500 psia Combustion Pressure (p_c)							
5	-1.132	0.095	3.266	-0.002	-0.538	-0.005	Forward
5	-1.926	0.094	3.175	-0.002	-0.534	-0.005	Return
1000 psia Combustion Pressure (p_c)							
5	-0.959	0.091	2.945	-0.001	-0.756	-0.006	Forward
5	-1.576	0.091	2.852	-0.001	-0.753	-0.006	Return

* The amplification effect is given in psi.

Table 2

Induction Zone

Numerical Values for the Amplification Parameters*

P_1	Velocity Increment	Heat Addition	Heat Transfer	Shock Direction
250 psia Combustion Pressure (p_c)				
5	0.428	0.057	0.342	Forward
5	-1.785	0.057	0.334	Return
25	3.910	0.054	0.328	Forward
25	-5.516	0.054	0.321	Return
500 psia Combustion Pressure (p_c)				
5	0.227	0.078	0.464	Forward
5	-1.634	0.078	0.450	Return
1000 psia Combustion Pressure (p_c)				
5	0.005	0.103	0.621	Forward
5	-1.419	0.103	0.594	Return

* The amplification effect is given in psi.

Table 3

Decomposition Zone

Numerical Values for the Amplification Parameters*

P_1	Velocity Increment	Heat Addition	Heat Transfer	Molecular Wt. Change Rate	Shock Direction
250 psia Combustion Pressure (p_c)					
5	1.545	2.230	-0.778	0.780	Forward
5	-3.505	2.143	-0.740	0.749	Return
25	10.978	3.119	-0.733	1.113	Forward
25	-10.861	2.843	-0.706	1.010	Return
500 psia Combustion Pressure (p_c)					
5	1.608	2.090	-1.573	0.729	Forward
5	-2.666	2.014	-1.495	0.701	Return
1000 psia Combustion Pressure (p_c)					
5	1.992	2.024	-3.158	0.704	Forward
5	-1.380	1.955	-3.002	0.680	Return

* The amplification effect is given in psi.

Table 4

Total Combustion Region

Numerical Values for the Amplifi[illegible] Parameters*

P_1	Velocity Increment	Heat Addition	Heat Transfer	Molecular Wt. Change Rate	Miscellaneous	Propellant	Net Effect
250 psia Combustion Pressure (p_c)							
5	-7.088	12.044	-1.605	1.530	0.184	-2.126	2.938
25	-6.541	14.994	-1.524	2.123	0.178	-8.489	0.740
500 psia Combustion Pressure (p_c)							
5	-5.523	10.703	-3.226	1.430	0.175	-2.485	1.074
1000 psia Combustion Pressure (p_c)							
5	-3.338	9.987	-6.454	1.384	0.167	-3.079	-1.333

* The amplification effect is given in psi.

The attenuating effect of the propellant was also included in the table. All of the effects were combined and presented in the last column as "Net Effect."

5.5 Experimental Data

The only experimental data available that can be compared quantitatively with the results of the investigation reported herein is that obtained from Rocketdyne through private communication with Mr. Carl Oberg. That data and a brief description of the experimental procedure employed to obtain them are given in Appendix E. For a combustion pressure of 400 psig and an initial shock amplitude before interaction with the combustion region of 8 psi, the ratio of final amplitude to initial amplitude, P_2/P_1, for two different tests were 1.03 and 1.08. Those two values are plotted as small crosses on Fig. 14.

Other experimental data that may be employed for a qualitative comparison with the theoretical results reported in the previous section are results obtained from T-burner experiments. Reference (20) gives a large quantity of experimental data obtained from burning various propellants under a number of combustion pressures. The result of the amplifying effect of the combustion region upon the pressure oscillation in the combustion chamber is given in the form of a growth rate constant α_g defined as follows:

$$\alpha_g = \frac{\ln (P_2) - \ln (P_1)}{\tau_2 - \tau_1} \tag{49}$$

where P_1 is the amplitude of the oscillation at some time τ_1 and P_2 is the amplitude of the oscillation at some later time τ_2 during the time when the amplitude of the oscillation is growing on successive oscillations. Equation 49 can be rearranged yielding a more convenient form. Thus

$$P_2/P_1 = e^{\alpha_g/\text{frequency}} \tag{50}$$

where P_2/P_1 is the now the ratio of pressure oscillation amplitudes on successive oscillations. Therefore, knowing the frequency of oscillation of the combustion pressure and the growth rate constant, the amplification of the oscillation per cycle can be calculated. Some of the data from reference (42) for frequency and growth rate constants along with the corresponding calculated amplification per cycle, P_2/P_1, are presented in Table 5 for combustion pressures of 200, 400, 800, and 1600 psig. The 200 and 400 psig combustion pressure data were obtained by employing only one-half of a T-burner and exhausting it into a surge tank. The rest of the data was obtained by employing a conventional T-burner with slabs of propellant at each end. In both experimental setups the pressure oscillation was measured by a pressure transducer placed behind the slab of propellant at the end of the motor.

Table 5

T-Burner Amplification Data*

Oscillation Frequency	Growth Rate Constant (α_g)	Calculated Amplification (P_2/P_1)
200 psig Combustion Pressure--surge tank		
10,100	160	1.0159
5,700	120	1.0212
3,450	121	1.0356
2,500	72	1.0292
400 psig Combustion Pressure--surge tank		
10,100	90	1.0089
5,600	71	1.0127
3,500	60	1.0176
2,500	38	1.0153
800 psig Combustion Pressure--double ended		
3,500	25	1.0072
2,550	14	1.0055
1,600 psig Combustion Pressure--double ended		
3,400	4	1.0012

* The frequency of oscillation and the growth rate data were taken from reference (20) for propellant A-1 (approximate composition: 80% AP and 20% PBAA and additives--no aluminum).

6.0 CONCLUSIONS

The results of the present investigation and related experimental data which had been collected were presented in the previous section. The T-burner data presented in Table 5 cannot be compared quantitatively with the results of the present investigation. They do, however, indicate qualitative agreement with the theoretical results. Although it is apparent from the T-burner data presented that those results are frequency dependent, it can be seen that for a given frequency the amplification of the pressure oscillation is a function of combustion pressure and that the amplification per cycle decreases with increasing combustion pressure. That result is in full agreement with the theoretical results as presented in Fig. 14. The amplification per cycle of the oscillation in the T-burner, although smaller, is of the same order of magnitude as the results calculated in the theoretical analysis. The lower value for the T-burner results could be partially attributed to the damping effects of the combustion cavity of the burner. The two results are in disagreement as to the rate at which the shock grows as a function of initial shock amplitude. The T-burner data indicate a constant rate of amplification per cycle of the pressure oscillation independent of oscillation amplitude until just before the maximum amplitude is reached. As is obvious in Fig. 14, the results of the present analysis show that the amplification of the shock is a function of shock amplitude. It may be that

the reflection from the propellant was analyzed in such a way that the attenuation of the larger amplitude shocks by the propellant was too severe. Even if the attenuating effect of the propellant was reduced to zero, however, the results would show a decreasing amplification of the shocks with increasing pulse initial amplitude. If the damping effect of the combustion cavity was included in the present analysis, the two results might show closer agreement on the effect of initial shock amplitude upon amplification.

The data obtained from Rocketdyne (see Appendix E) were taken from an experimental apparatus which closely approximates the model employed in the analysis reported herein. The experimental data obtained from that apparatus should be in good agreement with the theoretical results obtained. Unfortunately, data were available for only one combustion pressure and one initial pulse amplitude. The two points are plotted as crosses in Fig. 14. The two experimental data points were for a combustion pressure of 400 psig and an initial pulse amplitude of 8 psi. It can be seen from the figure that the measured amplification ratio is very close to that calculated theoretically. Interpolating linearly between 250 and 500 psia, the theory would give an amplification ratio of 1.17 compared with the actual measured results of 1.03 and 1.08. Considering the complexity of the theoretical problem being investigated and the difficulty of interpreting the pressure-time traces for the forward and reflected shock--an error of 1/64 of an inch in measuring the amplitude of the shock changes the amplification ratio by ± .05--the two results agree extremely well.

A more important result of the analysis than obtaining the net amplification of the nonuniform shock by the combustion region is the insight into the amplification mechanism of the combustion region which the theoretical investigation gives. Consider individually each of the terms contained on the right hand side of equation 48. Numerical values for the total effect of each of the terms for both the forward and return propagation of the shock in each zone are given in Tables 1 through 3. The data are for an initial pulse amplitude of 5 psi and combustion pressures of 250, 500, and 1000 psia, and for an initial amplitude of 25 psi and combustion pressure of 250 psia. The data are representative of the complete set of data calculated and show the effect of initial pulse amplitude and combustion pressure upon amplification of the shock. The complete set of data is tabulated in Appendix D. Table 4 presents the combination of the three previous tables and presents the data as a whole for the complete combustion region. The attenuation of the shock by the propellant is also included in the aforementioned table.

The first term is the velocity increment term, $(\overline{a\rho})_+ \Delta u$, and represents the effect of the steady state velocity gradient and a nonlinear effect related to amplitude change rate upon the amplification of the shock. The physical significance of the velocity increment term was discussed in detail in Section 5.4. The term is usually positive during the forward propagation and negative during the return as would be expected because the steady state velocity gradient is decreasing in the direction of shock propagation during the forward

motion and increasing upon return. In the flame zone, however, the heat release changes the strength of the shock so rapidly that the velocity increment term is negative during the forward propagation of the shock. The numerical value of the term increases with increasing shock amplitude because a_ρ increases behind the shock with increasing shock amplitude. The net effect of the velocity increment term is usually negative for the combustion region. The net effect might, however, become positive for large amplitude pulses. That is due to the fact that the large amplitude shock has a large plus value for the velocity increment term as it propagates forward; but it is greatly attenuated by the propellant and comes back as a much smaller shock, and as such the negative value for the velocity increment on return is much smaller than the plus forward value. If the amplitudes of the forward and return shocks are of about the same magnitude, the velocity increment term is negative.

The second term, the molecular weight change rate term, $\overline{(\rho T \frac{\Delta R}{\Delta \tau})}_+ \triangle \tau$, will occur only in the decomposition zone where the mass of the gas is assumed to be changed by the chemical reaction. The portion of the term $\Delta R/\Delta \tau$ is the rate of change of the gas constant for the mixture and is proportional to the negative of the time rate of change of the molecular weight of the mixture. As can be seen from Table 4, the molecular weight change rate effect is important. The molecular weight change rate effect will always amplify the shock if the molecular weight decreases as a result of the chemical reaction and vice versa. The amplifying effect increases with increasing shock

strength because the portion $\rho\bar{T}$ of the change rate term behind the shock increases with increasing shock amplitude. Also it can be stated that the larger the molecular weight change during the chemical reaction the larger the effect of the molecular weight change rate term.

Next, the two viscosity terms and the diffusion term will be considered as a group. As can be seen from an inspection of Table 1, all of those terms are of higher order. It was difficult to assign accurate values to the second coefficient of viscosity and the diffusion coefficient employed in the calculation of the three aforementioned terms. It is doubtful, however, that the values assigned are off by more than an order of magnitude. If the error was that large the contribution of the three terms would still not be important. It can safely be said that the diffusion and viscous effects could be neglected in any future analysis without introducing any appreciable amount of error.

The next term to be considered is the heat addition term. As can be seen from Table 4, it is the main effect by which the combustion region amplifies the shock. It is noted that the heat addition is not a very strong function of combustion pressure. Although the combustion rate increases with increasing combustion pressure, the width of the zone decreases so that the residence time of the shock in the zone decreases. As noted in equation 48, the heat addition rate is multiplied by the residence time of the shock in the increment,

$\Delta\tau$. The increased reaction rate and the decreased residence time just about compensate each other. Table 4 shows that the shock amplitude has a marked influence upon the amplifying effect of the heat addition. The larger the amplitude of the shock, the higher the temperature and density behind the shock which in turn produce a higher chemical reaction rate. The relaxation time for the chemical reaction was assumed to be zero for the calculation. If the relaxation time were assumed to be infinite, the heat addition term would decrease with increasing shock amplitude. That is because the reaction rate would be constant but the residence time would decrease as the shock amplitude, and hence its propagation speed, increased. The aforementioned observation would indicate then that the propellants with short chemical relaxation times should be more susceptible to combustion pressure oscillation than propellants with longer chemical relaxation times.

Another point to notice is that the chemical heat addition term is multiplied by the expression $(\gamma-1)$. That term came from the general character of the equations and not from any assumptions about the chemical processes. Therefore, the observation can be made that propellants which yield combustion region gases with a specific heat ratio close to unity should be more stable than propellants which yield gases with specific heat ratios much larger than unity. The above observation might help to explain why the addition of aluminum to a solid propellant helps to eliminate combustion pressure oscillation even though the aluminum increases the heat release rate. Although

the definition of the specific heat ratio of the combustion products of a propellant containing aluminum may be open to argument, reference (32) shows that the addition of about 20 per cent by weight of aluminum to a propellant reduces the factor $(\gamma-1)$ by about 20 per cent. Therefore, although the addition of aluminum to the propellant increased the heat release rate in the combustion region, the effectiveness of the heat release upon amplifying any pressure disturbances was reduced.

The last term to be considered is the heat transfer term $(\gamma-1)(k\frac{\partial^2 T}{\partial x^2})_+ \Delta\tau$. That term acts mainly to redistribute the effect of the chemical heat addition. An inspection of Tables 1 through 3 indicates the following: (1) In the flame zone the heat transfer effect upon amplification of the pulse is negative because a portion of the heat from the flame zone is transferred into the induction zone. (2) In the induction zone the heat transfer effect is positive because that zone receives more heat from the flame zone than it transmits into the decomposition zone. (3) In the induction zone the amplifying effect is about equal to the attenuating effect in the flame zone. (4) In the decomposition zone the heat transfer is negative because a large amount of heat is transferred into the propellant. Table 4 shows that the net effect of the heat transfer is to attenuate the shock, which is due to the loss of heat into the propellant. As the combustion pressure increases the reaction rate increases and the gradients in the zones of the combustion region become steeper. The heat transfer rate to the propellant increases

and so the attenuating effect of the heat transfer increases.

In addition to a summation of the numbers listed in Tables 1, 2, and 3, Table 4 contains the attenuating effect of the propellant. As can be seen, the attenuating effect of the propellant increases as the combustion pressure increases and as the pulse amplitude increases.

It is evident from Table 4 that the decrease in shock amplification with increase in combustion pressure results from the attenuating effect of the propellant. The attenuation by the propellant is accomplished in two ways: 1) the attenuation of the shock upon reflection from the propellant surface and 2) the attenuating effect of the heat transfer into the propellant. Both of the effects increase with increasing combustion pressure. The latter effect results because the heat transfer into the propellant increases with increasing combustion pressure. The attenuating effect of the heat transfer is a function of the heat transfer per unit volume not per unit mass of flowing combustion gases.

An inspection of Table 4 indicates that whether the shock is amplified or attenuated is determined by a balance between (1) the amplifying effects of the chemical heat addition and molecular weight change during chemical reaction, (2) the attenuating effects of heat transfer and the propellant as the pulse reflects from it, and (3) the amplifying or attenuating effect of the velocity gradient immediately behind the shock. The other effects are all higher order quantities. Under most circumstances the velocity gradient term will be an attenuating effect; therefore, whether or not the shock is amplified hinges upon

whether or not the heat release rate and the rate of change of the molecular weight in the combustion region are high enough.

The analysis reported herein would indicate that the more efficient a combustion chamber is, i.e., the higher the energy release rate per unit volume, the more susceptible the chamber will be to combustion pressure oscillation. The only possible solutions to the oscillation problem since the efficiency cannot be sacrificed is to add some type of damper in the combustion chamber such as baffles or acoustic liners; or in some way, either by putting additives in the propellant or by formulating a new propellant, reduce the specific heat ratio of the combustion gases. One other possible solution available if the present analysis is correct is to redesign the system to operate at a higher combustion pressure.

7.0 FUTURE PROGRAM

Unless some new and impressive ideas are presented, very little new information concerning combustion pressure oscillation will be gained from further investigations employing acoustic theory. In order to obtain more information, new theoretical work in the area of combustion pressure oscillation will have to employ nonacoustic methods of analysis. The present investigation is only an initial step into the field of nonacoustic theories for the study of the oscillation. The present work can be improved and extended, and the method of analysis employed herein can be applied to the study of other combustion pressure oscillation problems. In addition to further analytical work, an experimental program could be initiated to give experimental data with which to compare the analytical results. Some possible extensions of the present work will be given followed by other suggested areas which might be investigated. The order in which the ideas are presented does not necessarily indicate the order of importance or the order in which the work should be performed.

7.1 Extension of the Present Program

Future work related to the present program would involve improving and extending the results reported herein. The results can be improved by obtaining a more rigorous solution for the steady state conditions

in the flame and decomposition zones of the combustion region. In the present analysis the temperature and concentration profiles were approximated by polynomials which satisfied prescribed boundary conditions at the ends of the zones. One way of obtaining a more rigorous solution is to numerically integrate the steady state conservation equations. Once a more rigorous steady state solution is obtained, the present analysis can be extended to include the investigation of the influence of the total heat addition in the combustion region upon amplification of the shock. The numerical values for the physical and transport properties in the combustion region could also be varied. The effect of an infinite or some intermediate relaxation time for the chemical combustion rate could also be studied. A combustion region containing solid particles could be postulated so the attenuating effect of aluminum powder added to the solid propellant could be studied. However, because of the complexity of the problem it is doubtful that any meaningful results could be obtained.

7.2 Programs in Related Areas

The present method of analysis could be employed to study the interaction of a pressure disturbance with the combustion region of a premixed gaseous propellant. The burning surface of the propellant would be replaced by a constant mass source, reflecting wall which would approximate the premixed gas injector; and the decomposition zone would be dropped from the model of the combustion region. If a simple fuel and oxidizer are assumed in the analysis, such as hydrogen

and air or hydrogen and oxygen, the analysis of a premixed gaseous combustion region has the advantage that the combustion kinetics for the aforementioned mixtures are well understood and the physical and transport properties for the gases have been accurately determined. It is, therefore, possible to assign accurate values to the physical and transport properties. Also, because of the reduced complexity of the problem, it should be possible to develop an experimental program which closely approximates the model employed in the theoretical analysis. The pulsing could be performed by using a shock tube, and some of the difficulties involved in measuring the amplitude of the incident and reflected shock may be overcome by using the method employed by Rocketdyne (see Appendix E)(21) for measuring shock amplitudes.

With a less complex model for the combustion region it may be possible to improve the model for the pressure disturbance. Instead of employing a nonuniform shock for the pressure disturbance and treating it as the propagation of a normal shock, the rarefaction backside of the shock could be included in the calculation. A differently shaped pressure disturbance could also be employed in the analysis such as one-half of a sine wave, a triangular wave, or some other similar shape. Employing an improved model for the pressure disturbance would make it possible to check experimental data reported in reference (22). In experiments with a nonuniform shock wave interacting with a gaseous combustion region it was observed that, after the interaction, compression waves emanated from the combustion region--probably due to an increase in combustion rate--and caught up with the shock. It was

the compression waves catching up with the shock that produced most of the amplification of the shock. The appearance of the compression waves after the interaction indicates that relaxation times have a part to play in the interaction.

Another area of investigation to be considered in the light of the experimental procedure which has recently come into wide-spread practice of "bombing" motors to test susceptibility to combustion pressure oscillation is a program which would study the effect of pulse shape and energy upon the amplification of the pulse by a premixed gaseous combustion region. It may even be possible to extend the analysis to a series of pulses interacting with the combustion region. A parallel experimental program could also be initiated which would approximate the work being done analytically. The two programs carried on simultaneously may produce new useful information concerning the shape and amplitude of the pulse that is most likely to trigger combustion pressure oscillation.

Combustion pressure oscillation in liquid propellant rocket motors could also be investigated by the method reported herein. For the liquid motor, the solid propellant in the present analysis would be replaced by a constant mass source, reflecting wall. The evaporation of the propellant droplets could be approximated by a plane source function which is a function of selected flow parameters. The increased droplet breakup due to an interaction of the shock with the combustion region could be approximated by making the source function simulating evaporation also depend upon the pressure gradient. It may be possible

to include a damping effect for the droplets upon the pressure disturbance. The aforementioned investigation could also be coordinated with an experimental program similar to that mentioned for a premixed gas investigation. It would be much more difficult to correlate analytical results with experimental findings due to the increased complexity of the processes occurring. It may be worthwhile undertaking this type of investigation, however, because it is with the liquid propellant rocket motor that the most problems are encountered involving combustion pressure oscillation.

A study of the effect of pulse shape and energy, similar to that outlined for the gaseous combustion region, upon the triggering of combustion pressure oscillation could also be initiated. However, the program may have to be limited to experimental work because the analytical problem may be too complex.

8.0 NOMENCLATURE

Symbol	Concept	Dimension
a	Acoustic Velocity	L/τ
a_p	Velocity of Propagation of the Wave through the Propellant	L/τ
c_p	Heat Capacity, Constant Pressure	FL/MT
c_v	Heat Capacity, Constant Volume	FL/MT
D	Binary Diffusion Coefficient	L^2/τ
E	Activation Energy	FL/M
E_i	Internal Energy of i-th Species	FL/M
f	Mole Fraction	None
F	Force	F
g	Standard Acceleration of Gravity	L/τ^2
k	Thermal Conductivity	$F/T\tau$
k_T	Thermal Diffusion Ratio	None
m	Mass	M
M	Molecular Weight	None
Ma	Mach Number	None
$\dot{m}$	Mass Flow Rate	M/τ
p	Static Pressure	F/L^2
p_c	Combustion Pressure	F/L^2
P	Amplitude of the Shock	F/L^2

Symbol	Concept	Dimension
Q	Heat Transfer Function	$F/\tau L$
Q_{cc}	Heat Release Function	$F/L^2\tau$
R	Gas Constant	FL/MT
R_o	Universal Gas Constant	FL/MT
r	Rate at which Propellant Burns	L/τ
r_p	Pressure Ratio Across a Normal Shock	None
S	Slope of Stress-Strain Curve for the Propellant	F/L^2
SE	Energy Source	$FL/M\tau$
SM	Momentum Source	ML/τ^2
T	Static Temperature	T
U	Heat of Reaction	FL/M
u	Velocity	L/τ
v	Diffusion Velocity	L/τ
x	Coordinate Along Nozzle Axis	L
Y	Concentration	None
α	Combination Frequency-Steric Factor	$1/\tau$
γ	Specific Heat Ratio	None
ϵ	Strain Per Unit Length	None
η	Second Coefficient of Viscosity	$M/L\tau$
λ	Characteristic Direction	L/τ
μ	First Coefficient of Viscosity	$M/L\tau$
ρ	Density	M/L^3
σ_{kj}	Stress Tensor	F/L^2

Symbol	Concept	Dimension
τ	Time	τ
ω_i	Rate of Production of i-th Species	$M/\tau L^3$

Notation

$\overline{\quad}$	Bar over symbol indicates the average value
i	Subscript "i" indicates the i-th species
Δ	Indicates increment along the characteristic line defined by $d\tau/dx = 1/u$
$\overset{+}{\Delta}$	Indicates increment along the characteristic line defined by $d\tau/dx = 1/(u+a)$
$\overset{-}{\Delta}$	Indicates increment along the characteristic line defined by $d\tau/dx = 1/(u-a)$
$(\overline{\quad})$	Average value taken along the characteristic line defined by $d\tau/dx = 1/u$
$(\overline{\quad})_+$	Average value taken along the characteristic line defined by $d\tau/dx = 1/(u+a)$
$(\overline{\quad})_-$	Average value taken along the characteristic line defined by $d\tau/dx = 1/(u-a)$

Operators

$$\frac{\delta+}{\delta\tau} = \frac{\partial}{\partial\tau} + (u + a)\frac{\partial}{\partial x}$$

$$\frac{\delta-}{\delta\tau} = \frac{\partial}{\partial\tau} + (u - a)\frac{\partial}{\partial x}$$

$$\frac{D}{D\tau} = \frac{\partial}{\partial\tau} + u\frac{\partial}{\partial x}$$

$$\nabla = \underset{\sim}{i}\frac{\partial}{\partial x} + \underset{\sim}{j}\frac{\partial}{\partial y} + \underset{\sim}{k}\frac{\partial}{\partial z}$$

BIBLIOGRAPHY

9.0 BIBLIOGRAPHY

1. Technical Panel on Solid Propellant Instability of Combustion-Scientific Papers 1960-1963, The Johns Hopkins University, Applied Physics Laboratory, Silver Spring, Md., 1964.

2. Sirignano, W. A., Crocco, L., "A Shock Model of Unstable Rocket Combustors," AIAA Journal, Vol. 2, No. 7, pp. 1285-1296.

3. Brownlee, W. G., "Nonlinear Axial Combustion Instability in Solid Propellant Rocket Motors," AIAA Journal, Vol. 2, No. 2, pp. 215-284.

4. Chisnell, R. F., "The Normal Motion of a Shock Wave Through a Nonuniform One-Dimensional Medium," Royal Society of London Proceedings, Vol. 232, No. 1190, pp. 350-370.

5. Knudsen, J. R., "The Effects of Viscosity and Heat Conductivity on the Transmission of Plane Sound Pulses," The Journal of the Acoustical Society of America, Vol. 26, No. 1, pp. 51-57.

6. Whitham, G. B., "On the Propagation of Shock Waves Through Regions of Nonuniform Area or Flow," Journal of Fluid Mechanics, Vol. 4, pp. 337-360.

7. Rudinger, G., Wave Diagrams for Unsteady Flow in Ducts, D. Van Nostrand Co., Inc., New York, 1955.

8. Paterson, S., "The Reflection of a Plane Shock Wave at a Gaseous Interface," Physical Society of London, Vol. 61, No. 2, pp. 119-121.

9. Rudinger, G., "Shock Wave and Flame Interactions," Combustion and Propulsion (Third AGARD Colloquium), Butterworth's Scientific Publications, London, pp. 153-182, 1958.

10. Polachek, H., and Seeger, R. J., "On Shock-Wave Phenomena; Refraction of Shock Waves at a Gaseous Interface," Physical Review, Vol. 84, No. 5, pp. 922-929.

11. Courant, R., and Friedrichs, K. O., Supersonic Flow and Shock Waves, Interscience, New York, 1948.

12. Lehmann, G. M. and Murthy, S. N. B., "Interaction of a Weak Shock with a Combustion Region," Journal of Spacecraft and Rockets, pp. 828-830, Volume 2, No. 5, Sept.-Oct., 1965.

13. Price, E. W., "Combustion Instability in Solid Propellant Rockets," ARS Paper No. 1492-60, ARS 15th Annual Meeting, Washington, D. C., December 5-8, 1960.

14. Summerfield, M., and Suterland, G. S., "Burning Mechanism of Ammonium Perchlorate Propellants," Solid Propellant Rocket Research, pp. 141-182, Academic Press, New York, 1960.

15. Kantrowitz, A., "One-Dimensional Treatment of Nonsteady Gas Dynamics," High Speed Aero-Dynamics and Jet Propulsion, Volume III, pp. 350-415, Princeton University Press, Princeton, 1958.

16. Davids, N., Kumar, S., "A Contour Method for One-Dimensional Pulse Propagation in Elastic-Plastic Materials," Proceedings 3rd U. S. Congress of Applied Mechanics, pp. 503-512, 1958.

17. Zucrow, M. J., Aircraft and Missile Propulsion, Volume II, John Wiley and Sons, Inc., New York, 1958.

18. Agosta, V., "Shock Wave Interaction with a Burning Propellant," Presented at Third Meeting of the Technical Panel on Solid Propellant Combustion Instability, March 4-6, 1963.

19. Shapiro, A. H., The Dynamics and Thermodynamics of Compressible Fluid Flow, Volumes I and II, Ronald Press, New York, 1953.

20. Horton, M. D., "Testing the Dynamic Stability of Solid Propellants: Technique and Data," U. S. Naval Test Station, China Lake, Calif., August, 1964.

21. Huebner, A. L., Coltas, T. A., "Response of a Burning Solid Propellant to Pressure Waves of Finite Amplitude," Rocketdyne Report No. R-6213, June, 1965.

22. Salamandra, G. D., and Sevastyanova, I. K., "Formation of Weak Shock Waves Ahead of a Flame Front and Their Intensitifcation during Passage through the Flame," Combustion and Flame, pp. 169-174, Volume 7, June 1963.

23. Penner, S. S., and Mullins, B. P., Explosions, Detonations, Flammability and Ignition, Agardograph No. 31, Pergamon Press, New York, 1959.

24. Pai, S., Magnetogasdynamics and Plasma Dynamics, Prentice-Hall, Inc., Englewood Cliffs, New Jersey, 1962.

25. Schlichting, H., Boundary Layer Theory, McGraw Hill, New York, 1960.

26. Tsien, H. S., "The Equations of Gas Dynamics," High Speed Aerodynamics and Jet Propulsion, Volume III, pp. 3-63; Princeton University Press, Princeton, 1958.

27. Levy, J. B., and Friedman, R., "Further Studies of Pure Ammonium Perchlorate Deflagration," Eighth Symposium (International) on Combustion, pp. 633-672, The Williams and Wilkins Company, Baltimore, 1962.

28. Kuratanic, K., "Kinetics of Thermal Decomposition of Ammonium Perchlorate," Aeronautical Research Institute, University of Tokyo, Volume 28, No. 4, Report No. 372, July 1962.

29. Gross, D., Amster, A. B., "Thermal Explosions: Adiabatic Self-Heating of Explosives and Propellants," Eighth Symposium (International) on Combustion, The Williams and Wilkins Company, Baltimore, 1962.

30. Nachbar, W., and Williams, F. A., "On the Analysis of Linear Pyrolysis Experiments," Ninth Symposium (International) on Combustion, The Williams and Wilkins Company, Baltimore, 1963.

31. Powling, J. and Smith, W. A. W., "The Surface Temperature of Burning Ammonium Perchlorate." Combustion and Flame, Volume 7, pp. 269-275, December 1963.

32. Chemical Propulsion Information Agency, Propellant Manual SPIA/M2, Compiled by the Johns Hopkins University, Applied Physics Laboratory, Silver Spring, Md., Confidential.

33. Reid, R. C., and Sherwood, T. K., The Properties of Gases and Liquids, McGraw-Hill, New York, 1958.

34. Suehla, R. A., "Estimated Viscosities and Thermal Conductivities of Gases at High Temperatures," NASA Technical Report No. TR-R-132, 1962.

35. Penner, S. S., Chemical Reactions in Flow Systems, Agardograph No. 7, Butterworths, London, 1955.

36. Royal Society of London Proceedings, Volume 226 A, pp. 1-69, October 21, 1954.

37. Nettleton, R. E., "Intrinsic Bulk Viscosity in Monatomic and Diatomic Gases," Journal of Applied Physics, Volume 29, No. 2, pp. 204-212, 1958.

38. Hirschifelder, J. O., Curtiss, C. F., and Bird, R. B., Molecular Theory of Gases and Liquids, John Wiley and Sons, Inc., New York, 1954.

39. Price, E. W., Mathes, J. E., Crump, J. D., and McGie, M. R., "Experimental Research in Combustion Instability of Solid Propellants," Combustion and Flame, pp. 149-157, June 1961.

40. Price, E. W., "Analysis of Results of Combustion Instability Research on Solid Propellants," ARS Paper No. 1068-60, Presented at the Solid Propellant Rocket Research Conference, Princeton University, Princeton, January 1960.

41. Thompson, H. D., "Analysis of Three-Dimensional Flow in Rocket Motor Nozzles," Purdue University, Jet Propulsion Center, Report No. TM-64-1, February, 1964.

APPENDICIES

APPENDIX A

DERIVATION OF THE CONSERVATION EQUATIONS AND THE EQUATION OF STATE

The conservation equations for two-component gas mixtures can be found throughout the literature in different forms depending upon the assumptions made during their derivation. In the pages that follow, the conservation equations for a two-component gas mixture will be derived making assumptions which yield a system of conservation equations appropriate for analyzing the processes occurring in the combustion region of a rocket motor. The equations will be derived for one-dimensional, unsteady flow from the macroscopic point of view employing continuum theory. The effects of body forces and the first coefficient of viscosity will be neglected in the derivation. Equations for the gross properties of the medium will be obtained from the species equations by assuming simultaneous independent occupation of the same volume by each species; a method termed the Shavb-Zeldovich method by Penner (23). The utilization of the Shavb-Zeldovich method is illustrated in detail in Reference (24), Chapter 2, in the development of the conservation equations for magnetogasdynamics.

In deriving the conservation equations, it will be assumed that the physical and transport properties are not functions of the flow

properties, such as static temperature T and static pressure p. The effect of temperature and pressure upon the transport properties thermal conductivity k, diffusion coefficient D, and second coefficient of viscosity η will, however, be taken into account by employing calculated values evaluated at the local flow condition; the equations employed for calculating the appropriate values of k, D, and η are presented in Appendix B.

Conservation of Mass

The conservation of mass equation for each species can be written (23)

$$\frac{\partial \rho_i}{\partial \tau} + \frac{\partial \rho_i u_i}{\partial x} = \omega_i \qquad i = 1,2 \qquad (A-1)$$

where

ρ_i = density of the i-th species,

u_i = velocity of the i-th species, and

ω_i = the source function for the i-th species.

Letting i equal 1 and then 2 in equation A-1 and adding the two equations together gives

$$\frac{\partial}{\partial \tau}(\rho_1 + \rho_2) = \frac{\partial}{\partial x}(\rho_1 u_1 + \rho_2 u_2) = \omega_1 + \omega_2 = 0 \qquad (A-2)$$

The following gross properties are now defined:

$$\rho \equiv \rho_1 + \rho_2$$
$$\rho u = \rho_1 u_1 + \rho_2 u_2 \qquad (A-3)$$
$$u \equiv u_i - v_i$$

where

v_i = the diffusion velocity of the i-th species.

Employing the definitions given by equation A-3 the following result can be obtained:

$$\rho_1 v_1 + \rho_2 v_2 = 0 \tag{A-4}$$

Equation A-2 can now be written in terms of gross properties

$$\frac{\partial \rho}{\partial \tau} + \frac{\partial \rho u}{\partial x} = 0 \tag{A-5}$$

Note that the above equation is identical with the conservation of mass equation for a single component system.

Equation A-1, the conservation equation for species one and two, may be written in a different form for species one by employing equation A-3 and introducing the concentration $Y \equiv \rho_1/\rho$. Thus

$$\frac{\partial \rho Y}{\partial \tau} + \frac{\partial \left[\rho Y (u + v_1)\right]}{\partial x} = \omega_1 \tag{A-6}$$

Expanding equation A-6,

$$Y \left(\frac{\partial \rho}{\partial \tau} + \frac{\partial \rho u}{\partial x}\right) + \rho \left(\frac{\partial Y}{\partial \tau} + u \frac{\partial Y}{\partial x}\right) + \frac{\partial}{\partial x} (\rho Y v_1) = \omega_1 \tag{A-7}$$

Employing equation A-5,

$$\frac{\partial Y}{\partial \tau} + u \frac{\partial Y}{\partial x} = 1/\rho \left[\omega_1 - \frac{\partial}{\partial x} (\rho Y v_1)\right] \tag{A-8}$$

Equation A-8 is the mass conservation equation for species one.

Conservation of Momentum

The momentum equation is derived by starting with Newton's second law of motion in one dimension (19)

$$\sum F_i = \frac{D}{D\tau} (m_i u_i) \qquad \text{(A-9)}$$

where

$\frac{D}{D\tau} \equiv \frac{\partial}{\partial\tau} + u_i \frac{\partial}{\partial x}$ and the subscript i refers to the i-th species.

Writing equation A-9 in an expanded form,

$$\sum F_{i_E} + \sum F_{i_I} = m_i \frac{D}{D\tau}(u_i) + u_i \frac{D}{D\tau} (m_i) \qquad \text{(A-10)}$$

where

$\sum F_{i_I}$ = the sum of all forces of the i-th species acting on itself, and

$\sum F_{i_E}$ = the sum of all forces which arise due to interaction of the other species with the i-th species.

Equation A-10 can be rearranged to the form

$$\sum F_{i_I} = m_i \frac{D}{D\tau} (u_i) + \left[u_i \frac{D}{D\tau} (m_i) - \sum F_{i_E}\right] \qquad \text{(A-11)}$$

The terms inside the bracket in equation A-11 are momentum source terms. The first term represents the generation of momentum due to the production of the i-th species through chemical reaction, and the second term represents the generation of momentum due to interaction with the

other species. It is assumed that all the interactions between species take place through collisions; and, since momentum is conserved during collisions,

$$\sum_{i=1}^{n} \left[u_i \frac{D}{D\tau} (m_i) - \sum F_{i_E} \right] \equiv \sum_{i=1}^{n} SM_i = 0 \qquad \text{(A-12)}$$

Equation A-11 can be rewritten

$$\sum F_{i_I} = m_i \frac{D}{D\tau} (u_i) + SM_i \qquad \text{(A-13)}$$

If the last term were not present, equation A-13 would be identical to the equation from which the Navier-Stokes equation for a single-component gas is derived. The Navier-Stokes equation in one dimension taking into account the second but not the first coefficient of viscosity and neglecting body forces is (25)

$$\frac{\partial \rho_i u_i}{\partial \tau} + \frac{\partial \rho_i u_i^2}{\partial x} = \eta_i \frac{\partial^2 u_i}{\partial x^2} - \frac{\partial p_i}{\partial x} \qquad \text{(A-14)}$$

where

η_i = the second coefficient of viscosity of the i-th species.

Substituting equation A-14 for the first two terms of equation A-13 the momentum equation for the i-th species is obtained.

$$\frac{\partial \rho_i u_i}{\partial \tau} + \frac{\partial \rho_i u_i^2}{\partial x} = \eta_i \frac{\partial^2 u_i}{\partial x^2} - \frac{\partial p_i}{\partial x} + SM_i \qquad \text{(A-15)}$$

Letting i equal 1 and 2 in equation A-15 and adding the two equations together,

$$\frac{\partial}{\partial \tau}(\rho_1 u_1 + \rho_2 u_2) + \frac{\partial}{\partial x}(\rho_1 u_1^2 + \rho_2 u_2^2) + \frac{\partial}{\partial x}(p_1 + p_2) = \tag{A-16}$$

$$\eta_1 \frac{\partial^2 u_1}{\partial x^2} + \eta_2 \frac{\partial^2 u_2}{\partial x^2}$$

Defining an additional gross property, the static pressure p,

$$p = p_1 + p_2 \tag{A-17}$$

and substituting equations A-3 and A-17 into equation A-16 and collecting terms,

$$\frac{\partial \rho u}{\partial \tau} + \frac{\partial \rho u^2}{\partial x} + \frac{\partial p}{\partial x} = \eta_1 \frac{\partial^2 u_1}{\partial x^2} + \eta_2 \frac{\partial^2 u_2}{\partial x^2} - \frac{\partial}{\partial x}(\rho_1 v_1^2 + \rho_2 v_2^2) \tag{A-18}$$

By making the following definition

$$\eta \frac{\partial^2 u}{\partial x^2} \equiv \eta_1 \frac{\partial^2 u_1}{\partial x^2} + \eta_2 \frac{\partial^2 u_2}{\partial x^2} - \frac{\partial}{\partial x}(\rho_1 v_1^2 + \rho_2 v_2^2) \tag{A-19}$$

equation A-18 becomes

$$\frac{\partial \rho u}{\partial \tau} + \frac{\partial \rho u^2}{\partial x} + \frac{\partial p}{\partial x} = \rho \frac{Du}{D\tau} + \frac{\partial p}{\partial x} = \eta \frac{\partial^2 u}{\partial x^2} \tag{A-20}$$

Conservation of Energy

In the development of the energy equation a closed system is selected for making the energy balance; hence, the integral approach is employed. The energy balance equation for the i-th species in integral form is (26)

$$\frac{D}{D\tau}\int_{Vol.} \rho_i E_i d\,(Vol.) = -\int_{Surf.} \underset{\sim}{Q_i} \cdot d\,\underset{\sim}{(Surf.)} + \int_{Surf.} \delta\,Work_i + \int_{Vol.} \rho_i\,(SE_i)\,d(Vol.) \qquad \text{(A-21)}$$

where

E_i = the internal energy of the i-th species,

$\underset{\sim}{Q_i}$ = the rate of heat transfer to the i-th species (a vector quantity), and

SE_i = the energy source related to the i-th species. The surface work can be expressed in terms of the stress tensor

$$-\int_{Surf.} \delta\,Work_i = \int_{Surf.} \underset{\sim}{(\sigma_{kj}\,u_j)_i} \cdot d\,\underset{\sim}{(Surf.)} \qquad \text{(A-22)}$$

where

σ_{kj} = the stress tensor.

Employing Gauss's Theorem from vector analysis, the surface integrals in equation A-21 can be written in terms of volume integrals

$$\int_{\text{Surf.}} \underset{\sim}{Q_j} \cdot d\,(\text{Surf.}) = \int_{\text{Vol.}} \nabla \cdot \underset{\sim}{Q_i}\, d(\text{Vol.})$$

(A-23)

$$\int_{\text{Surf.}} \underset{\sim}{(\sigma_{kj} u_j)_i} \cdot d\,(\text{Surf.}) = \int_{\text{Vol.}} \nabla \cdot (\sigma_{kj} u_j)_i\, d\,(\text{Vol.})$$

Taking the total derivative of the first term of equation A-21 and substituting the above relations into Equation A-21 the following equation is obtained:

$$\int_{\text{Vol.}} \left[\frac{\partial \rho_i E_i}{\partial \tau} + u_i \frac{\partial \rho_i E_i}{\partial x} + E_i \rho_i \frac{\partial u_i}{\partial x}\right] d\,(\text{Vol.}) =$$

(A-24)

$$\int_{\text{Vol.}} \left[- \nabla \cdot \underset{\sim}{Q_i} + \nabla \cdot \underset{\sim}{(\sigma_{kj} u_j)_i} + \rho_i\,(SE_i)\right] d\,(\text{Vol.})$$

Equating integrands and reducing the different terms to one dimension,

$$\frac{\partial \rho_i E_i}{\partial \tau} + u_i \frac{\partial \rho_i E_i}{\partial x} + E_i p_i \frac{\partial u_i}{\partial x} = - \frac{\partial Q_i}{\partial x} + \frac{(\sigma_k u)_i}{\partial x} + \rho_i\,(SE_i)$$

(A-25)

The energy equation is obtained for the gross properties of the gas by letting i equal 1 and 2 in equation A-25 and adding the two equations together. By noting

$$(\sigma_k u)_i = - u_i p_i + u_i \eta_i \frac{\partial u_i}{\partial x} \quad \text{Reference (25)} \qquad \text{(A-26)}$$

$$\sum_{i=1}^{2} \rho_i \, (SE_i) = 0 \tag{A-27}$$

and

$$E_i = \frac{u_i^2}{2} + c_{v_i} \, T + e_{c_i} \tag{A-28}$$

where

e_{c_i} = the chemical energy of the i-th species, and making the following definitions,

$$\rho \, c_v \equiv \rho_1 \, c_{v_1} + \rho_2 \, c_{v_2}$$

$$U \equiv e_{c_1} - e_{c_2} = \text{constant} \tag{A-29}$$

$$Y \equiv \rho_1/\rho$$

$$Q \equiv Q_1 + Q_2$$

the sum of the two equations becomes

$$\frac{\partial}{\partial \tau} \left(\frac{\rho_1 u_1^2}{2} + \frac{\rho_2 u_2^2}{2} + \rho \, c_v \, T + Y \, U\right) + \frac{\partial}{\partial x} \left[\rho_1 u_1 \left(\frac{u_1^2}{2} + c_{v_1} \, T + e_{c_1}\right)\right.$$

$$\left. + \rho_2 u_2 \left(\frac{u_2^2}{2} + c_{v_2} \, T + e_{c_2}\right)\right] = - \frac{\partial Q}{\partial x} \tag{A-30}$$

$$- \frac{\partial}{\partial x} (u_1 p_1 + u_2 p_2) + \frac{\partial}{\partial x} \left(u_1 \eta_1 \frac{\partial u_1}{\partial x} + u_2 \eta_2 \frac{\partial u_2}{\partial x}\right)$$

Expanding equation A-30 and collecting terms,

$$\frac{\partial}{\partial\tau}\left[\frac{\rho u^2}{2} + u\,(\rho_1 v_1 + \cancelto{0}{\rho_2 v_2}) + \frac{\rho_1 v_1^2}{2} + \frac{\rho_2 v_2^2}{2} + \rho\, c_v\, T + \rho\, Y\, U\right]$$

$$+ \frac{\partial}{\partial x}\left[\rho\,\frac{u^3}{2} + \frac{3}{2}\,u\,(\rho_1 v_1 + \rho_2 v_2^2) + u\,\rho\,c_v\,T + u\,\rho\,Y\,U\right.$$

$$\left. + \frac{\rho_1 v_1^3}{2} + \frac{\rho_2 v_2^3}{2} + \rho_1 v_1 c_{v_1} T + \rho_2 v_2 c_{v_2} T + \rho_1 v_1 e_{c_1} + \rho_2 v_2 e_{c_2}\right.$$

$$\left. + \frac{3}{2}u^2\,(\rho_1 v_1 + \cancelto{0}{\rho_2 v_2})\right] = \frac{\partial}{\partial x}\left[-Q - pu - p_1 v_1\right. \qquad \text{(A-31)}$$

$$\left. - p_2 v_2 + u\,(\eta_1 \frac{\partial u_1}{\partial x} + \eta_2 \frac{\partial u_2}{\partial x}) + v_1 \eta_1 \frac{\partial u_1}{\partial x} + v_2 \eta_2 \frac{\partial u_2}{\partial x}\right]$$

Employing equation A-5, equation A-31 becomes

$$\rho u \frac{Du}{D\tau} + \rho\, c_v \frac{DT}{D\tau} + \rho\, U \frac{DY}{D\tau} + \frac{\partial}{\partial\tau}\left[\frac{\rho_1 v_1}{2}(v_1 - v_2)\right]$$

$$+ \frac{\partial}{\partial x}\left[\frac{u}{2}(\rho_1 v_1^2 + \rho_2 v_2^2) + \frac{\rho_1 v_1}{2}(v_1^2 - v_2^2) + \rho_1 v_1 (c_{v_1} T + \frac{p_1}{\rho_1})\right.$$

$$\left. + \rho_2 v_2 (c_{v_2} T + \frac{p_2}{\rho_2}) + \rho_1 v_1 U\right] = \qquad \text{(A-32)}$$

$$\frac{\partial}{\partial x}\left[-Q + u\,(\eta_1 \frac{\partial u_1}{\partial x} + \eta_2 \frac{\partial u_2}{\partial x} - \rho_1 v_1^2 - \rho_2 v_2^2)\right.$$

$$\left. - pu + v_1 \eta_1 \frac{\partial u_1}{\partial x} + v_2 \eta_2 \frac{\partial u_2}{\partial x}\right]$$

Equation A-32 can be further reduced by utilizing equation A-20

$$\rho\, c_v \frac{DT}{D\tau} + \rho\, U \frac{DY}{D\tau} + \frac{\partial}{\partial\tau}\left[\frac{\rho_1 v_1}{2}(v_1 - v_2)\right]$$

$$+ \frac{\partial}{\partial x}\left[\frac{u}{2}(\rho_1 v_1^2 + \rho_2 v_2^2) + \frac{\rho_1 v_1}{2}(v_1^2 - v_2^2)\right] \qquad \text{(A-33)}$$

$$+ \rho_1 v_1 T\,(c_{p_1} - c_{p_2}) + \rho_1 v_1 U = -\,p\frac{\partial u}{\partial x}$$

$$+ \eta\left(\frac{\partial u}{\partial x}\right)^2 + \frac{\partial}{\partial x}\left[-Q + v_1\eta_1\frac{\partial u_1}{\partial x} + v_2\eta_2\frac{\partial u_2}{\partial x}\right]$$

Substituting equation A-8 into equation A-33

$$\rho\, c_v \frac{DT}{D\tau} + \omega_1 U + \frac{\partial}{\partial\tau}\left[\frac{\rho_1 v_1}{2}(v_1 - v_2)\right] + \frac{\partial}{\partial x}\left[\frac{u}{2}(\rho_1 v_1^2 + \rho_2 v_2^2) + \frac{\rho_1 v_1}{2}(v_1^2 - v_2^2)\right.$$

$$\left. + \rho_1 v_1 T\,(c_{p_1} - c_{p_2})\right] = -\,p\frac{\partial u}{\partial x} + \eta\left(\frac{\partial u}{\partial x}\right)^2 - \frac{\partial Q}{\partial x} + \frac{\partial}{\partial x}\left[v_1\eta_1\frac{\partial(u+v_1)}{\partial x} + v_2\eta_2\frac{\partial(u+v_2)}{\partial x}\right]$$

(A-34)

Making the assumption that v_i, $\frac{\partial v_i}{\partial x}$, and $c_{p_1} - c_{p_2}$ are small; and dropping all terms of second order and higher; equation A-34 becomes

$$\rho\, c_v \frac{DT}{D\tau} = -\,\omega_1 U - p\frac{\partial u}{\partial x} + \eta\left(\frac{\partial u}{\partial x}\right)^2 - \frac{\partial Q}{\partial x} + \frac{\partial}{\partial x}\left[(v_1\eta_1 + v_2\eta_2)\frac{\partial u}{\partial x}\right] \qquad \text{(A-35)}$$

Equation of State

The equation of state for each component of the mixture is assumed to be

$$p_i = \rho_i \frac{R_o}{M_i} T \tag{A-36}$$

Letting i equal 1 and 2 in equation A-35 and adding the two equations

$$p = \rho R T \tag{A-37}$$

where

$$R = R_o \frac{Y (M_2 - M_1) + M_1}{M_1 M_2} \tag{A-38}$$

Employing equation A-37 to remove the variable p from the conservation equations, the conservation equations in a form suitable for solution by the method of characteristics are as follows:

conservation of mass

species one

$$\frac{\partial Y}{\partial \tau} + u \frac{\partial Y}{\partial x} = 1/\rho \left[\omega_1 - \frac{\partial}{\partial x} (\rho Y v_1)\right] \tag{A-8}$$

mixture

$$\rho \frac{\partial u}{\partial x} + \frac{\partial \rho}{\partial \tau} + u \frac{\partial \rho}{\partial x} = 0 \tag{A-39}$$

conservation of momentum

$$\rho R \frac{\partial T}{\partial x} + \rho \frac{\partial u}{\partial \tau} + \rho u \frac{\partial u}{\partial x} + RT \frac{\partial \rho}{\partial x} = - \rho T \frac{\partial R}{\partial x} + \eta \frac{\partial^2 u}{\partial x^2} \tag{A-40}$$

conservation of energy

$$\rho\, c_v \frac{\partial T}{\partial \tau} + \rho\, u\, c_v \frac{\partial T}{\partial x} + \rho\, RT \frac{\partial u}{\partial x} = -\omega_1 U + \eta \left(\frac{\partial u}{\partial x}\right)^2$$

$$- \frac{\partial Q}{\partial x} + \frac{\partial}{\partial x}\left(v_1 \eta_1 + v_2 \eta_2\right) \frac{\partial u}{\partial x} \qquad \text{(A-41)}$$

APPENDIX B

PROCESS EQUATIONS AND PHYSICAL AND TRANSPORT PROPERTIES

To employ the conservation equations (equations A-8, A-37, A-38, and A-39) for the calculation of the propagation of the pressure disturbance through the combustion region the following are required: (1) the expressions for the processes of heat transfer, molecular diffusion, and chemical reaction indicated in the foregoing equations; (2) numerical values for the transport and physical properties (thermal conductivity k, second coefficient of viscosity η, diffusion coefficient D, specific heat ratio γ, activation energy E, etc.). The expressions for the processes and the numerical values assigned to the physical and transport properties depend upon the type of propellant assumed to be burned. The subject report is concerned with the combustion of a composite propellant having a composition, by weight, of 80 per cent ammonium perchlorate and 20 per cent polybutadiene-acrylic acid. Experiments with propellants whose composition approximates that of the subject propellant have demonstrated that they are readily susceptible to combustion pressure oscillation.

It is difficult to assign meaningful values to the physical and transport properties in the various zones of the combustion region. The difficulty arises because of the following reasons:

(1) The composition of the gases at each section of a zone is not known accurately. The combustion region is thin (20 - 4000 microns) and is at a high temperature (1600 - 4700^{o}R); consequently, it is extremely difficult to make accurate measurements in any zone in the combustion region and the processes occurring in the combustion region are too complicated to analyze analytically.

(2) There are few data pertinent to the physical and transport properties for the high molecular weight gases occurring adjacent to the burning surface.

(3) Ammonium perchlorate decomposes upon heating and, therefore, its physical properties are not easily determined.

(4) The flow in the combustion region is turbulent which influences the transport processes and, hence, the values of the transport properties.

In view of the above, the numerical values assigned to the transport and physical properties of the flow media should be considered as being order of magnitude quantities. Consequently, the calculated results obtained for the propagation of a disturbance in the combustion region, since they are based on order of magnitude values for the physical and transport properties, should be considered to be only first order approximations.

This appendix is divided into four sections organized as follows:

(1) In the first section the chemical composition upon which the calculations for physical and transport properties are based is assumed for each zone of the combustion region.

(2) The second section contains expressions obtained for the processes of heat transfer, molecular diffusion, and chemical reaction. The transport and physical properties which appear in those expressions are evaluated for each zone employing the pertinent chemical composition assumed in part (1). The transport properties of thermal conductivity k and diffusion coefficient D are assumed to be functions of the flow properties of temperature T, and temperature T and pressure p respectively.

(3) In the third section the remaining physical and transport properties which appear in the conservation equations are calculated for each zone employing the respective chemical composition assumed in part (1). The physical properties for the solid propellant are also given. The second coefficient of viscosity η is assumed to be a function of the flow temperature T.

(4) The last section contains the steady state profile assumed for the combustion region.

Chemical Composition

There is considerable published information regarding the decomposition of ammonium perchlorate (14)(27)(28)(29)(30)(31). No information, however, could be found by the author concerning the decomposition and combustion of polybutadiene-acrylic acid. Since the propellant under consideration is 80 per cent by weight ammonium perchlorate, it is assumed that the gases near the propellant surface are entirely those obtained from decomposing the ammonium perchlorate.

The process of decomposition for ammonium perchlorate assumed below is based on the studies presented in References (14)(27), and (31). The first step in the decomposition of ammonium perchlorate occurs at the burning surface of the propellant and is the following reaction. Thus

$$NH_4ClO_4{}_{solid} \longrightarrow NH_3{}_{gas} + HClO_4{}_{gas} \qquad \text{(B-1)}$$

The ammonia NH_3 and perchloric acid $HClO_4$ decompose further according to the following chemical reaction (27). Thus

Reactant		Product
$NH_3 + HClO_4$	$\longrightarrow$	$0.265N_2 + 0.12N_2O + 0.23NO$
		$+ 1.015O_2 + 1.62H_2O + 0.76HCl + 0.12Cl_2$

(B-2)

Further data concerning the chemical reaction between the product given on the right hand side of equation B-2 and the decomposed polybutadiene-acrylic acid are not available. However, data for the composition of the combustion products after the chemical reaction has taken place are available (32). The major components of the combustion products and their approximate per cents by volume are tabulated in Table 6.

Based upon the aforementioned information the following assumptions were made concerning the chemical composition of the three zones of the combustion region. (1) The compostion of the gases leaving the flame

Table 6

Assumed Composition of Combustion Products

Leaving Flame Zone*

Component	% by Volume
H_2O	27.8
H_2	18.0
CO	24.9
CO_2	6.1
N_2	7.6
HCl	15.1

* The above table is based on information presented in reference (32). Only the major constituents found in the combustion products were included in the above table.

zone are that tabulated in Table 6. (2) Since the physical and transport properties were assumed to be unaffected by the chemical reaction in the flame zone, the composition of gases tabulated in Table 6 is employed to calculate the properties of the gases entering the flame zone. (3) The properties in the induction zone were assumed to remain constant; therefore, the calculations for the properties in the induction zone are made employing the gas composition tabulated in Table 6. (4) The chemical composition of the decomposition zone is assumed to change according to equation B-2. The left hand side of the equation is assumed to be the composition of the gases entering the zone and the right hand side of the equation is assumed to be the composition of the gases leaving the zone.

Figure 15 summarizes the aforementioned information; the figure shows the molecular chemical composition assumed for the flowing medium as it enters and leaves each zone of the combustion region. The chemical compositions do not necessarily indicate the processes that are assumed to be occurring in the zones, but only give a chemical composition upon which to base calculations for the physical and transport properties for each zone.

Process Equations and Related Physical and Transport Properties

The rapid exothermic chemical reaction that occurs in the flame zone as well as the exothermic decomposition of ammonium perchlorate that occurs in the decomposition zone produce steep temperature gradients

DECOMPOSITION ZONE

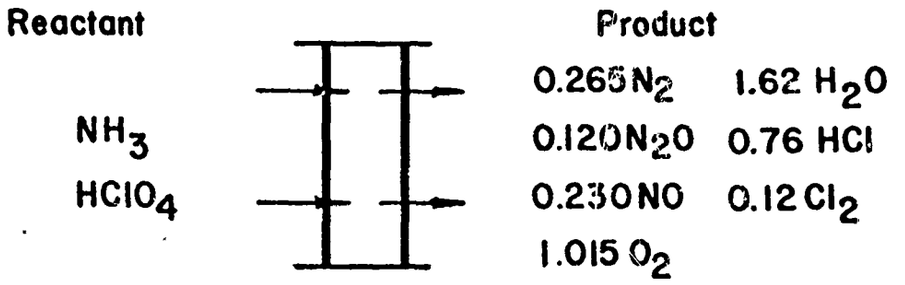

INDUCTION ZONE

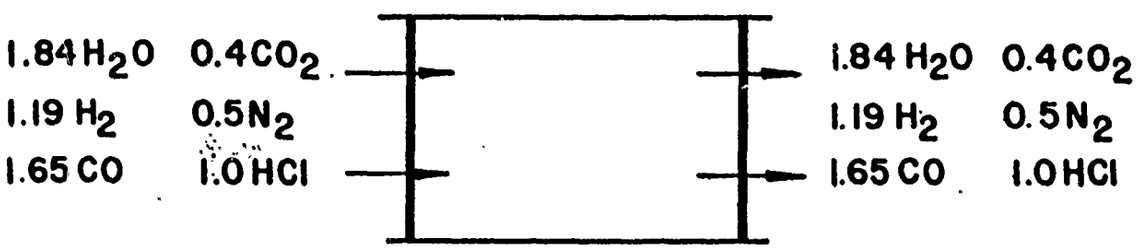

FLAME ZONE

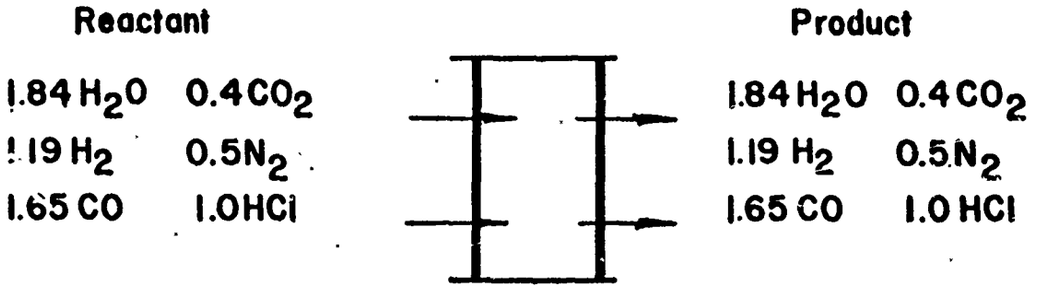

Figure 15 Assumed Molecular Composition of the Flowing Medium Entering and Leaving Each Zone

in the flowing medium in the combustion region. As a result of those gradients, heat is transferred at a high rate from the flame zone into the induction zone and from the decomposition zone into the propellant. There is only a very low rate of heat transfer from the induction zone into the decomposition zone.

In the subject report the usual assumption is made that the rate of heat transfer is a linear function of the local static temperature gradient. Thus

$$Q = - k \frac{\partial T}{\partial x} \qquad \text{(B-3)}$$

where

k is the overall thermal conductivity for the flowing medium.

The overall thermal conductivity for the gas mixture in the various zones is calculated by employing a mixing relationship proposed by Brokaw and presented in Reference (33). The thermal conductivity for an n component gas mixture is

$$k = \frac{1}{2} (k_r + k_s) \qquad \text{(B-4)}$$

where

$$k_s = \sum_{i=1}^{n} f_i \, k_i$$

$$\frac{1}{k_r} = \sum_{i=1}^{n} \frac{f_i}{k_i}$$

f_i = the mole fraction and k_i = the thermal conductivity of the i-th species.

Plots of the thermal conductivity k of each gaseous component of the assumed combustion mixture gas (34) were plotted as a function of the gas temperature for the range of temperatures (2300 - 4700^{o}R) encountered in the flame and induction zones. The resulting curves demonstrated that for each gaseous component the thermal conductivity k was practically a linear function of temperature T. It was, therefore, assumed that in each zone of the combustion region the thermal conductivity of the pertinent gaseous mixture is given by the following equation. Thus

$$k = A + BT \qquad \text{(B-5)}$$

where

A and B are constants.

The constants A and B were evaluated for the gas mixture by employing the data presented in Reference (34) and equation B-4 (the mixing rule); the result obtained for the flame and induction zones are presented below.

<u>thermal conductivity in the flame and induction zones</u>

$$k = 6.7 \times 10^{-6} + 7.8 \times 10^{-9} \, (T) \, \frac{BTU}{ft\text{-}sec\text{-}^{o}R} \quad (T \text{ in } ^{o}R) \qquad \text{(B-6)}$$

The constants A and B for the gas mixture leaving the decomposition zone (product) were calculated by employing the chemical composition presented in Fig. 15. The calculations for the constants

A and B of the gas mixture entering the decomposition zone (reactant) were based on the thermal conductivity of NH_3 because the thermal conductivity of $HClO_4$ was not available. The results of the aforementioned calculations are presented below.

thermal conductivity in the decomposition zone

(a) gas mixture entering the zone

$$k_1 = -7.2 \times 10^{-6} + 1.8 \times 10^{-8} (T) \frac{BTU}{ft\text{-}sec\text{-}^oR} \quad (T \text{ in } ^oR) \qquad (B\text{-}7)$$

(b) gas mixture leaving the zone

$$k_2 = -3.0 \times 10^{-7} + 7.4 \times 10^{-9} (T) \frac{BTU}{ft\text{-}sec\text{-}^oR} \quad (T \text{ in } ^oR) \qquad (B\text{-}8)$$

The thermal conductivity at any location in the decomposition zone is calculated by combining equations B-7, B-8, and B-4.

The diffusion velocity v_1 for component 1 of a binary mixture is a function of the pressure, temperature, and concentration gradients for the mixture. The diffusion velocity v_1 is given by (35)

$$v_1 = -D\{\frac{d\ ln(Y)}{dx} - (\frac{Y}{M_1} + \frac{1-Y}{M_2})(M_2-M_1)(1-Y) \frac{d\ ln(p)}{dx} + \frac{[M_2Y + M_1(1-Y)]^2}{M_1\ M_2} \frac{k_T}{Y} \frac{d\ ln(T)}{dx}\} \qquad (B\text{-}9)$$

where

D = binary diffusion coefficient,

M_i = molecular weight of i-th species, and

k_T = thermal diffusion ratio.

It is assumed that the pressure and temperature gradients have small effects upon the diffusion of one gas into another. In view of the aforementioned assumption, equation B-9 is greatly simplified and one can write the following equations. Thus

$$v_1 = -D \frac{1}{Y} \frac{dY}{dx} \tag{B-10}$$

and

$$v_2 = D \frac{1}{1-Y} \frac{dY}{dx} \tag{B-11}$$

Equation B-11 employs the relation that the concentration of the second species is (1-Y).

The diffusion coefficient D for a binary mixture is a function of pressure and temperature. Thus (33, p. 267)

$$D = \frac{N \sqrt{T^3}}{p} \tag{B-12}$$

where

N is a constant.

To obtain an estimate of the value of the constant N in equation B-12, a study was made of the data for the diffusion of air into various polyatomic gases (33). Based on that study the value $N = 1.3 \times 10^{-6}$ was selected for N. The diffusion coefficient D in

the flame zone is presented below.

diffusion coefficient in the flame zone

$$D = \frac{1.3 \times 10^{-6} \sqrt{T^3}}{p} \quad ft^2/sec \quad (T \text{ in } {}^oR, \text{ p in psi}) \qquad (B\text{-}13)$$

No attempt was made to improve the equation for the diffusion coefficient D, because the numerical calculations indicated that the effect of diffusion in the flame zone had only a second order effect on the propagation of a normal shock (see Table 1). Moreover, in view of the latter result, the effects of diffusion in the decomposition zone were assumed to be negligible.

The source function ω that appears in the conservation equations represents the rate at which a species is produced by the chemical reaction present in the zone. The chemical reactions that occur in the decomposition and flame zones are both assumed to have reaction rates governed by an Arrhenius type function of the following form (35). Thus the source function is assumed to be

$$\omega_1 = -\alpha \rho Y e^{-E/R_o T} \quad lb/ft^3\text{-sec} \qquad (B\text{-}14)$$

where

α = a combination frequency and steric factor,

E = the activation energy,

R_o = the universal gas constant, and

ω_1 = the rate of production of species one.

It is assumed that the activation energy for the decomposition zone is approximately equal to that for the thermal decomposition of ammonium perchlorate (28).

activation energy for the decomposition zone

$$E/R_o = 36{,}200\ ^oR \qquad \text{(B-15)}$$

The factor α in equation B-14 is estimated to have the following value for the decomposition zone.

combination frequency and steric factor for the decomposition zone

$$\alpha = 1 \times 10^{13}\ 1/sec \qquad \text{(B-16)}$$

The value was assigned to give a chemical reaction rate compatible with the steady state temperature profile assumed for the decomposition zone.

The activation energy for the flame zone is assumed to have the value given below.

activation energy for the flame zone

$$E/R_o = 45{,}320\ ^oR \qquad \text{(B-17)}$$

Equation B-17 is based on the data for the activation energies for the combustion of relatively light hydrocarbons (23). For the flame zone, the combination frequency and steric factor α is assumed to have the value presented below.

combination frequency and steric factor for the flame zone

$$\alpha = 8 \times 10^{10}\ 1/sec \qquad \text{(B-18)}$$

Equation B-18 was determined from calculations for a reaction rate that is consistent with the steady state temperature profile assumed for the flame zone.

Ammonium perchlorate gradually decomposes upon heating. It is difficult, therefore, to determine accurately the values of the specific heat, heat of sublimation, and heat of decomposition. Moreover, no information could be found concerning the decomposition of polybutadiene-acrylic acid. In view of the foregoing, it is difficult to determine accurately the amount of heat released by chemical reaction in each zone of the combustion region. From a study of the available data (27)(30)(32) and some rough energy calculations, the values listed below were assigned as the amounts of heat released U in each zone by the chemical processes. The total heat released is equal to the amount of heat estimated to be released by the burning of the subject propellant.

the amount of heat released in the flame zone

$$U = 1{,}570 \text{ Btu/lb} \tag{B-19}$$

the amount of heat released in the induction zone

$$U = 80 \text{ Btu/lb} \tag{B-20}$$

the amount of heat released in the decomposition zone

$$U = 1{,}000 \text{ Btu/lb} \tag{B-21}$$

Physical and Transport Properties

There is only a small body of literature concerned with either the determination of or the values for the second coefficient of viscosity

η, also called the bulk viscosity (36)(37). No accurate values for η could be found for polyatomic gases. For a monatomic gas the second coefficient of viscosity is calculated from the following equation (25). Thus

$$\mu + \frac{3}{2}\eta = 0 \qquad \text{(B-22)}$$

where

μ is the dynamic viscosity of the gas.

Equation B-22 does not hold for a polyatomic gas. It is probably true, however, that the second coefficient of viscosity η is of the same order of magnitude as the dynamic viscosity μ but of opposite sign. It is assumed that η and the temperature T are related in the same manner as μ and T. Hence the relation between the second coefficient of viscosity and temperature is given by the expression

$$\eta = -A\sqrt{T} \qquad \text{(B-23)}$$

where

A is a constant.

Equation B-23 is the relation developed for μ by Hirshfelder (38) by applying statistical methods. The constant A in equation B-23 was obtained for the flame zone by calculating μ for the gas mixture by the method presented in Reference (33). The corresponding magnitude of η was assumed to be equal to the calculated magnitude of μ. The following expression was obtained for the second coefficient of viscosity.

the equation for the second coefficient of viscosity in the flame zone

$$\eta = -7 \times 10^{-7} \sqrt{T} \text{ lb/(ft-sec)} \qquad (T \text{ in } {}^{o}R) \qquad \text{(B-24)}$$

No attempt was made to improve equation B-24 because the numerical calculations (see Table 1) showed that the effect of η on the propagation of a normal shock within the flame zone was a second order effect.

In each of the zones the molecular weight of the gas mixture $\overline{M}$ is calculated by means of the formula

$$\overline{M} = \sum_{i=1}^{n} f_i M_i \qquad \text{(B-25)}$$

where

f_i = the mole fraction and

n = the number of components.

The gas constant for the gas mixture is obtained from the equation

$$R = \frac{R_o}{\overline{M}} \qquad \text{(B-26)}$$

where

R_o is the universal gas constant = 1.9865 Btu/(mole-${}^{o}R$).

It is assumed the induction and flame zones are occupied by gas mixtures having the same molecular weight and the same gas constant.

The molecular weights and gas constants for the decomposition zone were calculated by assuming the reactant in equation B-2 represented the composition of the gas mixture entering the zone, and

the product in the same equation represented the composition of the gas mixture leaving the zone.

molecular weight and gas constant for the flame and induction zones

$$\overline{M} = 22.84 \tag{B-27}$$

$$R = 67.7 \frac{\text{ft-lb}}{\text{lb-}^{o}R} \tag{B-28}$$

molecular weights and gas constants for the decomposition zone

(a) gas mixture entering the decomposition zone

$$\overline{M}_1 = 58.75 \tag{B-29}$$

$$R_1 = 26.3 \frac{\text{ft-lb}}{\text{lb-}^{o}R} \tag{B-30}$$

(b) gas mixture leaving the decomposition zone

$$\overline{M}_2 = 28.56 \tag{B-31}$$

$$R_2 = 54.11 \frac{\text{ft-lb}}{\text{lb-}^{o}R} \tag{B-32}$$

The molecular weight and gas constant at any point in the decomposition zone were found by considering the gases to be a two-component mixture, product and reactant, and then employing equations B-25 and B-26 respectively.

The specific heat at constant pressure $\overline{c_p}$ for the gas mixture in each zone of the combustion region is calculated by the following relation.

$$\overline{c_p} = \sum_{i=1}^{n} f_i \, c_{pi} \tag{B-33}$$

where

c_{pi} = specific heat at constant pressure of the i-th component.

An investigation of the value of $\overline{c_p}$ over the range of temperatures encountered in the combustion region showed that $\overline{c_p}$ did not vary significantly with temperature. Therefore, the specific heat at constant pressure was assumed to be a constant.

Once the specific heat at constant pressure has been determined the specific heat ratio can be calculated by the following equation.

$$\overline{\gamma} = \frac{1}{1-R/\overline{c_p}} \tag{B-34}$$

Since R is a constant and $\overline{c_p}$ is assumed to be a constant, it is noted from equation B-34 that $\overline{\gamma}$ will also be constant. It will be recalled that it was assumed that the gas mixture in the decomposition zone had the same transport and physical properties as ammonia. The composition of the gas mixture leaving the decomposition zone is assumed to be that of the product in equation B-2.

The values of $\overline{\gamma}$ and $\overline{c_p}$ for the gas mixtures in the different zones of the combustion region are given below.

<u>the specific heat at constant pressure and specific heat ratio for the flame and induction zones</u>

$$\overline{c_p} = 0.48 \text{ Btu/(lb-}^{\circ}\text{R)} \tag{B-35}$$

$$\overline{\gamma} = 1.24 \qquad \text{(B-36)}$$

the specific heat at constant pressure and the specific heat ratio for the decomposition zone

(a) gas mixture entering the zone

$$\overline{c_{p_1}} = 0.24 \text{ Btu/(lb-}^{o}\text{R)} \qquad \text{(B-37)}$$

$$\overline{\gamma} = 1.17 \qquad \text{(B-38)}$$

(b) gas mixture leaving the zone

$$\overline{c_{p_2}} = 0.317 \text{ Btu/(lb-}^{o}\text{R)} \qquad \text{(B-39)}$$

$$\overline{\gamma} = 1.28 \qquad \text{(B-40)}$$

The following were assumed to be the physical properties for the subject propellant, based upon a study of Reference (32).

density of propellant

$$\rho_p = 102 \text{ lb/ft}^3 \qquad \text{(B-41)}$$

slope of stress-strain curve in region of interest

$$\overline{S} = 400 \text{ lb/in}^2 \qquad \text{(B-42)}$$

the equation for the burning rate of the propellant

$$r = 0.00132p^{0.432} \text{ ft/sec} \qquad \text{(p in psia)} \qquad \text{(B-43)}$$

Steady State Combustion Region Profile

The calculation of the propagation of the nonuniform shock through the combustion region is a boundary-valued problem. One boundary

condition is the initial strength of the shock; the other condition is a solution for the flow properties as a function of location in the steady state combustion region. Assigning an initial strength to the shock causes no problem; however, defining a solution for the flow properties in the steady state combustion region that approximates the actual conditions at the surface of a burning solid propellant presents a very difficult problem. As mentioned at the beginning of this appendix, the combustion region at the surface of a burning solid propellant is so thin and at such a high temperature that it is difficult to make experimental measurements in the region; and the processes are so complex that the region cannot be studied to any great degree of accuracy analytically. After the available literature has been studied (14)(32)(39)(40), widths for each zone and the temperature rise through each zone were assigned which should reasonably approximate the actual conditions in the combustion region at the surface of a propellant composed of 80 per cent ammonium perchlorate and 20 per cent polybutadiene-acrylic acid by weight. The combustion temperature in each zone was assumed to be independent of combustion pressure since data showed (32) that a change in combustion pressure over the range encountered in the present analysis changed the combustion products' temperature only a few per cent. In the analysis the chemical reaction rate was assumed to be proportional to the gas density; therefore, the combustion rate will increase directly with the combustion pressure. The zone widths during steady state combustion

were, therefore, assumed to vary inversely as the combustion pressure. The zone widths for each of the combustion regions as a function of combustion pressure and the entrance and exit temperatures assumed for the steady state combustion region are given below in Tables 7 and 8 respectively.

Table 7

Zone Widths Assumed

Combustion Pressure psia	Flame Zone Width (ft)	Induction Zone Width (ft)	Decomposition Zone Width (ft)
250	6.67×10^{-5}	8.0×10^{-4}	4.0×10^{-5}
500	3.33×10^{-5}	4.0×10^{-4}	2.0×10^{-5}
1000	1.67×10^{-5}	2.0×10^{-4}	1.0×10^{-5}

Table 8

Temperature Rise Assumed

Position	Flame Zone ^{o}R	Induction Zone ^{o}R	Decomposition Zone ^{o}R
Entrance	3600	2300	1600
Exit	4700	3600	2300

The combustion pressure through the entire combustion region can be assumed to be constant without introducing much error (6, p. 108). With the aforementioned assumption and the assigned values for zone width and temperature rise, an analytical solution for the conservation equations for the temperature profile--equations A-37 and A-39 with the unsteady and nonapplicable terms dropped out--can be obtained for the induction zone. Thus

$$T = T_o - B\left[1 - \exp\left(\frac{\dot{m}\overline{c_p}x}{k}\right)\right] + \frac{Q}{\overline{c_p}}\left(\frac{x}{x_o}\right)^2 + \frac{2kQ}{x_o\dot{m}\overline{c_p}^2}\left(\frac{x}{x_o}\right) \qquad \text{(B-44)}$$

where

$$B = \left[T_o - T_1 + \frac{Q}{\overline{c_p}} + \frac{2kQ}{x_o\dot{m}\overline{c_p}^2}\right]\left[1-\exp\left(\frac{\dot{m}\overline{c_p}x_o}{k}\right)\right]^{-1}$$

$\dot{m}$ = mass flow rate per unit area,

Q = total heat added per unit mass flow,

T_o = static temperature of the gas entering the induction zone,

T_1 = static temperature of the gas leaving the induction zone,

x_o = the zone width, and

x = the distance measured from the fore end of the zone in the direction of gas flow.

In the other two zones the conservation equations cannot be solved directly. The steady state solutions for the temperature and concentration profiles can be approximated for the two zones, however, by a polynomial which satisfies specified conditions at each end of the zone. Thus

$$T = E + F\,(x/x_0) + G(x/x_0)^2 + H(x/x_0)^3 \qquad \text{(B-45)}$$

$$Y = E + F\,(x/x_0) + G(x/x_0)^2 + H(x/x_0)^3 \qquad \text{(B-46)}$$

The concentration is assumed to be one as the gases enter the flame and decomposition zones and zero as they leave. The slope of the concentration curve is assumed to be zero at each end of the zones. Thus equation B-46 for both the flame and decomposition zones reduces to

$$Y = 1 - 3(x/x_0)^2 + 2(x/x_0)^3 \qquad \text{(B-47)}$$

where

the coordinate x is measured from the edge of the zone in the direction of gas flow.

The slope of the temperature curve is assumed to be zero at the interface between the flame zone and the combustion products region. Also, the slopes at the ends of the flame and decomposition zones that are adjacent to the induction zone are assumed to have the same slopes as the induction zone at those points. Further, for the decomposition zone the second derivative of the slope of the temperature curve is also assumed to match the induction zone slope. With the aforementioned slopes and the temperatures at the ends of the zones given, the four constants in equation B-45 can be evaluated. Table 9 gives the values for the constants in equation B-45 for each combustion pressure for the flame and decomposition zones respectively.

Table 9

Coefficients for Equation B-45*

Combustion Pressure	E	F	G	H
Flame Zone				
250	2.30×10^3	2.49×10^7	-1.55×10	-5.42×10^2
500	2.30×10^3	3.38×10^7	1.04×10^3	-1.07×10^3
1000	2.30×10^3	4.54×10^7	1.79×10^3	-1.44×10^3
Decomposition Zone				
250	1.60×10^3	1.31×10^2	-8.19	0.17
500	1.60×10^3	5.24×10^2	-1.31×10^2	1.09×10
1000	1.60×10^3	2.10×10^3	-2.09×10^3	6.98×10^2

* x is measured from the edge of the zone in the direction of gas flow.

APPENDIX C

CHARACTERISTIC CURVES AND COMPATIBILITY EQUATIONS

Several methods for determining the characteristic curves and the compatibility equations pertinent to them for a system of hyperbolic partial differential equations have been published (7)(11)(19)(41). Of the methods available, the one outlined in Section 3-1 of Reference (41) is probably the easiest to execute if three or more equations are involved and is employed herein. The method of Reference (41) is first explained step-by-step for a general case. After that the method is employed to find the characteristic curves and corresponding compatibility equations for the conservation equation derived in Appendix A.

Assume given a system of hyperbolic partial differential equations, the characteristic curves are determined first by employing the following procedure: (1) each of the partial differential equations is multiplied by a different unknown function σ_i, (2) all of the equations are added to form one equation, and (3) the resultant equation is factored into the following form:

$$\sum_{i=1}^{n} G_i \left(\frac{\partial h_i}{\partial \tau} + \Gamma_i \frac{\partial h_i}{\partial x}\right) = H \qquad \text{(C-1)}$$

where

x and τ are the independent variables of length and time respectively and the G_i's, Γ_i's and H are functions of the dependent variables and the unknown multiplying functions σ_i's; the h_i's are the dependent variables; and n is the number of dependent variables. For the problem investigated herein the dependent variables are such physical properties as static temperature T, static pressure p, velocity u, etc. Assume that all of the Γ_i's are identical, then equation 1 represents the total derivative taken in the direction where the slope is $dx/d\tau = \Gamma_i$. Replacing $dx/d\tau$ by λ, one obtains the following:

$$\begin{aligned}
\Gamma_1 &= \frac{dx}{d\tau} = \lambda \\
\Gamma_2 &= \frac{dx}{d\tau} = \lambda \\
&\cdot \quad \cdot \quad \cdot \\
&\cdot \quad \cdot \quad \cdot \\
\Gamma_n &= \frac{dx}{d\tau} = \lambda
\end{aligned} \tag{C-2}$$

By rearranging equations C-2 a system of homogeneous equations linear in the unknown functions σ_i's is obtained.

$$\begin{aligned}
a_{11}\ \sigma_1 + a_{12}\ \sigma_2 + \ldots + a_{1n}\ \sigma_n &= 0 \\
a_{21}\ \sigma_1 + a_{22}\ \sigma_2 + \ldots + a_{2n}\ \sigma_n &= 0 \\
\cdot \qquad \cdot \qquad \cdot \qquad \cdot &\\
\cdot \qquad \cdot \qquad \cdot \qquad \cdot &\\
a_{n1}\ \sigma_1 + a_{n2}\ \sigma_2 + \ldots + a_{nn}\ \sigma_n &= 0
\end{aligned} \tag{C-3}$$

where the a_{ij}'s are functions of the dependent variables and the slope λ. If equations C-3 are to have a nontrivial solution, the determinant of the coefficients of the σ_i's must be zero. Solving the determinant of equations C-3 yields "n" roots for λ which are called the characteristic directions. The curves which satisfy the expression $dx/d\tau = \lambda_i$ are the characteristic curves discussed earlier. It can be shown that only when the initial system of partial differential equation is hyperbolic will all of the n roots be real functions (7)(11)(19).

The corresponding compatibility equation for each characteristic direction is determined in the following manner: (1) substitute the particular value of λ_i into equations C-3 and obtain equations relating the different unknown functions, σ_i's; (2) substitute those relations into equation C-1; (3) cancel the unknown functions (σ_i's) out of the equation leaving the desired compatibility equation; (4) steps (1), (2), and (3) are repeated for each of the other characteristic directions.

The procedure outlined above will now be applied to determine the set of characteristic directions and compatibility equations for the conservation equations derived in Appendix A. Assume that the higher order derivatives and the powers of the derivatives that appear in the heat transfer, diffusion, and viscosity terms of the conservation equations are known functions of the independent variables. In that case the conservation equations may be treated as a system of first order partial differential equations. The unsteady one-dimensional conservation equations from Appendix A are presented below.

conservation of mass

$$\rho \frac{\partial u}{\partial x} + \frac{\partial \rho}{\partial \tau} + u \frac{\partial \rho}{\partial x} = 0 \qquad \text{(C-4)}$$

where

ρ = density,

u = velocity,

τ = time, and

x = distance.

The species conservation of mass equation (equation A-8) is already a compatibility equation that must be solved along characteristic curve $\lambda = u$.

conservation of momentum

$$\rho R \frac{\partial T}{\partial x} + \rho \frac{\partial u}{\partial \tau} + \rho u \frac{\partial u}{\partial x} + RT \frac{\partial \rho}{\partial x} = - \rho T \frac{\partial R}{\partial x} + \eta \frac{\partial^2 u}{\partial x^2} \qquad \text{(C-5)}$$

where

R = gas constant,

T = static temperature, and

η = second coefficent of viscosity.

conservation of energy

$$\rho c_v \frac{\partial T}{\partial \tau} + \rho u c_v \frac{\partial T}{\partial x} + \rho RT \frac{\partial u}{\partial x} = - \omega_1 U + \eta \left(\frac{\partial u}{\partial x}\right)^2 - \frac{\partial Q}{\partial x} + \frac{\partial}{\partial x} (v_1 \eta_1 + v_2 \eta_2) \frac{\partial u}{\partial x} \qquad \text{(C-6)}$$

where

c_v = specific heat at constant volume,

U = heat of reaction,

ω_1 = rate of production of reactants,

Q = heat transfer function, and

v = diffusion velocity.

Multiply equations C-4, C-5, and C-6 by the unknown functions σ_1, σ_2, and σ_3 respectively. Add the resulting equations and factor into the form of equation C-1.

$$\sigma_3 \rho c_v \left[\frac{\partial T}{\partial \tau} + \frac{\sigma_3 \rho u c_v + \sigma_2 \rho R}{\sigma_3 \rho c_v} \frac{\partial T}{\partial x}\right]$$

$$+ \sigma_2 \rho \left[\frac{\partial u}{\partial \tau} + \frac{\sigma_3 \rho RT + \sigma_2 \rho u + \sigma_1 \rho}{\sigma_2 \rho} \frac{\partial u}{\partial x}\right] \qquad \text{(C-7)}$$

$$+ \sigma_1 \left[\frac{\partial \rho}{\partial \tau} + \frac{\sigma_2 RT + \sigma_1 u}{\sigma_1} \frac{\partial \rho}{\partial x}\right]$$

$$= \sigma_3 A + \sigma_2 B$$

where

$$A \equiv -\omega_1 U + \eta \left(\frac{\partial u}{\partial x}\right)^2 - \frac{\partial Q}{\partial x} + \frac{\partial}{\partial x}\left[(v_1 \eta_1 + v_2 \eta_2) \frac{\partial u}{\partial x}\right]$$

$$B \equiv -\rho T \frac{R}{x} + \eta \frac{\partial^2 u}{\partial x^2}$$

Assuming equation C-7 represents a total derivative in some direction λ,

then

$$\frac{\sigma_3 \, u \, c_v + \sigma_2 \, R}{\sigma_3 \, c_v} = \lambda$$

$$\frac{\sigma_3 \, R \, T + \sigma_2 \, u + \sigma_1}{\sigma_2} = \lambda \qquad \text{(C-8)}$$

$$\frac{\sigma_2 \, RT + \sigma_1 \, u}{\sigma_1} = \lambda$$

Equations C-8 corresponds to equations C-2 of the general case. Rearrange equations C-8 into the form of equations C-3. Thus

$$0 - R \, \sigma_2 + c_v \, (\lambda - u) \quad \sigma_3 = 0$$

$$\sigma_1 - (\lambda - u) \quad \sigma_2 + RT \quad \sigma_3 = 0 \qquad \text{(C-9)}$$

$$(\lambda - u) \, \sigma_1 - RT \quad \sigma_2 + 0 \quad = 0$$

A nontrivial solution is desired for equations C-9. Hence, its determinant must vanish. Thus

$$c_v \, (\lambda - u)^3 - (\lambda - u) \, R^2 T - c_v \, R \, T \, (\lambda - u) = 0 \qquad \text{(C-10)}$$

Factoring equation C-10 yields

$$(\lambda - u) \, (\lambda - u + \sqrt{\gamma RT}) \, (\lambda - u - \sqrt{\gamma RT}) = 0 \qquad \text{(C-11)}$$

The roots of equation C-11 are

$$\lambda_1 = u; \quad \lambda_2 = u + \sqrt{\gamma RT}\ ; \quad \lambda_3 = u - \sqrt{\gamma RT} \tag{C-12}$$

To determine the compatiblity equations proceed as follows: (1) select $\lambda_1 = u$ as the first characteristic direction. (2) Substitute $\lambda = u$ into equations C-9 and obtain the relations between the σ_i's.

$$\sigma_3 = \sigma_3\ ; \quad \sigma_2 = 0\ ; \quad \sigma_1 = -\ RT\ \ \sigma_3 \tag{C-13}$$

(3) Substitute equations C-13 into equation C-7 and obtain the compatibility equation in the characteristic direction $\lambda = u$. Thus

$$\rho\, c_v \frac{DT}{D\tau} - R\bar{T} \frac{D\rho}{D\tau} = -\ \omega_1\, U + \eta \left(\frac{\partial u}{\partial x}\right)^2$$

$$- \frac{\partial Q}{\partial x} + \frac{\partial}{\partial x}\ \left[\ (v_1\, \eta_1 + v_2\, \eta_2)\ \frac{\partial u}{\partial x}\ \right] \tag{C-14}$$

where

$$\frac{D}{D\tau}\ \equiv \frac{\partial}{\partial \tau}\ + u\ \frac{\partial}{\partial x}$$

In an analogous manner the remaining two compatibility equations are obtained.

The compatibility equation for $\lambda = u + \sqrt{\gamma RT}$ is accordingly

$$\frac{\delta+p}{\delta\tau} + a\rho\ \frac{\delta+ u}{\delta\tau} = \rho\ T\ \frac{DR}{D\tau} + a\eta\ \ \frac{\partial^2 u}{\partial x^2} \tag{C-15}$$

$$+ (\gamma-1)\ \{- \omega_1\, U + \eta\ \left(\frac{\partial u}{\partial x}\right)^2 - \frac{\partial Q}{\partial x} + \frac{\partial}{\partial x}\ [\ (v_1\, \eta_1 + v_2\, \eta_2)\ \frac{\partial u}{\partial x}\ ]\}$$

where

$$a \equiv \sqrt{\gamma\ RT}$$

$$\frac{\delta+}{\delta\tau} \equiv \frac{\partial}{\partial\tau} + (u + a)\ \frac{\partial}{\partial x}$$

The compatibility equation for $\lambda = u - \sqrt{\gamma RT}$ is

$$\frac{\delta-p}{\delta\tau} - a\ \rho\ \frac{\delta-u}{\delta\tau} = \rho\ \ T\ \frac{DR}{D\tau} - a\eta\ \ \frac{\partial^2 u}{\partial x^2} \qquad (C\text{-}16)$$

$$+ (\gamma-1)\ \{ - \omega_1\ U + \eta\ \left(\frac{\partial\ u}{\partial\ x}\right)^2 - \frac{\partial Q}{\partial x} + \frac{\partial}{\partial x}\ [(v_1\ \eta_1 + v_2\ \eta_2)\ \frac{\partial u}{\partial x}\ ]\}$$

where

$$\frac{\delta-}{\delta\tau}\ \equiv \frac{\partial}{\partial\tau} + (u-a)\ \frac{\partial}{\partial x}$$

APPENDIX D

TABULATION OF CALCULATED DATA

The present appendix contains a tabulation of all of the results calculated during the investigation. Tables 10, 11, and 12 contain the numerical values for the amplification parameters in the flame zone for combustion pressures of 250, 500, and 1000 psia respectively. The first column in the tables contains the initial amplitude of the shock as it enters the combustion region and the last column indicates the direction of propagation of the shock. The "Forward" indicates a shock traveling toward the propellant surface and "Return" indicates a shock traveling away from the propellant surface. Tables 13 through 15 and 16 through 18 contain similar data for the induction and decomposition zones respectively.

Tables 19, 20, and 21 contain the numerical values of the amplification parameters for the total combustion region for combustion pressures of 250, 500, and 1000 psia respectively. The aforementioned tables represent a summation of Tables 10 through 18. The amplifying effects of diffusion and viscosity were combined and entered in the table under the heading "Misc." The attenuation by the propellant of the shock as it reflects from the propellant surface was entered in the table under the heading "Propellant." The amplifying effect of all of the parameters was added together and entered in the

last column of the table under the heading "Net Effect."

In Table 22 the amplification ratio P_2/P_1 calculated for each pressure ratio across the shock r_p and combustion pressures of 250, 500, and 1000 psia are tabulated. The corresponding initial shock amplitude P_1 for each pressure ratio is also given. The data tabulated in Table 22 for initial pressures up to 50 psi are plotted in Fig. 14.

Table 10

Flame Zone

Numerical Values for the Amplification Parameters*

250 psia Combustion Pressure (p_c)

P_1	Velocity Increment	Viscosity	Heat Addition	Viscous Heat	Heat Transfer	Diffusion	Shock Direction
2.5	-1.545	0.099	3.725	-0.002	-0.385	-0.005	Forward
2.5	-2.162	0.098	3.674	-0.002	-0.379	-0.003	Return
5.0	-1.407	0.099	3.810	-0.002	-0.383	-0.004	Forward
5.0	-2.354	0.097	3.744	-0.002	-0.378	-0.003	Return
12.5	-1.016	0.097	4.068	-0.002	-0.377	-0.004	Forward
12.5	-2.940	0.096	3.960	-0.002	-0.373	-0.003	Return
25.0	-0.345	0.095	4.517	-0.002	-0.368	-0.004	Forward
25.0	-3.986	0.094	4.405	-0.002	-0.365	-0.002	Return
37.5	0.347	0.093	4.991	-0.002	-0.360	-0.003	Forward
37.5	-4.963	0.092	4.710	-0.002	-0.358	-0.002	Return

* The amplification effect is given in psi.

Table 11

Flame Zone

Numerical Values for the Amplification Parameters*

500 psia Combustion Pressure (p_c)

P_1	Velocity Increment	Viscosity	Heat Addition	Viscous Heat	Heat Transfer	Diffusion	Shock Direction
2.5	-1.285	0.095	3.229	-0.002	-0.540	-0.005	Forward
2.5	-1.792	0.095	3.150	-0.002	-0.535	-0.005	Return
5.0	-1.132	0.095	3.266	-0.002	-0.538	-0.005	Forward
5.0	-1.926	0.094	3.175	-0.002	-0.534	-0.005	Return
10.0	-0.825	0.095	3.340	-0.002	-0.535	-0.005	Forward
10.0	-2.228	0.094	3.231	-0.002	-0.531	-0.005	Return
25.0	0.112	0.093	3.570	-0.002	-0.527	-0.005	Forward
25.0	-3.061	0.093	3.385	-0.002	-0.525	-0.005	Return
50.0	1.728	0.091	3.969	-0.001	-0.515	-0.004	Forward
50.0	-4.441	0.091	3.642	-0.001	-0.516	-0.004	Return
75.0	3.404	0.089	4.390	-0.001	-0.504	-0.004	Forward
75.0	-5.793	0.090	3.895	-0.001	-0.508	-0.004	Return

* The amplification effect is given in psi.

Table 12

Flame Zone

Numerical Values for the Amplification Parameters*

1000 psia Combustion Pressure (p_c)

P_1	Velocity Increment	Viscosity	Heat Addition	Viscous Heat	Heat Transfer	Diffusion	Shock Direction
2	-1.155	0.091	2.925	-0.001	-0.757	-0.006	Forward
2	-1.463	0.091	2.842	-0.001	-0.753	-0.006	Return
5	-0.959	0.091	2.945	-0.001	-0.756	-0.006	Forward
5	-1.576	0.091	2.852	-0.001	-0.753	-0.006	Return
10	-0.632	0.091	2.980	-0.001	-0.754	-0.006	Forward
10	-1.780	0.091	2.871	-0.001	-0.752	-0.006	Return
20	0.026	0.091	3.048	-0.001	-0.751	-0.005	Forward
20	-2.147	0.090	2.904	-0.001	-0.749	-0.005	Return
50	2.040	0.089	3.259	-0.001	-0.740	-0.005	Forward
50	-3.258	0.090	3.004	-0.001	-0.743	-0.005	Return
100	5.511	0.087	3.627	-0.001	-0.724	-0.005	Forward
100	-4.940	0.089	3.157	-0.001	-0.734	-0.005	Return
150	9.118	0.086	4.016	-0.001	-0.709	-0.004	Forward
150	-6.471	0.088	3.296	-0.001	-0.727	-0.005	Return

* The amplification effect is given in psi.

Table 13

Induction Zone

Numerical Values for the Amplification Parameters*

250 psia Combustion Pressure (p_c)

P_1	Velocity Increment	Heat Addition	Heat Transfer	Shock Direction
2.5	0.099	0.057	0.343	Forward
2.5	-1.330	0.057	0.336	Return
5.0	0.428	0.057	0.342	Forward
5.0	-1.785	0.057	0.334	Return
12.5	1.435	0.056	0.336	Forward
12.5	-3.180	0.056	0.329	Return
25.0	3.910	0.054	0.328	Forward
25.0	-5.516	0.054	0.321	Return
37.5	5.020	0.052	0.320	Forward
37.5	-8.071	0.052	0.314	Return

* The amplification effect is given in psi.

Table 14

Induction Zone

Numerical Values for the Amplification Parameters*

500 psia Combustion Pressure (p_c)

P_1	Velocity Increment	Heat Addition	Heat Transfer	Shock Direction
2.5	-0.092	0.078	0.466	Forward
2.5	-1.279	0.078	0.451	Return
5.0	0.227	0.078	0.464	Forward
5.0	-1.634	0.078	0.450	Return
10.0	0.877	0.077	0.462	Forward
10.0	-2.438	0.077	0.448	Return
25.0	2.867	0.075	0.454	Forward
25.0	-4.663	0.076	0.442	Return
50.0	6.317	0.072	0.443	Forward
50.0	-8.391	0.074	0.434	Return
75.0	9.883	0.070	0.432	Forward
75.0	-12.224	0.075	0.450	Return

* The amplification effect is given in psi.

Table 15

Induction Zone

Numerical Values for the Amplification Parameters*

1000 psia Combustion Pressure (p_c)

P_1	Velocity Increment	Heat Addition	Heat Transfer	Shock Direction
2	-0.377	0.103	0.622	Forward
2	-1.102	0.104	0.595	Return
5	0.005	0.103	0.621	Forward
5	-1.419	0.103	0.594	Return
10	0.645	0.103	0.619	Forward
10	-1.990	0.103	0.593	Return
20	1.937	0.102	0.616	Forward
20	-3.024	0.103	0.591	Return
50	5.893	0.100	0.605	Forward
50	-6.158	0.102	0.586	Return
100	12.741	0.096	0.590	Forward
100	-10.941	0.100	0.578	Return
150	19.822	0.093	0.575	Forward
150	-15.328	0.098	0.572	Return

* The amplification effect is given in psi.

Table 16

Decomposition Zone

Numerical Values for the Amplification Parameters*

250 psia Combustion Pressure (p_c)

P_1	Velocity Increment	Heat Addition	Heat Transfer	Molecular Wt. Change Rate	Shock Direction
2.5	0.448	2.134	-0.780	0.745	Forward
2.5	-2.653	2.067	-0.745	0.721	Return
5.0	1.545	2.230	-0.778	0.780	Forward
5.0	-3.505	2.143	-0.740	0.749	Return
12.5	4.950	2.537	-0.761	0.894	Forward
12.5	-6.131	2.387	-0.727	0.839	Return
25.0	10.978	3.119	-0.733	1.113	Forward
25.0	-10.861	2.843	-0.706	1.010	Return
37.5	17.575	3.824	-0.707	1.380	Forward
37.5	-15.701	3.335	-0.687	1.195	Return

* The amplification effect is given in psi.

Table 17

Decomposition Zone

Numerical Values for the Amplification Parameters*

500 psia Combustion Pressure (p_c)

P_1	Velocity Increment	Heat Addition	Heat Transfer	Molecular Wt. Change Rate	Shock Direction
2.5	0.516	2.045	-1.579	0.712	Forward
2.5	-2.016	1.985	-1.499	0.690	Return
5.0	1.608	2.090	-1.573	0.729	Forward
5.0	-2.666	2.014	-1.495	0.701	Return
10.0	3.834	2.183	-1.561	0.763	Forward
10.0	-4.119	2.082	-1.487	0.726	Return
25.0	10.719	2.481	-1.526	0.873	Forward
25.0	-8.180	2.273	-1.466	0.797	Return
50.0	23.009	3.047	-1.472	1.086	Forward
50.0	-15.143	2.613	-1.431	0.923	Return
75.0	36.402	3.714	-1.418	1.338	Forward
75.0	-22.206	2.972	-1.400	1.058	Return

* The amplification effect is given in psi.

Table 18

Decomposition Zone

Numerical Values for the Amplification Parameters*

1000 psia Combustion Pressure (p_c)

P_1	Velocity Increment	Heat Addition	Heat Transfer	Molecular Wt. Change Rate	Shock Direction
2	0.677	1.998	-3.166	0.694	Forward
2	-0.812	1.942	-3.005	0.675	Return
5	1.992	2.024	-3.158	0.704	Forward
5	-1.380	1.955	-3.002	0.680	Return
10	4.190	2.069	-3.146	0.721	Forward
10	-2.397	1.979	-2.996	0.688	Return
20	8.656	2.161	-3.122	0.755	Forward
20	-4.224	2.022	-2.985	0.704	Return
50	22.576	2.455	-3.053	0.864	Forward
50	-9.860	2.155	-2.955	0.753	Return
100	47.413	3.013	-2.944	1.073	Forward
100	-18.534	2.366	-2.908	0.831	Return
150	74.338	3.668	-2.832	1.320	Forward
150	-26.636	2.567	-2.868	0.906	Return

* The amplification effect is given in psi.

Table 19

Total Combustion Region

Numerical Values for the Amplification Parameters*

250 psia Combustion Pressure (p_c)

P_1	Velocity Increment	Heat Addition	Heat Transfer	Molecular Wt. Change Rate	Misc.	Propellant	Net Effect
2.5	-7.143	11.718	-1.611	1.466	0.184	-1.339	3.275
5.0	-7.088	12.044	-1.605	1.530	0.184	-2.126	2.938
12.5	-6.883	13.065	-1.573	1.734	0.181	-4.501	2.022
25.0	-6.541	14.994	-1.524	2.123	0.178	-8.489	0.740
37.5	-5.793	16.966	-1.478	2.576	0.174	-14.651	-2.206

* The amplification effect is given in psi.

Table 20

Total Combustion Region

Numerical Values for the Amplification Parameters*

500 psia Combustion Pressure (p_c)

P_1	Velocity Increment	Heat Addition	Heat Transfer	Molecular Wt. Change Rate	Misc.	Propellant	Net Effect
2.5	-5.948	10.567	-3.236	1.403	0.176	-1.088	1.873
5.0	-5.523	10.703	-3.226	1.430	0.175	-2.485	1.074
10.0	-4.899	10.993	-3.206	1.489	0.175	-4.573	-0.021
25.0	-2.203	11.863	-3.149	1.671	0.173	-12.889	-4.534
50.0	3.079	13.420	-3.059	2.010	0.170	-28.171	-12.549
75.0	9.465	15.118	-2.949	2.397	0.167	-46.844	-22.644

* The amplification effect is given in psi.

Table 21

Total Combustion Region

Numerical Values for the Amplification Parameters*

1000 psia Combustion Pressure (p_c)

P_1	Velocity Increment	Heat Addition	Heat Transfer	Molecular Wt. Change Rate	Misc.	Propellant	Net Effect
2	-4.234	9.917	-6.466	1.370	0.167	-0.634	0.120
5	-3.338	9.987	-6.454	1.384	0.167	-3.079	-1.333
10	-1.964	10.107	-6.436	1.410	0.166	-6.855	-3.572
20	1.224	10.343	-6.401	1.459	0.166	-15.326	-8.534
50	11.233	11.078	-6.300	1.617	0.164	-41.512	-23.717
100	31.249	12.361	-6.143	1.904	0.162	-91.343	-51.807
150	54.842	13.740	-5.989	2.227	0.160	-148.970	-83.988

* The amplification effect is given in psi.

Table 22

Net Amplification of the Nonuniform Shock

Pressure Ratio (r_p)	Initial Shock Amplitude (P_1)*	Amplification Ratio (P_2/P_1)
250 psia Combustion Pressure (p_c)		
1.01	2.5	2.231
1.02	5.0	1.550
1.05	12.5	1.141
1.10	25.0	1.005
1.15	37.5	0.950
500 psia Combustion Pressure (p_c)		
1.005	2.5	1.673
1.01	5.0	1.181
1.02	10.0	0.978
1.05	25.0	0.811
1.10	50.0	0.745
1.15	75.0	0.713
1000 psia Combustion Pressure (p_c)		
1.002	2.0	0.974
1.005	5.0	0.700
1.01	10.0	0.627
1.02	20.0	0.564
1.05	50.0	0.525
1.10	100.0	0.486
1.15	150.0	0.457

* Initial shock amplitude given in psi.

APPENDIX E

EXPERIMENTAL DATA FROM ROCKETDYNE

Two datum points were calculated from experimental information collected at Rocketdyne, Inc., Canoga Park, California. The information was obtained from Mr. Carl Oberg through personal communication. The conditions under which the information was collected approximated the model postulated for the analysis reported herein.

A simple sketch of the equipment employed at Rocketdyne to obtain the experimental information is given in Fig. 16. The equipment is basically a closed shock tube. The low pressure end of the tube is divided in half longitudinally by a flow divider. On one side of the divider a slab of solid propellant is burned; on the other side is an empty chamber. A pressure transducer is aligned at the surface of the propellant and another transducer is placed opposite it in the empty chamber. The propellant is pulsed by bursting the diaphragm which restrains the high pressure air at the other end of the tube. As the nonuniform shock produced by bursting the diaphragm travels down the tube it is separated by the flow divider. One half of the nonuniform shock reflects from the burning propellant surface and a time-pressure trace of the interaction is measured by the transducer located at the propellant surface. The other half of the nonuniform shock travels past the second transducer and the time-pressure trace for the forward

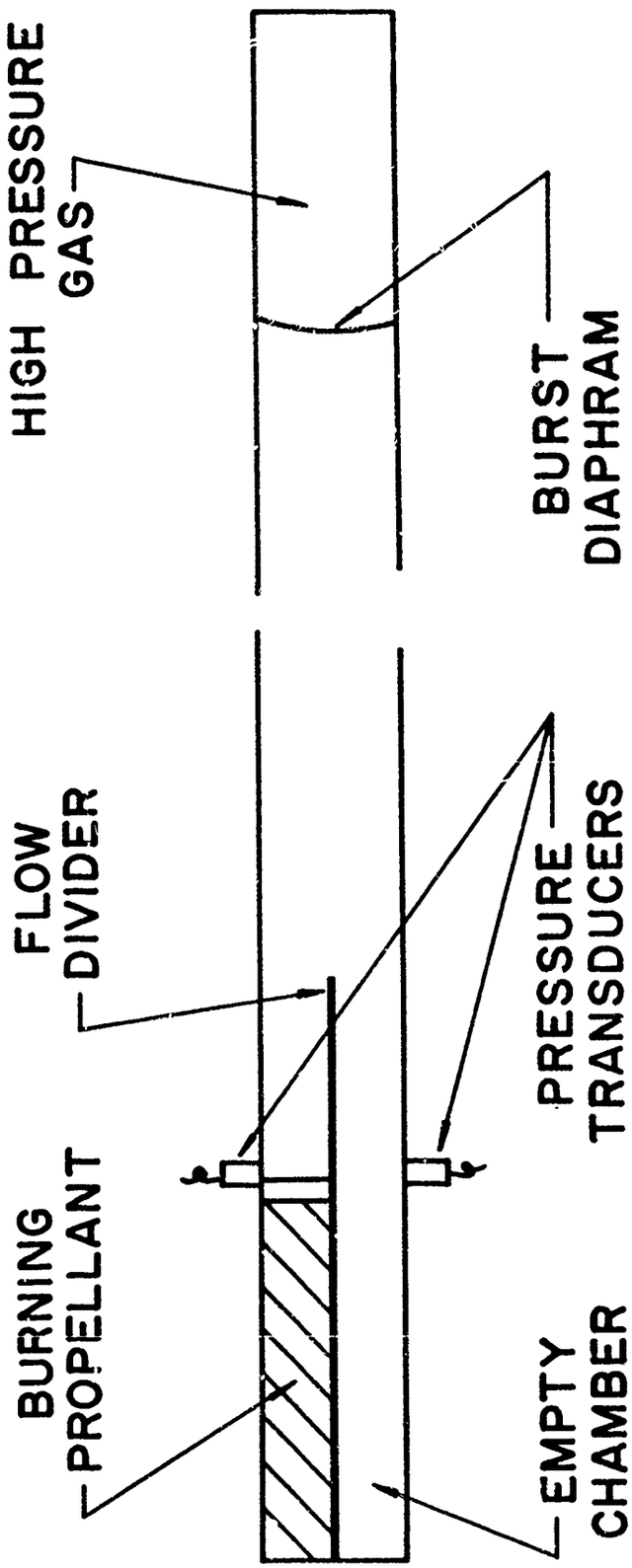

Figure 16 Sketch of Apparatus Employed at Rocketdyne

propagating nonuniform shock is obtained. The difference between the two traces should approximate the time-pressure trace for the reflected nonuniform shock.

Figure 17 presents pictures of oscilloscope traces for two interactions. The upper trace in each picture is the pressure-time trace for the interaction at the surface of the propellant and the lower trace is from the empty chamber. The pulse amplitude at the time of interaction was about 8 psi and the combustion pressure was about 400 psig.

As can be seen from the traces, it is difficult to determine amplitudes for the pulses. Table 23 lists the values that were estimated to be the amplitudes of the pulses. The calculated amplification ratio for each interaction is also given. The amplification ratio was calculated under the assumption that the pressure-time trace at the surface of the propellant represents the sum of the forward and reflected pulses. The amplification ratio was calculated according to the formula,

$$\text{amplification ratio} = \frac{\text{propellant amplitude} - \text{empty chamber amplitude}}{\text{empty chamber amplitude}} \qquad \text{(E-1)}$$

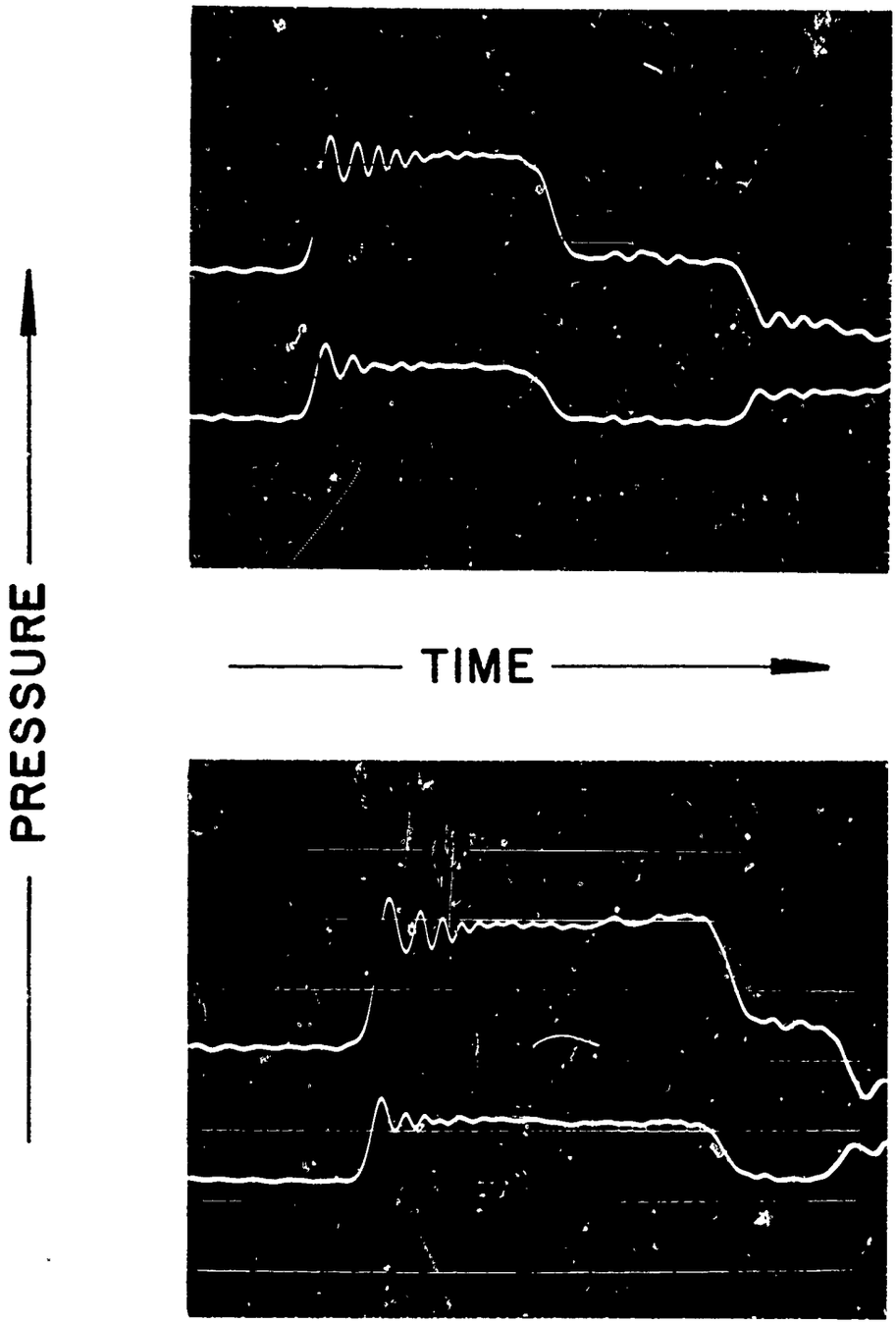

Figure 17 Pressure-Time Traces Obtained at Rocketdyne

Table 23

Experimental Data -- Rocketdyne

Noninteraction Amplitude (in)	Interaction Amplitude (in)	Amplification Ratio (P_2/P_1)
0.281	0.585	1.08
0.320	0.650	1.03

UNCLASSIFIED
Security Classification

DOCUMENT CONTROL DATA - R&D

(Security classification of title, body of abstract and indexing annotation must be entered when the overall report is classified)

1. ORIGINATING ACTIVITY (Corporate author)
Jet Propulsion Center, Purdue University
School of Mechanical Engineering
Lafayette, Indiana

2a. REPORT SECURITY CLASSIFICATION
Unclassified

2b. GROUP

3. REPORT TITLE
THE INTERACTION OF A FINITE AMPLITUDE PRESSURE DISTURBANCE WITH A COMBUSTION REGION

4. DESCRIPTIVE NOTES (Type of report and inclusive dates)
Scientific Report

5. AUTHOR(S) (Last name, first name, initial)
Lehmann, G. M.

6. REPORT DATE	7a. TOTAL NO. OF PAGES	7b. NO. OF REFS
February 1966	192	41

8a. CONTRACT OR GRANT NO
NONR 1100(21) AFOSR 753-65

b. PROJECT NO.
9711-01

c. 61445014

d.

9a. ORIGINATOR'S REPORT NUMBER(S)
TM-66-1

9b. OTHER REPORT NO(S) (Any other numbers that may be assigned this report)
AFOSR 66-0892

10. AVAILABILITY/LIMITATION NOTICES
Distribution of this document is unlimited

11. SUPPLEMENTARY NOTES

12. SPONSORING MILITARY ACTIVITY
Power Branch, Office of Naval Research
Air Force Office of Scientific Research (SREP)
Washington, D. C. 20333

13. ABSTRACT

The method for calculating the interaction of a nonuniform shock with the combustion region at the surface of a burning solid propellant is presented. Interactions were calculated for initial nonuniform shock amplitudes ranging from 2.5 to 150 psi. at combustion pressures of 250, 500, and 1000 psia. (U)

Results indicated that the amplification of the nonuniform shock by the combustion region decreases with increasing combustion pressure and increasing initial shock amplitude. It was found that the major factor that lead to the amplification of the nonuniform shock was the heat addtion in the combustion region. The major attenuating effects were the heat transfer into the propellant, the energy absorbed by the propellant as the shock reflected from its surface, and the steady state velocity gradient in the combustion region. (U)

DD FORM 1473

UNCLASSIFIED

Security Classification

14. KEY WORDS	LINK A		LINK B		LINK C	
	ROLE	WT	ROLE	WT	ROLE	WT
combustion instability						
shock interaction						

INSTRUCTIONS

1. ORIGINATING ACTIVITY: Enter the name and address of the contractor, subcontractor, grantee, Department of Defense activity or other organization *(corporate author)* issuing the report.

2a. REPORT SECURITY CLASSIFICATION: Enter the overall security classification of the report. Indicate whether "Restricted Data" is included. Marking is to be in accordance with appropriate security regulations.

2b. GROUP: Automatic downgrading is specified in DoD Directive 5200.10 and Armed Forces Industrial Manual. Enter the group number. Also, when applicable, show that optional markings have been used for Group 3 and Group 4 as authorized.

3. REPORT TITLE: Enter the complete report title in all capital letters. Titles in all cases should be unclassified. If a meaningful title cannot be selected without classification, show title classification in all capitals in parenthesis immediately following the title.

4. DESCRIPTIVE NOTES: If appropriate, enter the type of report, e.g., interim, progress, summary, annual, or final. Give the inclusive dates when a specific reporting period is covered.

5. AUTHOR(S): Enter the name(s) of author(s) as shown on or in the report. Enter last name, first name, middle initial. If military, show rank and branch of service. The name of the principal author is an absolute minimum requirement.

6. REPORT DATE: Enter the date of the report as day, month, year; or month, year. If more than one date appears on the report, use date of publication.

7a. TOTAL NUMBER OF PAGES: The total page count should follow normal pagination procedures, i.e., enter the number of pages containing information.

7b. NUMBER OF REFERENCES: Enter the total number of references cited in the report.

8a. CONTRACT OR GRANT NUMBER: If appropriate, enter the applicable number of the contract or grant under which the report was written.

8b, 8c, & 8d. PROJECT NUMBER: Enter the appropriate military department identification, such as project number, subproject number, system numbers, task number, etc.

9a. ORIGINATOR'S REPORT NUMBER(S): Enter the official report number by which the document will be identified and controlled by the originating activity. This number must be unique to this report.

9b. OTHER REPORT NUMBER(S): If the report has been assigned any other report numbers *(either by the originator or by the sponsor)*, also enter this number(s).

10. AVAILABILITY/LIMITATION NOTICES: Enter any limitations on further dissemination of the report, other than those imposed by security classification, using standard statements such as:

(1) "Qualified requesters may obtain copies of this report from DDC."

(2) "Foreign announcement and dissemination of this report by DDC is not authorized."

(3) "U. S. Government agencies may obtain copies of this report directly from DDC. Other qualified DDC users shall request through _____."

(4) "U. S. military agencies may obtain copies of this report directly from DDC. Other qualified users shall request through _____."

(5) "All distribution of this report is controlled. Qualified DDC users shall request through _____."

If the report has been furnished to the Office of Technical Services, Department of Commerce, for sale to the public, indicate this fact and enter the price, if known.

11. SUPPLEMENTARY NOTES: Use for additional explanatory notes.

12. SPONSORING MILITARY ACTIVITY: Enter the name of the departmental project office or laboratory sponsoring *(paying for)* the research and development. Include address.

13. ABSTRACT: Enter an abstract giving a brief and factual summary of the document indicative of the report, even though it may also appear elsewhere in the body of the technical report. If additional space is required, a continuation sheet shall be attached.

It is highly desirable that the abstract of classified reports be unclassified. Each paragraph of the abstract shall end with an indication of the military security classification of the information in the paragraph, represented as *(TS), (S), (C), or (U)*.

There is no limitation on the length of the abstract. However, the suggested length is from 150 to 225 words.

14. KEY WORDS: Key words are technically meaningful terms or short phrases that characterize a report and may be used as index entries for cataloging the report. Key words must be selected so that no security classification is required. Identifiers, such as equipment model designation, trade name, military project code name, geographic location, may be used as key words but will be followed by an indication of technical context. The assignment of links, roles, and weights is optional.